Modeling 2013 in Massachusetts Bay using the unstructured-grid Bays Eutrophication Model

Massachusetts Water Resources Authority
Environmental Quality Department
Report 2015-03

Modeling 2013 in Massachusetts Bay
Using the Unstructured-Grid Bays Eutrophication Model

Submitted to

Massachusetts Water Resources Authority
Environmental Quality Department
100 First Avenue
Charlestown Navy Yard
Boston, MA 02129
(617) 242-6000

Prepared by

Liuzhi Zhao and Changsheng Chen

School for Marine Science and Technology

University of Massachusetts-Dartmouth

New Bedford, MA 02744

Robert C. Beardsley

Woods Hole Oceanographic Institution

Woods Hole, MA 02543

Daniel L. Codiga, Wendy S. Leo, and Michael J. Mickelson

Massachusetts Water Resources Authority

Boston, MA 02129

April 2015

Citation:

Zhao L, Chen C, Beardsley RC, Codiga DL, Leo WS, Mickelson MJ. 2015. **Modeling 2013 in Massachusetts Bay Using the Unstructured-Grid Bays Eutrophication Model.** Boston: Massachusetts Water Resources Authority. Report 2015-03. 102p.

Acronyms

Model names

BEM	Bays Eutrophication Model (water quality model UG-RCA and hydrodynamics model MB-FVCOM coupled to each other)
FVCOM	Finite-Volume Community Ocean Model
GoM/GB-FVCOM	FVCOM applied to the Gulf of Maine/Georges Bank[1]
MB-FVCOM	FVCOM applied to Massachusetts Bay[2]
RCA	Row Column Advanced (RCA), a water quality model from Hydroqual
UG-RCA	Unstructured-grid version of RCA

Model forcing and methods

OA	Objective Analysis, creates OBC from observations located on/off boundary
OBC	Open Boundary Condition, values on offshore boundary of model domain
NERACOOS	Northeast Regional Association for Coastal Ocean Observing Systems
WRF	Weather Research and Forecast meteorological model[3]

Geographic names

BH	Boston Harbor
CCB	Cape Cod Bay
MB	Massachusetts Bay, sometimes inclusive of Cape Cod Bay and Boston Harbor
WMCC	Western Maine Coastal Current

State variables and rates

DIN	Dissolved Inorganic Nitrogen (=Sum of N in NH_4^+, NO_3^-, and NO_2^-)
DO	Dissolved Oxygen
DOC, DON, DOP	Dissolved Organic Carbon, Nitrogen, and Phosphorous
NH_4^+, NO_3^-, NO_2^-	Ammonium, Nitrate, Nitrite
PO_4^{3-}, SiO_3^{2-}	Phosphate, Silicate
POC, PON, POP	Particulate Organic Carbon, Nitrogen, and Phosphorous
SOD	Sediment Oxygen Demand

[1] http://fvcom.smast.umassd.edu/research_projects/GB/index.html
[2] http://fvcom.smast.umassd.edu/research_projects/MassBay/index.html
[3] http://fvcom.smast.umassd.edu/research_projects/GB/WRF/index.html

EXECUTIVE SUMMARY

MWRA contracted University of Massachusetts Dartmouth to simulate hydrodynamic fields (including currents, temperature, and salinity) and water quality parameters (including nutrients, chlorophyll, and dissolved oxygen, DO) in Massachusetts Bay, Cape Cod Bay, and Boston Harbor for calendar year 2013. This report presents the simulation results, with comparisons to observations to assess the model performance. It also discusses scenario simulations examining potential impacts of hypothetical changes in nutrient loads from the MWRA outfall effluent on bay-wide ecosystem function such as algal production and DO levels.

Methods were the same as in the simulations of 2012. The hydrodynamic model was driven (a) at the sea surface by a regional weather model, and by satellite temperature observations; (b) at its offshore boundary, an arc from north of Portsmouth NH to 25 km offshore from Cape Cod, by a larger regional Gulf of Maine simulation; (c) by freshwater discharge from rivers at the coast, and from the MWRA outfall; and (d) using available oceanographic observations, including from the A01 mooring operated by the Northeast Regional Association of Coastal Ocean Observing Systems south of Cape Ann with partial support from MWRA. Hydrodynamic model results captured the main observed characteristics of tidal and non-tidal residual currents and of temperature and salinity distributions, including the seasonal cycle of stratification.

Inputs to the water quality model consist of (a) hydrodynamic model outputs; (b) observed sunlight characteristics; (c) conditions at the offshore boundary, an arc from Cape Ann to the offshore edge of Cape Cod, as estimated from MWRA monitoring observations in the bay; and (d) nutrient and carbon loadings from the MWRA outfall, other effluent outfalls, rivers, non-point sources, and atmospheric sources. Modeled phytoplankton growth depends on sunlight and nutrient availability, and modeled zooplankton grazing increases as temperature increases. The model incorporates cycling of nutrients and dissolved and particulate forms of organic carbon, nitrogen, and phosphorous. Model DO levels are determined by air-sea exchange, sediment oxygen demand, water column mixing, and phytoplankton production and respiration.

The water quality simulation captured general patterns in observed seasonal variations and vertical structure for many variables. This included the spring/summer reduction in near-surface dissolved inorganic nitrogen (DIN), due to phytoplankton uptake, and its replenishment in fall when stratification breaks down. Modeled chlorophyll showed a spring increase which, though weaker and later than in other years, did not agree well with the unusually low observed 2013

levels. The model exhibited the observed seasonal DO cycle, with peak shallow values in spring due to solubility and phytoplankton growth, continuous decreases through summer and early fall at all depths, and replenishment during the winter mixed period. Modeled dissolved and particulate organic nitrogen showed modest agreement with observations, while model particulate organic carbon did not capture well the observed seasonal variations or vertical structure. In general, as in prior years, most modeled water quality variables exhibited a smaller range of values, and smaller surface-bottom differences during stratified conditions, as compared to observations.

To isolate MWRA outfall influences, a scenario was run with the outfall nutrient load removed but all other conditions unchanged. Results of this scenario for 2013 were as in prior years. The outfall had little perceptible effect on chlorophyll and DO, and effluent nutrients comprised a very small percentage of natural background levels except within 10-20 km of the outfall. Effluent was trapped nearer to the bottom during summer stratification than in winter. In winter, increased winds and mixing caused effluent to reach the surface and disperse over longer distances, but reduced light levels slowed phytoplankton growth such that nutrients were not efficiently converted into biomass by phytoplankton. These results for 2013 support conclusions from the MWRA monitoring program that bay-wide ecological function is not appreciably influenced by the outfall.

Additional scenario simulations investigated the potential influence of hypothetical increases to MWRA outfall nutrient loads. These runs scaled up by 10% and 100% (doubled) the effluent nutrient concentrations. A 10% increase has practical relevance, as estimates suggest an increase of up to 5% could result from a co-digestion program under consideration for the treatment plant; the 100% increase is a hypothetical extreme to investigate the level at which ecological effects might begin to be seen. Response to the 10% increase was most pronounced in DIN, which increased detectably only very near to the outfall and the seafloor, but effects on chlorophyll and DO were essentially imperceptible. Response to the 100% increase included substantially higher DIN (~53%) local to the outfall, modest increases (~7%) to chlorophyll, and changes of less than 0.5% in DO. Even for the extreme case of doubled MWRA outfall nutrient load, conditions far from the outfall (for example, Cape Cod Bay) were very similar to the simulation with actual 2013 loading.

The scenario simulations demonstrated that effects on water quality and ecosystem function would be very minor, even in the immediate vicinity of the discharge, for MWRA outfall nutrient load changes of approximately 10%. This is because most nutrients in Massachusetts and Cape Cod Bays originate from the Gulf of Maine. Outfall nutrients are only a small percentage of the total.

Table of Contents

EXECUTIVE SUMMARY 3
1. Introduction 10
1.1 Project overview 10
1.2 Background 10
1.3 Summary of observed 2013 conditions 10
2. Methods 11
3. Results 13
3.1 Forcing conditions 13
3.1.1 Wind, heat flux, and Merrimack River 13
3.1.2 Loading of organic carbon, nitrogen, and phosphorous 13
3.1.3 UG-RCA open boundary 14
3.2 Physical fields 16
3.2.1 Model-observation comparisons 16
3.2.2 Model monthly-mean surface circulation, temperature, and salinity 18
3.2.3 Comparison with simulations of previous years 19
3.3 Water quality fields 20
3.3.1 Model fields including comparisons to observations 20
3.3.1.1 Chlorophyll 21
3.3.1.2 Dissolved inorganic nitrogen 22
3.3.1.3 Primary productivity 23
3.3.1.4 Dissolved and particulate organic nitrogen 23
3.3.1.5 Particulate organic carbon 24
3.3.1.6 Dissolved oxygen 24
3.3.1.7 Sediment fluxes 25
3.3.1.8 Summary 26
3.3.2 Comparison with previous years' simulations 26
4. Scenario experiments 27
4.1 Scenario without MWRA outfall nutrient load 27
4.2 Scenarios with hypothetically increased MWRA outfall nutrient loads 29
5. Summary 32
6. References 34

Table of Figures

Figure 1.1 Geographic features, bathymetry, MWRA outfall location, and site of meteorological station 44013. 37

Figure 2.1 Model grids. 38

Figure 2.2 Schematic of water quality model (reproduced from Hydroqual, 2004). 39

Figure 3.1 Monthly-averaged wind (upper panel) and heat flux (mid panel) and daily-averaged discharge from Merrimack River in 2013 (black) and the 18-year (1995-2012) average (red). 40

Figure 3.2 Mean daily loads of carbon, nitrogen and phosphorus from non-oceanic sources in 2013. 41

Figure 3.3 MWRA outfall mean annual flow and daily carbon, nitrogen and phosphorus loads 2005-2013. 42

Figure 3.4 Stations. Subsets grouped together in later plots: northern (green), southern (yellow), harbor (blue). 43

Figure 3.5 Open boundary chlorophyll, nutrients, DO and organics concentrations. 44

Figure 3.6 Inter-annual variations in open boundary nitrate (μM). 2013 (left), 2012 (middle) and 2011 (right) in winter. January 30 (upper) and March 1 (lower). 45

Figure 3.7 Temperature and salinity: vessel-survey observations (circles) and model output (line) at select northern/southern subset stations in 2013. 46

Figure 3.8 Near-surface temperature (upper, ^{o}C) and salinity (lower, PSS), Feb (left group), Apr (middle group), and Jun (right group). Observed (left in each pair) and model (right in each pair). Note differences in temperature colorscales. 47

Figure 3.9 Near-surface temperature (upper, ^{o}C) and salinity (lower, PSS), Aug (left group), and Oct (right group). Observed (left in each pair) and model (right in each pair). Note differences in temperature colorscales. 48

Figure 3.10 Monthly-mean model surface currents: Jan to Apr 2013. 49

Figure 3.11 Monthly-mean model surface currents: May to Aug 2013. 50

Figure 3.12 Monthly-mean model surface currents: Sep to Dec 2013. 51

Figure 3.13 Model surface temperature at the end of each month of 2013. Note differences in temperature colorscales. 52

Figure 3.14 Model surface salinity at the end of each month of 2013. 53

Figure 3.15 Inter-annual variation in monthly-mean surface currents: Apr (upper) and Sep (lower) during 2013 (left) and 2012 (right). 54

Figure 3.16 Inter-annual variation in monthly-mean surface temperatures (left group, ^{o}C) and salinities (right group, PSS): Apr (upper) and Sep (lower) during 2013 (left) and 2012 (right). 55

Figure 3.17 Model-observation correlations and regressions (solid lines) of key parameters, all stations outside BH, 2013. 56

Figure 3.18 Chlorophyll: observed (dots) and modeled (lines) at northern subset stations in 2013. 57

Figure 3.19 Chlorophyll: observed (dots) and modeled (lines) at southern subset stations in 2013. 58

Figure 3.20 Chlorophyll: observed (dots) and modeled (lines) at harbor subset stations in 2012. 59

Figure 3.21 Model chlorophyll (μg L^{-1}): west-east transect through MWRA outfall, end of each month, 2013. 60

Figure 3.22 DIN: observed (dots) and modeled (lines) at northern subset stations in 2013. 61

Figure 3.23 DIN: Observed (dots) and modeled (lines) at southern subset stations in 2013. 62

Figure 3.24 DIN: observed (dots) and modeled (lines) at harbor subset stations in 2013. 63

Figure 3.25 Model DIN (μM): west-east transect through MWRA outfall, end of each month, 2013..... 64

Figure 3.26 Model vertically-integrated primary production in 2013 (heavy line), with 1995-2010 observations (box-whiskers), at select MB stations..... 65

Figure 3.27 DON: observed (dots) and modeled (lines) at northern subset stations in 2013. 66

Figure 3.28 DON: observed (dots) and modeled (lines) at southern subset stations in 2013. 67

Figure 3.29 Model DON (μM): west-east transect through MWRA outfall, end of each month, 2013. 68

Figure 3.30 PON: observed (dots) and modeled (lines) at northern subset stations in 2013. 69

Figure 3.31 PON: observed (dots) and modeled (lines) at southern subset stations in 2013. 70

Figure 3.32 Model PON (μM): west-east transect through MWRA outfall, end of each month, 2013. 71

Figure 3.33 POC: observed (dots) and modeled (lines) at northern subset stations in 2013. 72

Figure 3.34 POC: observed (dots) and modeled (lines) at southern subset stations in 2013. 73

Figure 3.35 Model POC (μM): west-east transect through MWRA outfall, end of each month, 2013. 74

Figure 3.36 DO (mg L^{-1}): observed (dots) and modeled (lines) at northern subset stations in 2013. 75

Figure 3.37 DO (mg L^{-1}): observed (dots) and modeled (lines) at southern subset stations in 2013. 76

Figure 3.38 Model DO (mg L^{-1}): west-east transect through MWRA outfall, end of each month, 2013. 77

Figure 3.39 DO saturation (%): observed (dots) and modeled (lines) at northern subset stations in 2013. 78

Figure 3.40 DO saturation (%): observed (dots) and modeled (lines) at southern subset stations in 2013. 79

Figure 3.41 DO saturation (%): observed (dots) and modeled (lines) at harbor subset stations in 2013. 80

Figure 3.42 Model DO saturation (%): west-east transect through MWRA outfall, end of each month, 2013. 81

Figure 3.43 Model sediment NH_4^+ flux in 2013 (heavy line), with 2001-2010 observations (box-whiskers), at select sediment flux study stations. 82

Figure 3.44 Model sediment oxygen demand in 2013 (heavy line), with 2001-2010 observations (box-whiskers), at select sediment flux study stations. 83

Figure 3.45 Seasonal and interannual variations, model surface chlorophyll, select MB stations: 2011 (red lines), 2012 (blue lines), and 2013 (black lines). 84

Figure 3.46 Seasonal and interannual variations, model surface DIN at select MB stations: 2011 (red lines), 2012 (blue lines), and 2013 (black lines). 85

Figure 3.47 Seasonal and interannual variations, model bottom DO (mg L^{-1}) at select MB stations: 2011 (red lines), 2012 (blue lines), and 2013 (black lines). 86

Figure 3.48 Seasonal and interannual variations, model bottom DO saturation (%) at select MB stations: 2011 (red lines), 2012 (blue lines), and 2013 (black lines). 87

Figure 4.1 Scenario experiment surface chlorophyll: control run (black line) and non-sewage (red line) at select MB stations in 2013. 88

Figure 4.2 Scenario experiment surface DIN: control run (black line) and non-sewage (red line) at select MB stations in 2013. 89

Figure 4.3 Scenario experiment bottom DIN: control run (black line) and non-sewage (red line) at select MB stations in 2013. 90

Figure 4.4 Scenario experiment bottom DO (mg L^{-1}): control run (black line) and non-sewage (red line) at select MB stations in 2013. 91

Figure 4.5 Scenario experiment surface DO saturation (%): control run (black line) and non-sewage (red line) at select MB stations in 2013. 92

Figure 4.6 Differences in bottom NH_4^+ (μM) between control and non-sewage experiments at end of each month, 2013. 93

Figure 4.7 Differences in NH_4^+ concentration (μM) between control and non-sewage experiments on west-east transect across MWRA outfall at end of each month, 2013. 94

Figure 4.8 Differences in bottom NH_4^+ (μM) between run with nutrient load of 1.1X relative to the control, and the control, at end of each month in 2013. 95

Figure 4.9 Differences in NH_4^+ (μM) between run with nutrient load of 1.1X relative to the control, and the control, on west-east transect across MWRA outfall at end of each month in 2013. 96

Figure 4.10 Differences in bottom NH_4^+ (μM) between run with nutrient load of 2X relative to the control, and the control, at end of each month in 2013. 97

Figure 4.11 Differences in NH_4^+ (μM) between run with nutrient load of 2X relative to the control, and the control, on west-east transect across MWRA outfall at end of each month in 2013. 98

Figure 4.12 Surface DIN concentrations in runs with nutrient load of 1X (black), 1.1X (red), and 2X (blue) relative to the control, at select MB stations in 2013. 99

Figure 4.13 Bottom DIN concentrations in runs with nutrient load of 1X (black), 1.1X (red), and 2X (blue) relative to the control, at select MB stations in 2013, shown as in Figure 4.12. 100

Figure 4.14 Surface chlorophyll concentrations in runs with nutrient load of 1X (black), 1.1X (red), and 2X (blue) relative to the control, at select MB stations in 2013, shown as in Figure 4.12. 101

Figure 4.15 Bottom DO (mg L^{-1}) concentrations in runs with nutrient load of 1X (black), 1.1X (red), and 2X (blue) relative to the control, at select MB stations in 2013, shown as in Figure 4.12. 102

Table of Tables

Table 1.1 Scenario simulations with outfall loading changes. Average conditions over month of August 2013. 36

1. Introduction

1.1 *Project overview*

The Massachusetts Water Resources Authority (MWRA) has established a long-term monitoring program to evaluate the impact of MWRA sewage treatment plant effluent on the ecosystem function and water quality in Boston Harbor (BH), Massachusetts Bay (MB) and Cape Cod Bay (CCB). The monitoring program primarily consists of an array of field observations, but is complemented by water quality modeling as required by the MWRA permit for effluent discharge into MB. This report presents the results of the Bays Eutrophication Model (BEM), which consists of the MB-FVCOM (Finite Volume Community Ocean Model) hydrodynamic model and the UG-RCA (Unstructured Grid Row Column Advanced) water quality model, for the 2013 calendar year simulation period including details of forcing treatment, model setup, model-data comparisons, scenario runs, and interpretation of findings.

1.2 *Background*

Massachusetts Bay and Cape Cod Bay (Figure 1.1) comprise a temperate coastal embayment. Readers unfamiliar with its geography and the current understanding of physical and biological oceanographic processes in it are referred to, for example, the introductory summaries in sections 1.2 and 1.3 of Zhao et al. (2012), the annual MWRA water column monitoring report (e.g., for calendar year 2013, Libby et al., 2014), and references therein.

1.3 *Summary of observed 2013 conditions*

To provide context for descriptions of model simulations of 2013 throughout the remainder of this report, a brief summary is given here of the observed conditions based on MWRA monitoring results (Libby et al., 2014). In the early months of 2013 the winter/spring was characterized by relatively higher than normal temperatures and salinities, and lower than normal precipitation and freshwater runoff. In spring the nutrient concentrations were anomalously low and remarkably there was essentially no spring phytoplankton bloom. Although observations during peak winter months were limited, it has been suggested that during that time some continued algal growth may have been sustained by the higher than normal temperatures, depleting nutrients and contributing to the absence of the spring bloom. During the summer, temperatures remained higher than normal but river runoff became higher than normal. There was a larger than typical diatom bloom in the

summer, and summer zooplankton abundances were at normal to high levels. In the summer and fall the density stratification was anomalously strong as a result of vertical gradients in both temperature (higher than normal surface values) and salinity (lower than normal surface values due to the high summertime runoff). In the fall, runoff was lower than normal, the phytoplankton bloom strength was normal to high, and stratification persisted longer than normal as the onset of strong winds was later than normal. Dissolved oxygen (DO) levels were generally lower than normal throughout the year. Despite somewhat lower DO levels when stratification developed, and a summertime period of decreasing DO that persisted longer in fall than typical, DO minima in late summer and fall were typical of most years except in one portion of CCB where they were slightly lower than normal. In summary, there was lower than average annual-mean runoff, no spring phytoplankton bloom, historically low biomass based on chlorophyll and particulate organic carbon (POC), strong stratification in summer that persisted late into fall, and DO that was lower than normal but followed a typical annual cycle and did not have a particularly low minimum.

2. Methods

The present-day BEM is the result of extensive development begun in the early 1990s. Complete background information on BEM is in MWRA Technical Reports, where the model development and updating process has been documented fully. Zhao et al. (2015) includes a comprehensive listing (their Table 1.1) of MWRA Technical Reports about the modeling, including for each a summary of the topic, highlighted aspects of its content, the full citation, and a hyperlink to the downloadable PDF file in the online repository. Section 1.4 of Zhao et al. (2012) reviews some of the key improvements incorporated, with emphasis on recent years. Simulations of years from 2008 onward use MB-FVCOM for hydrodynamics and UG-RCA for water quality.

Methods used in 2013 simulations are the same as for simulations of 2012 (Zhao et al., 2015), which incorporate some improvements (detailed in Zhao et al., 2015) relative to the methods used for simulations of 2011 (described in detail by Zhao et al., 2012). A brief summary is as follows.

The hydrodynamic model MB-FVCOM (FVCOM on grid spanning MB; Figure 2.1) was driven at the surface with calibrated wind stress, heat flux/shortwave irradiance, and precipitation/evaporation from the mesoscale meteorological model WRF (Weather Research and Forecast). Forcing at the open boundary, including tides, is by nesting in the regional Gulf of Maine and Georges Bank FVCOM (GoM/GB-FVCOM; Figure 2.1). Freshwater discharges enter at the coast from all local rivers. Effluent from the MWRA outfall enters at the seafloor. MB-FVCOM

also assimilated available observations, including sea surface temperature and timeseries of water column temperature and salinity from moorings.

The water quality model UG-RCA is driven by transport and eddy diffusivity from the hydrodynamic model output. The grids for MB-FVCOM and UG-RCA are the same, except that UG-RCA does not extend as far eastward (Figure 2.1). Horizontal resolution ranges from about 0.29 km near the coast to 0.7-2.5 km at the eastern boundary of UG-RCA and 5–10 km near the MB-FVCOM nested boundary. In the vertical a hybrid fixed/terrain-following coordinate is used with 30 grid levels.

UG-RCA is based on RCA-v3.0 (Hydroqual, 2004) and has 26 state variables and 23 sediment variables (Figure 2.2). Growth of phytoplankton is based on solar radiation and nutrient availability, and subject to zooplankton grazing parameterized as a first-order temperature-dependent transformation to particulate and dissolved organic matter. Three phytoplankton functional groups are included: a winter-spring group favoring low temperatures, low light, and high nutrients (representative of diatoms); a summer group that favors higher temperature and light conditions, and tolerates lower nutrients (representative of a mixture of species including dinoflagellates); and a fall group most responsive to moderate temperatures and lower nutrients (representative of a second diatom group). Nutrients (including ammonium NH_4^+, nitrate NO_3^- and nitrite NO_2^-, phosphate PO_4^{3-} and dissolved silica SiO_3^{2-}) are formed through mineralization of organic substances in the water column and at the sediment-water interface. Cycling of labile and refractory forms of dissolved and particulate organic carbon, nitrogen, and phosphorous is treated. DO is computed by the reaeration flux at the sea surface, sediment oxygen demand (SOD) at the bottom, and biological and biogeochemical dynamics in the water column including phytoplankton photosynthetic production, consumption by respiration, biogeochemical oxygen demand through the mineralization of particulate and dissolved organic matter, and nitrification. Open boundary condition (OBC) fields are specified using objective analysis (OA) of MWRA monitoring program observations. Non-oceanic (meaning not derived from exhange with offshore Gulf of Maine waters) nutrient and carbon loadings are specified with recent observations when available, or historic observations and estimates, and include the MWRA effluent outfall from the Deer Island Treatment Plant, non-MWRA point sources, non-point sources, river discharge and atmospheric sources.

3. Results

3.1 *Forcing conditions*

3.1.1 Wind, heat flux, and Merrimack River

Wind, heat flux, and Merrimack River discharges in 2013 are shown in Figure 3.1 and compared with the climatological mean values averaged over the prior 18 years (1995–2012). Northwest (southeastward) wind prevailed in January, February and March in both 2013 and the 18-year average, though in comparison to the 18-year average the direction in 2013 was more eastward in January and more southward in March. January and March 2013 both had notably stronger winds than the long-term average. April saw northward wind that was opposite in direction to the long-term average. From April through August, 2013 winds were northward, with July wind speeds stronger than the long-term average. From September through December 2013, southeastward-eastward wind prevailed, with wind speeds in September/October and November of 2013 notably weaker and stronger (two times as strong) than the long-term average, respectively.

Surface heat flux in 2013 followed a seasonal cycle mostly comparable to the long-term average, with high values in summer and low values in winter and late fall. However, other than April and September, surface heat flux was visibly lower in 2013 than in the long-term average, and was particularly low in June and July.

The annual Merrimack River discharge in 2013 (6.81×10^9 m^3) was about 16% less than the long-term average (8.12×10^9 m^3). Discharge in 2013 was lower than the long-term average in the winter and spring, then higher than average in summer. The spring discharge was characterized by four peaks: one at ~400 m^3/s in early February, a 2nd peak >600 m^3/s around mid-March, and 3rd and 4^{th} peaks of nearly 600 m^3/s in early and mid-April. Three summer peaks occurred, in late May through July, the last with a peak value higher than any spring rate. Discharge in fall 2013 was substantially lower than the long-term average.

3.1.2 Loading of organic carbon, nitrogen, and phosphorous

There are both oceanic and non-oceanic sources of organic materials and nutrients to the bays. The oceanic component stems from exchange with adjacent offshore waters of the Gulf of Maine. These offshore waters are not characterized by particularly high concentrations, but the volume of the exchange is very large. A systemwide budget for nitrogen in the bays concluded that more than

90% originated offshore in the Gulf of Maine (Hunt et al., 1999; Hydroqual, 2000). Consequently, oceanic input is by far the single largest source of organic materials and nutrients to the bays.

Non-oceanic sources include rivers, terrestrial runoff other than rivers (referred to as non-point sources), atmospheric deposition, and sewage outfalls (referred to as point sources). Point sources include both the MWRA outfall and non-MWRA outfalls. Among these non-oceanic sources, in 2013 the non-MWRA outfalls contributed most (32%) to organic carbon loading, followed by the MWRA outfall (21%), atmospheric deposition (18%), non-point sources (15%) and rivers (14%) (Figure 3.2). The MWRA outfall was the largest input (47%) to nitrogen loading, followed by atmospheric deposition (28%), non-MWRA outfalls (13%), non-point sources (8%), and rivers (4%). For phosphorus loading, the MWRA outfall again contributed the largest portion (48%), followed by non-MWRA outfalls (29%), non-point sources (15%), rivers (5%) and atmospheric deposition (3%). Note that for non-MWRA outfalls, use has been made of the only available dataset (Menzie et al., 1991), for which there are recognized limitations to applicability given that treatment levels at some non-MWRA outfalls have changed since that study. The relatively low runoff conditions in 2013 led to low loads (Figure 3.3). For both carbon and phosphorous, the MWRA outfall load in 2013 was lower than the average load from 2005 to 2012, and the 2nd lowest load in recent years (higher than only 2012). The MWRA outfall nitrogen load in 2013 was 2.2% higher that in 2012 and lower than many recent years.

3.1.3 UG-RCA open boundary

The open boundary condition (OBC) values for UG-RCA are determined using objective analysis (OA) on field survey observations from the MWRA monitoring program at the green, yellow, and black MB stations in Figure 3.4 (excluding those not sampled in 2013: N10, N16, and stations of the Alexandrium Rapid Response Study, denoted AF). Because they are representative of the annual cycle and have been examined in reports describing prior years, results for April 15 and August 15 are used to illustrate OBC fields (Figure 3.5; colorscale ranges are the same as in earlier reports for ease of comparison). As explained in Zhao et al. (2012), for dissolved organic carbon and biogenic silica (not shown), which are no longer being sampled, OBC values are from a seasonal cycle constructed by averaging observations from all prior years. Given the low frequency of field observations and large distance between the open boundary and observation sites, particularly for the South Passage, the OA-mapped results should be viewed with caution.

Chlorophyll concentrations in April were modest with peak values at the northern end of the boundary, while in August they were notably low across the entire boundary. The distribution of NO_3^- was similar in April and August, with peak values (about 6 mmol m^{-3} in April and >8 mmol m^{-3} in August) in the deep channel and reduced concentrations in shallower water, and a distinct nutricline at about 20-40 m in August. In April, NH_4^+ increased at depth to about 2 mmol m^{-3}, with a sharp vertical gradient at a depth of ~5-10 m in the south and north but ~30-40 m deep over the deeper region; in contrast, August NH_4^+ was much lower (<0.2 mmol m^{-3}) above 60 m on the mid- and northern boundary with a maximum of ~1.0-1.5 mmol m^{-3} around 20 m deep on the southern end. The dissolved oxygen (DO) concentration was higher on the northern end and decreased southward in both April and August, with maximum values at depth in the upper water column of ~11-12 mg L^{-1} in April and of ~8-9 mg L^{-1} in August, consistent with expectations based on patterns of inflow from the Western Maine Coastal Current (WMCC). Distributions of SiO_3^{2-} and PO_4^{3-} were similar in April and August and similar to each other: lower near the surface and increased with depth, with the larger vertical gradient in August than in April. Particulate organic carbon (POC) and nitrogen (PON) distributions were similar to each other, in April increasing toward the surface and slightly toward the north, then in August differing mainly in that near-surface values were lower, so the maxima were at mid-depth in the north. Dissolved organic carbon (DOC) in both April and August was relatively uniform and high (>100 mmol m^{-3}). Dissolved organic nitrogen (DON) was relatively uniform spatially (4-6 mmol m^{-3}) in April and August, with slightly higher values in April near the bottom in the north. The particulate organic phosphorous (POP) concentration in April had slightly higher (~0.15 mmol m^{-3}) concentrations in the upper 20 m and a subsurface minimum of ~0.05 mmol m^{-3} in a depth range of 40-60 m in the north, then in August levels were lower overall with a minima at the surface in the south. Dissolved organic phosphorous (DOP) changed from vertically banded concentrations peaking in the south during April to generally higher levels and horizontally banded structure with surface minima in August.

Interannual variability of OA-mapped OBC forcing is illustrated in Figure 3.6 using nitrate concentration in 2013, 2012, and 2011; the late January and early March dates are included, representing well-mixed and early stratified periods respectively, as in prior reports. Nitrate concentrations in 2013 were generally lower than in 2012 and 2011. The south-north distribution in 2013 was similar to that of 2011, lowest in the south and relatively uniform elsewhere, while in

contrast in 2012 there were stronger north-south and vertical gradients and peak values at depth in the north.

3.2 *Physical fields*

3.2.1 Model-observation comparisons

The physical circulation has strong influence on water quality, which is the focus of BEM, so performance of UG-RCA simulations depends on the capability of MB-FVCOM to capture realistic MB physical processes. For this reason, we have assimilated temperature and salinity observations into MB-FVCOM to increase the accuracy of physical fields. Assimilated observations included satellite-derived sea-surface temperature (SST), temperature and salinity profiles from MWRA monitoring surveys, and time series measurements from mooring A01 (Figure 3.4) operated by NERACOOS (Northeast Regional Association of Coastal Ocean Observing Systems).

Figure 3.7 shows comparisons between modeled and observed temperature and salinity at select MWRA monitoring stations spanning MB. Stations N01 and N07, located near the MWRA outfall, and station F22 to the northeast, are part of the “northern subset” (the six green stations in Figure 3.4) that appears grouped together in a number of later figures; stations F10, F06, and F13, to the south and near the coast, are in the “southern subset” (the six yellow stations in Figure 3.4) that appears grouped together in a number of later figures. In the station F22 panel of Figure 3.7, the green and pink lines are observations near the surface and bottom respectively from mooring A01 located (see Figure 3.4) about 5 km northeast from F22. Assimilation of SST and hydrographic cast measurements made the modeled temperature and salinity match the observations well. Nonetheless there was substantial temporal variabity in the model at the surface and bottom, which was not resolved by the approximately monthly MWRA field surveys.

The vertical stratification started to develop in April and peaked in July, with the largest surface-bottom temperature difference in mid-July reaching ~15°C. The water temperature became vertically well mixed again in late fall (around day 300) which remained true through the end of the year. We ran the model without assimilation of temperature and salinity observations, to test its importance; as expected the simulation accuracy was degraded at short timescales but gross features of seasonal variability in vertical stratification of temperature and salinity were still captured, confirming that vertical mixing is performing adequately in the model.

The largest vertical gradient of salinity (salinity is given in units on the Practical Salinity Scale throughout this report) was a surface-bottom difference of ~2, which occurred in late May, later than typical climatologically. (For ease of comparison the range of the vertical axis scale of salinity plots in Figure 3.7 is the same as in reports describing prior years, when salinities reached lower values than occurred in 2013.) This timing was consistent with the river discharge record (Figure 3.1), which showed multiple freshwater discharge peaks occurring in late spring through summer of 2013. The seasonal variability of surface salinity was similar at all stations and the bottom salinity did not show substantial seasonality, suggesting that the response to these wet summer conditions had a bay-wide scale and was surface intensified.

Figure 3.8 and Figure 3.9 show model-observation comparisons for spatial structure of near-surface temperature and salinity in select months of 2013. The observed fields in these figures are computed using measurements from all stations (black dots) sampled during each month-long period. For most months there was one one-day survey in MB; BH stations are sampled weekly or biweekly. The model fields in these figures are computed using model outputs from the dates and locations corresponding to the associated set of observations.

The assimilation worked well to reproduce observed fields of temperature and salinity. In February, observed temperature was relatively higher offshore and decreased onshore, with an offshore-onshore difference of ~1.2°C. The model temperatures were similar except in and near BH where they were about 0.1-0.2°C higher, a result attributed to uncertainty in the assimilated satellite-derived SST. February observed and modeled salinity distributions were similar, increasing by up to ~2 offshore relative to onshore. In April, model conditions were very similar to the observations in all respects, including higher temperatures everywhere, and broad offshore-onshore gradients with warming and freshening onshore more so than offshore. In June after further warming the observed offshore-onshore gradients remained as in April, observed salinities showed the freshened area extending farther offshore, and agreement of the model fields with observation was again very strong except for slightly lower temperatures in and near BH. In August the model captured all features of the observations reasonably well: temperatures fell onshore, particularly in a narrow area along the northern coast, while the spatial structure of salinities remained the same but with increases offshore. Finally, in October the spatial patterns were generally similar to August and except for a lower range of temperatures the model conditions agreed well with observations.

3.2.2 Model monthly-mean surface circulation, temperature, and salinity

The monthly-averaged surface circulation from January through April (Figure 3.10) was characterized by two major features:

(1) Offshore, an extension of the WMCC flowing south-southeastward from the Western GoM Coast across Stellwagen Bank toward the offshore side of Cape Cod, which was well-defined in January, most intensified in February, weaker in March, and weaker and farther offshore in April;

(2) A current that bifurcates at the North Passage entrance, with one branch departing from the south-southeastward flow and entering MB southwestward. Water entering MB remained close to the coast and affected the onshore coastal region while moving southward, then turned in a counterclockwise direction and moved offshore eastward to rejoin the south-southeastward WMCC extension flow in the northeastern CCB region. In March, this onshore current was stronger than in January and February, and a separate cyclonic circulation formed mid-bay. In April the onshore flow and bay-wide cyclonic flow merged and were nearly as strong as in March. Winter and spring conditions were therefore influenced strongly by WMCC inflow to MB along the northern boundary.

Circulation was substantially different during May through August (Figure 3.11), a period of weak and southerly winds (Figure 3.1). The inflow to MB along the northern boundary was essentially absent during these months. The south-southeastward flow was re-established offshore during May and June, then very weak or absent in July and August. In May and June a weak partial anticyclonic eddy formed in the northern coastal region offshore from and south of Cape Ann, there was southward flow in most of MB, and CCB had a diffuse flow generally parallel to the inner Cape Cod coastline that ultimately fed a narrow eastward current just north of Cape Cod that joined the southwestward offshore flow. In July and August a single cyclonic eddy occupied most of Northern MB outside of BH, with flow on its southern side in central and southern MB directed offshore, while in CCB currents were diffuse and weaker.

In September and October (Figure 3.12) currents remained weak with several smaller eddies throughout the region. In November and December the south-southeastward flow was re-established offshore, though of modest strength and influenced by multiple eddies, and most of MB had generally southward currents leading into CCB where flow was weakly eastward. The onshore flow from the WMCC entering MB at its northern boundary did not occur during these months.

To examine the seasonal variability of water properties, we present the model surface temperature (Figure 3.13) and salinity (Figure 3.14) fields at the end of each month. Recall that the time series of surface and bottom temperatures and salinities (Figure 3.7) indicated that the water was seasonally stratified in MB; the end-of-month surface fields reveal more complete spatial structure. During February to March, temperatures were colder onshore, particularly in western CCB, with onshore-offshore differences of up to 6°C. April and May temperatures were more uniform, varying by less than about 2°C across the domain. In June, July, and August, the spatial structure of temperature was reversed compared to winter months, with values increasing onshore and southward, and peak values in western CCB. In September a relatively weak north-south gradient persisted and then during seasonal cooling of October through December temperatures were quite uniform across the domain.

The salinity distribution (Figure 3.14) in January through April showed variability attributable as responses to river discharge (e.g. Figure 3.1). In January low salinities occurred along the inner shelf of the northwestern Gulf of Maine including where the Merrimack River enters, and in February they had expanded to the entire shelf region with areas farther south in MB increasingly freshened as well. In March the freshening influence expanded in northern MB where salinities were about 29-30. In April most of the GoM region was substantially freshened including as far south as offshore of MB. In May through August, the unusually wet conditions led to salinities of 29-30 across nearly the entire region. In September through December eastward and southeastward winds become dominant, saltier water was pushed onshore by the associated onshore Ekman transport, and the low-salinity area shrank. In MB the salinities in September had a complex spatial structure, then were higher and relatively uniform spatially in October, before an offshore-onshore gradient was established in November and December with freshest water in a narrow band along the northern and western shores.

3.2.3 Comparison with simulations of previous years

The monthly-mean surface current, temperature, and salinity at the end of April and September were selected as examples to illustrate inter-annual variations by comparing 2013 with 2012 (Figure 3.15 and Figure 3.16). In April (Figure 3.15, upper panels), the 2013 conditions had inflow to MB along the northern shore that was similar to that of 2012, and an alongshore southward flow in the central MB region that was stronger than in 2012, but the southwestward current in the

offshore area between Cape Ann and Cape Cod was much weaker in 2013 compared to 2012. In September (Figure 3.15, lower panels), the 2013 conditions included modestly strong counter-rotating eddies within MB and a modest southwestward current offshore from it, while in 2012 there was a single eddy and a much weaker southwestward current offshore. Surface temperatures in 2013 were considerably colder than in 2012 in both April and September (Figure 3.16), although the months prior to April and to September (not shown) were considerably warmer in 2013 than in a typical year. The temperature was more spatially uniform in September 2013 than September 2012. April and September salinities in 2013 were quite similar to those in 2012, although the months between April and September 2013 were much wetter than the same period in 2012, as described above.

3.3 *Water quality fields*

3.3.1 Model fields including comparisons to observations

Model-observation correlation and regression analyses of key variables—including surface chlorophyll, NO_3^-, SiO_3^{2-}, NH_4^+, and bottom DO concentration (mg L^{-1}) and DO saturation (%) — are presented in Figure 3.17 from all stations outside BH (the northern and southern subsets of stations, and black stations in Figure 3.4, excluding those not sampled in 2013: N10, N16, and stations of the Alexandrium Rapid Response Study, denoted AF). There is no meaningful correlation for near-surface chlorophyll or for silicate. The model greatly underestimates the chlorophyll when its concentration is higher than about 2 μg L^{-1}. For NO_3^- near the surface, high observed values tended to be associated with high modeled values, but there is a high degree of scatter in model results corresponding to lower NO_3^- values. Overall the model tended to overestimate the corresponding nitrate values, although the range of values is similar between model and data. The correlation coefficient was 0.91 for surface nitrate. For near-surface ammonium, there is no clear relationship at higher concentrations, and the model tended to exceed observations toward the low end of the concentration range. A better-defined model-data relationship is seen for DO, including a correlation coefficient of 0.95 for bottom DO. The DO saturation was not directly modeled, rather it was calculated based on temperature, salinity and DO concentration; biases in the simulation of these different parameters could all influence the accuracy of DO saturation estimates.

The remainder of this section describes the 2013 annual progressions of key model variables, including plots that facilitate visual comparisons to observations. Many individual figures show results from subsets of all stations in each of three geographic domains (as shown in Figure 3.4): "northern subset" (F22, N04, N01, N18, Outfall/N21, and N07), "southern subset" (F15, F13, F10, F06, F29, and F01), and "harbor subset" (024, 139, 140, 142, 124, and F23).

3.3.1.1 Chlorophyll

Model chlorophyll showed less variation over the year than observations, and less surface-bottom difference (Figure 3.18 to Figure 3.20). There was a springtime increase in chlorophyll in the model, although it was later and less abrupt than spring blooms typical of past years, and did not capture particularly well the unusually low observed levels in 2013. It is interesting to note that modeled chlorophyll in bottom waters never reaches the very low levels seen in summer field measurements, generally remaining above 1 µg L^{-1} throughout the study area all year. We checked vertical mixing of temperature and salinity in the model, and confirmed that the observed stratification in late spring through early fall was properly captured, which implies the small vertical gradient in modeled chlorophyll originates in biological rather than physical processes.

The vertical distribution of 2013 model chlorophyll along a west-east transect (line, upper frame of Figure 3.4) across the outfall to the model boundary is shown in Figure 3.21. There were significant variations from month to month. In January, mixing kept chlorophyll relatively uniform vertically, with moderate levels (~2-3 µg L^{-1}) onshore, lower levels (< 1 µg L^{-1}) in the deep central region, and peaks of > 3 µg/l near the open boundary offshore. In February, levels were ~1 µg/l or less from the middle of the transect shoreward, and moderate offshore. In March, the lower layer in the deep region and offshore areas were depleted, and an isolated relatively high concentration core appeared in the upper 20 m in the deep region. This subsurface maximum increased to > 4 µg L^{-1} and shifted slightly offshore in April, when levels increased over the entire transect due to rapid phytoplankton growth. In May with the onset of stratification, the transition was underway towards mainly vertical structure, with concentrations more uniform horizontally than vertically and decreasing with depth. June exemplified this horizontally layered structure with near-surface levels of 2-3 µg L^{-1} overlying levels of 0-1 µg L^{-1} throughout nearly the entire transect. In July there was little vertical gradient but it returned in August and September when conditions were more like June. In October through December levels were generally lower with spatial structure consisting mainly of a vertical gradient with higher near-surface values.

3.3.1.2 Dissolved inorganic nitrogen

Modeled and observed dissolved inorganic nitrogen (DIN) showed typical seasonal variation near the surface and bottom at most of the monitoring stations (Figure 3.22 to Figure 3.24). DIN was generally depleted in surface waters during March and April due to consumption by phytoplankton, remained at low levels in summer through early fall, and was then replenished in late fall and winter by vertical mixing. In contrast to surface waters, DIN in the bottom layer stayed at a relatively high level through the summer and fall seasons; a vertical gradient in DIN concentration occurred in the model and observations at most of the monitoring stations. At the outfall (N21) during three springtime surveys observed DIN levels were highest near the surface, in contrast to other stations (Figure 3.22). The simulation did not capture this feature, which is likely associated with the details of circulation within the zone of initial dilution (e.g. Blumberg et al., 1996), and if so would not be expected to be represented particularly well in the model.

At some stations the model underestimated the observed DIN concentration in the bottom layer (Figure 3.22, Figure 3.23). For example, observed summer DIN reached up to 7 μM in bottom waters at western MB stations F06 and F13, in water depths of about 32 m and 28 m respectively. Near-bottom depths at these stations are below the euphotic zone, i.e., nutrient uptake by phytoplankton does not occur. It is possible the model underestimation of DIN at depth there is due to local nutrient sources not captured well by the model, such as groundwater sources (Becker, 1992, Jiang et al. 2007) which the model bases on historical estimates without inclusion of geographic variations.

At most BH stations, including F23 at the harbor mouth, the magnitudes and seasonal cycles of DIN in the model were similar to observations (Figure 3.24). Nutrient depletion affected the full water column and vertical gradients were small. Simulated near-bottom DIN concentrations were higher at stations 024 and 124, at the inner harbor mouth and in southeastern BH in Hingham Bay respectively, a vertical gradient that was not seen in observations.

In end-of-month snapshots on the west-east transect across the outfall (Figure 3.25), the DIN signature of the outfall plume was concentrated at depth throughout the year with December the only exception. Near-surface DIN was lowest from March to September as expected in association with stratification, and higher during the generally higher mixing levels in other months.

3.3.1.3 Primary productivity

Primary productivity in the 2013 model run is shown in Figure 3.26 at three monitoring stations (F23 at the mouth of BH; N04 to the northeast of the outfall; and N18 nearest to the outfall) where observations of primary productivity had been made in past years. Ongoing field sampling no longer includes primary productivity measurements, but for context the observations from 1995-2010 (a review of the field results is included as part of Keay et al 2012; methods are described in Appendix C of Libby et al., 2005) are superimposed as box-whisker plots on the model outputs. The box-whisker plots consist of a box with the 25th and 75th percentiles at its lower and upper bounds and a horizontal line bisecting the box at the median, with whiskers that extend to the 9th and 91st percentiles. Instead of peaks for spring and fall blooms as typify many other years, in 2013 primary productivity in the model increased in late spring then remained high with fluctuations on several-day timescales through mid to late summer when it decreased and then rose again briefly in early fall before tapering off to low winter levels again.

3.3.1.4 Dissolved and particulate organic nitrogen

Seasonal variations of DON (Figure 3.27, Figure 3.28) were weaker in the model than observed. (There were no observations of DON, or of PON which is discussed below, at F29 or F01 in 2013.) Model DON along the west-east transect (Figure 3.29) was relatively uniform vertically and slightly higher from January to April, and in December, compared to other months.

Model PON values were moderate from spring through late summer and again for a short period in fall, with low values during winter (Figure 3.30, Figure 3.31). Near-surface PON in the model generally agreed with observations but near-bottom model PON overestimated observations so the model did not capture the observed vertical structure of PON well. Model PON along the west-east transect (Figure 3.32) was highest and generally surface-intensified in April through June, lowest and generally spatially uniform from November to March, and intermediate from July to October.

In summary, model-observation agreement was modest for DON and PON. In both model and observations, there was no anomalous signal near the outfall in either DON or PON, showing that the organic nitrogen pools were essentially controlled by internal dynamics within the water column and not detectably altered by outfall effluent.

3.3.1.5 Particulate organic carbon

Model-observation agreement was weak for seasonal variations and vertical distributions of POC (Figure 3.33 and Figure 3.34; there were no POC observations at F29 or F01 in 2013). Observed seasonal variations in surface POC differed from site to site. In contrast, seasonal variations in model POC were generally the same across all sites and displayed two dominant events, an extended increase through late spring and a weaker, shorter one in early fall. Observed deep POC varied little seasonally but was generally substantially lower than surface values. In contrast, model deep POC had seasonal variations parallel to those of model surface POC, and was higher than surface POC during most of the year. Because seasonal variations in stratification are captured by the model, as described above, these biases in vertical structure of model POC are apparently due to parameterization of biogeochemical processes in RCA.

Model POC on the west-east transect (Figure 3.35) was relatively low in January to March and intermediate in April and June through August, had elevated levels in September through December, and peaked in May. Peak values generally occurred at the offshore eastern end of the transect at mid-depth, and the spatial structure generally included a vertical gradient with higher values at or just below the surface.

3.3.1.6 Dissolved oxygen

Fairly good agreement was found between simulated and observed DO (Figure 3.36 and Figure 3.37). The seasonal cycle (peak in spring, decrease through summer to minimum in late fall, then increase) was reproduced by the model reasonably well. The model had a noticeable bias toward underestimation at both the surface and bottom, compared to observations. As noted above (Figure 3.17) the correlation between modeled and observed DO concentrations was 0.95 near the bottom, with root-mean square (RMS) error of 0.59 mg L^{-1}.

The spring maximum and fall minimum concentrations averaged across 12 stations (northern subset, Figure 3.36; and southern subset, Figure 3.37) were 11.53±0.91 mg L^{-1} and 7.79±0.73 mg L^{-1} near the surface and 11.07±1.03 mg L^{-1} and 6.71±0.77 mg L^{-1} near the bottom. Corresponding model values were 10.57±0.46 mg L^{-1} and 6.98±1.46 mg L^{-1} near the surface and 10.88±2.58 mg L^{-1} and 6.72±0.24 mg L^{-1} near the bottom. The observation-model difference was 0.96±1.05 mg L^{-1} at the surface and 0.19±2.87 mg L^{-1} at the bottom during the spring peak and 0.80±1.77 mg L^{-1} at the surface and -0.02±0.70 mg L^{-1} at the bottom during the fall minima. This level of model-observation difference is similar in magnitude to previous years.

Model DO on the west-east transect (Figure 3.38**)** showed the same general patterns as those found in previous years. Concentrations are highest in spring and lowest in late summer, with values near the surface generally higher than near the bottom.

Xue et al. (2014) investigated mechanisms controlling DO and concluded that a dominant factor is reaeration, or air-sea interaction, as governed partly by vertical mixing and partly by DO over/under-saturation. DO saturation depends on temperature and salinity as well as oxygen concentration, and is a useful quantity to help understand the relative influence of temperature and photosynthesis on DO; percent saturation above 100% can result from photosynthetic production. We computed DO saturation from observations of DO concentration, temperature, and salinity using the approximate relation given in equation 2.3 of Zhao et al. (2012). Comparisons between this result and modeled DO saturation (Figure 3.39 to Figure 3.41) reveal reasonable agreement between model and observations, and a similar pattern at most MB stations. In winter, DO saturation levels are modest and vertical mixing keeps them nearly vertically uniform; in spring, photosynthesis increases surface values, which reach a maximum in early summer. Then both surface and deep values both gradually decrease through late fall or early winter, when they are homogenized again. The model underestimated the saturation value at most stations in 2013, similarly to simulations from earlier years, which could indicate that photosynthetic oxygen production is underestimated by the model.

For most stations in BH, observed DO saturation (Figure 3.41) varied relatively weakly seasonally and vertically, compared to MB. Model DO saturation in BH was consistent with this variability at most stations, with the exception of 024 and 124 where the model DO saturation was more similar to that in MB. Model DO saturation along the west-east transect (Figure 3.42) was most uniform vertically in November through February, in other months was mostly horizontally uniform with a gradient from high values at the surface to lower values at depth, and took peak values near the surface in March through July.

3.3.1.7 Sediment fluxes

Sediment NH_4^+ fluxes and sediment oxygen demand (SOD) from the 2013 simulation are shown in Figure 3.43 and Figure 3.44 at BH and MB stations (Figure 3.4; BH02, BH03, BH08A, MB01, MB03 and MB05) where flux measurements had been made in earlier years. Ongoing field sampling no longer includes benthic fluxes, but to provide context the observations from 2000-

2010 (the field program and its results are described in MWRA technical reports, for example Tucker et al., 2010) are superimposed as box-whisker plots (as described in Section 3.3.1.3) on the model results. Observations from prior to 2001 were not included, because diversion of the outfall to its current location occurred in 2000. At BH stations the model NH_4^+ flux was nearly zero except during about 5 months centered on summertime, and systematically lower than the range of observed values. At MB stations it was nearly zero except between May and December, and had values within the range of prior observations although with notable bias lower than them at MB05. At BH stations the model SOD had seasonality, and low bias relative to observations, similar to the NH_4^+ flux there. At MB stations, model SOD had similar seasonality to the NH_4^+ flux there, and values on the lower end of the range of observations.

3.3.1.8 Summary

In summary, the UG-RCA 2013 simulation captured many of the observed seasonal and vertical variations of an array of key parameters examined here. Among them, agreement of the model with observations was generally strongest for DIN and DO, modest for DON, and PON, and poor for DOC. There was an increase, though weak, in springtime chlorophyll in the model despite that observed 2013 levels were unusually low. Other notable differences of model fields with observations included underestimation of fall chlorophyll concentrations and overestimation of bottom POC. The model typically does not capture the extremes of observed values, and at most stations it has smaller surface-bottom differences than are observed.

3.3.2 Comparison with previous years' simulations

We now compare UG-RCA simulations for 2011, 2012 and 2013 in order to provide context for inter-annual variability in the model. Overall, as noted above the 2013 chlorophyll simulation had a clear spring increase, though of weaker magnitude and appearing later compared to a typical observed bloom, and a weak fall increase (Figure 3.45). In contrast, the warm winter in 2012 led to an early spring bloom, and the fall peaks in 2011 were markedly larger than in 2012 and 2013.

The DIN seasonal cycle was generally similar among the three years, with high values in winter, low values in summer and replenishment in late fall (Figure 3.46). In 2013 the winter peak in January was particularly high, then levels dropped to normal or lower than normal in February, before remaining there unusually long through March and April before being depleted. The longer persistence of high concentrations through April is consistent with the weak spring bloom.

For bottom DO concentration (Figure 3.47) and bottom DO saturation (Figure 3.48), differences among the three years were minor. In all three years, high values occurred during springtime and low values occurred in late summer and early fall. The pattern in 2013 was very similar to that of 2012 in January through October and very similar to that of 2011 in November and December.

4. Scenario experiments

This section describes a series of scenario experiments designed to assess the potential influence of the MWRA outfall on MB water quality and ecosystem function during 2013. The first experiment is the same as in prior MWRA modeling reports, a comparison of simulations without and with MWRA outfall nutrient load. Next, an analysis is made of those results together with additional simulations in which the nutrient load from the MWRA outfall is increased by 10% and 100% relative to the maximal-realism simulation described in prior sections.

4.1 *Scenario without MWRA outfall nutrient load*

We refer to the simulation of current conditions described in prior sections, with the MWRA outfall nutrient load included, as the "control" and to the simulation without the MWRA outfall nutrient load as the "non-sewage" run. We compared the chlorophyll, DIN, DO, and NH_4 fields in the two simulations. The control and non-sewage simulations had nearly identical intensities and seasonal variations of chlorophyll concentration (Figure 4.1). The seasonal cycle of surface DIN was also very similar in the two simulations (Figure 4.2); in summer they were almost identical while in winter the non-sewage case had lower surface DIN concentration than the control. In bottom DIN (Figure 4.3) the non-sewage case was notably lower than the control at stations near the outfall, and very similar at other stations. This result is consistent with field measurements that show elevated levels of DIN near the outfall (e.g., Libby et al., 2014). The DO results (Figure 4.4 and Figure 4.5) were practically identical for the two simulations.

These results for 2013 are consistent with prior non-sewage scenario runs (HydroQual 1995; Jiang and Zhou 2006b; Tian et al. 2009; Chen et al. 2010; Tian et al. 2010, Zhao et al. 2011, 2012, 2015). They are also in keeping with the conclusion drawn by MWRA, based on comparing field observations between pre-diversion (prior to relocation of the outfall to MB from BH) and post-diversion periods, that effects of the outfall are confined to within about 10-20 km and consist

mainly of elevated ammonium levels there. While the outfall influences nutrients in its immediate vicinity, it does not have a notable influence on system-wide nutrients, chlorophyll, or DO.

To investigate the extent of the difference in ammonium—the most abundant form of nitrogen in the outfall discharge— between the two runs, we plotted the spatial distribution of the difference between bottom-layer ammonium in the control and non-sewage cases at the end of each month (Figure 4.6). Generally, as in past years, the bottom ammonium difference (Figure 4.6) was perceptibly higher in summer months than in winter months, as expected due to effluent trapping by summer stratification. Also, as in past years, months when dispersal of the plume extended larger distances southward toward CCB occurred in winter, for example January. This dispersion has been previously shown (Fitzpatrick and Isleib, 2003) to be insensitive to the location of the outfall in BH, where it was prior to 2000, as compared to its current location in MB. These results are also consistent with nitrogen stable isotope studies (Tucker et al. 1999; Tucker and Giblin 2002; Montoya et al., 2003) which show the effects of sewage derived nitrogen on the food web confined to areas relatively near the outfall in summer, but as far away as the northern edge of CCB in winter months.

We also plotted the ammonium difference (Figure 4.7) at the end of each month along the west-east transect through the outfall (line in the December frame of Figure 4.6). The height of the effluent plume, as inferred from the ammonium concentration, varied from month to month and was confined vertically by stratification more so in summer than winter, as expected. The plume was mostly restricted to the bottom 10 m or so from January to September. Only in October, November and December, the well mixed season, did the plume reach the surface in the coastal region. These results are in approximate agreement with the rise height of 5-15 m predicted by Blumberg et al. (1996) using nearfield and farfield models. The depth of the plume changes as it spreads. It surfaced during weak stratification, suggesting that its upward spread is controlled mainly by vertical mixing. In these end-of-month snapshots, the plume did not extend as near to the surface in winter as it did in simulations of some past years.

To summarize, the no-outfall scenario simulation for 2013 indicated similar results as in prior years. The outfall plume influence consists almost entirely of increased NH_4 concentrations, typically remains within about 10-20 km of the outfall, and is concentrated in the deeper part of the water column except in winter. Dispersal of the plume can occur over longer horizontal distances during winter, but both light and vertical mixing are unfavorable to phytoplankton growth at that

time. Consequently, the conclusion that there are no important influences of the outfall on ecosystem function (e.g., biomass, DO distributions) is supported.

4.2 *Scenarios with hypothetically increased MWRA outfall nutrient loads*

To investigate how the bays respond to hypothetically increased nutrient loading from the MWRA outfall, two additional simulations were carried out. In these simulations, the nutrient concentrations (NH_4^+, NO_2^-, NO_3^-, and PO_4^{3-}) in the MWRA outfall effluent were increased, relative to the control run, by 10% and 100% respectively. The 10% increase scenario has practical relevance as an approximate upper bound of the effect of a new program for co-digestion of engineered food waste under consideration by MWRA at its Deer Island treatment plant; estimates of the increase to the nutrient load at the outfall are roughly 5%, if the program is implemented. The 100% increase (doubling) scenario is intended solely to help explore the sensitivity of the system, and is a hypothetical extreme case. The non-sewage, control, 10%-increase load, and 100%-increase load runs are referred to as the 0X, 1X, 1.1X, and 2X simulations.

Graphical comparisons of the 1.1X and 1X simulations were made by differencing their 2013 end-of-month concentrations of NH_4^+, which as explained above is the property most likely to reveal changes. From May to October, an increase in near-bottom differences of up to ~1 mmol m^{-3} occurred in an very small area local to the outfall, while during winter months (Figure 4.8) increases were appreciably less than ~1 mmol m^{-3} everywhere. The vertical structure of these differences (Figure 4.9) revealed that they extended at most about 15 m off the seafloor. It can be concluded that the 1.1X case results in insignificant changes to NH_4^+, the most sensitive aspect of the system, and thus that potential effects on ecosystem function will be difficult to discern.

To examine the difference between the 2X and 1X simulations, the same pair of NH_4^+ concentration difference plots was made (Figure 4.10 and Figure 4.11). In this case, the signature of the outfall effluent is readily discernable. The geographic and vertical structure of the NH_4^+ concentration differences between 2X and 1X, and their month to month variations, are strikingly similar to the differences between 1X and 0X shown earlier in Figure 4.6 and Figure 4.7. This is indicative that the response of the system to nutrient loading from the MWRA outfall, with respect to NH_4^+ distributions, is largely linear for loads in the range 0X to 2X relative to the control run. In other words, the increase or decrease in NH_4 concentrations, relative to the control run, that results

from an increase or decrease to MWRA outfall nutrient load is nearly linearly proportional to the amount of the load change relative to that of the control run.

Next we use comparisons of timeseries model ouput at select stations, from the 1X, 1.1X, and 2X cases, to assess other aspects of the system response: surface DIN, bottom DIN, surface chlorophyll, and DO. For surface DIN (Figure 4.12) and bottom DIN (Figure 4.13) the results are similar in structure to those for NH_4^+ described above, as expected given that DIN is dominated by NH_4^+. In surface DIN the differences between 1.1X and 1X are very minor at all stations, and the differences between 2X and 1X are very minor at stations far from the outfall; for stations near the outfall, the 2X case shows increases of up to 2-3 mmol m^{-3} during September to December. In bottom DIN the 1.1X case shows small differences (less than 2-3 mmol m^{-3}) from 1X, most often at stations near the outfall, and only for parts of the year. For the bottom DIN 2X case, relative to 1X, the responses vary from increases of less than about 2 mmol m^{-3} during short temporary periods, at the more distant stations, to levels elevated year round by as much as 15-20 mmol m^{-3} at stations nearer the outfall.

Surface chlorophyll (Figure 4.14) and bottom DO (Figure 4.15) remained almost identical for the three cases. The maximum difference in surface chlorophyll among the 1X, 1.1X, and 2X cases was at these stations was 0.067 µg l^{-1} (about 6.3%). The maximum difference among them in bottom DO was 0.037 mg l^{-1}, about 0.45% relative to the annual mean DO value. This latter result was consistent with our previous findings (Xue et al., 2014) that the total net DO flux was mainly controlled by reaeration, while other biogeochemical processes offset each other.

A summary of the scenario simulation results (Table 1.1) for surface chlorophyll, surface DIN, bottom DIN, bottom DO concentration, and surface DO saturation from the 0X, 1X, 1.1X, and 2X cases at three representative stations (near-outfall, central western MB, and CCB), averaged over the month of August, helps quantify these results during the stratified period. The magnitude of the percent changes relative to 1X reaches a maximum (for 0X and 2X) of about 7% for surface chlorophyll, 9% for surface DIN, 53% for bottom DIN, 0.25% for bottom DO concentration, and 0.35% for surface DO saturation. Comparing the percent change values from the 0X and 2X cases in the table underscores that the reponse of these variables, for this range of nutrient loads (from 0 to 2X relative to the control run), is nearly linear. That is, the percent change values for 0X and 2X for a given station and parameter are roughly equal in magnitude and opposite in sign. Chlorophyll levels increase/decrease with increased/decreased nutrient load, as expected, and the magnitude of

the response is similar at the three stations. The magnitude of percent change in surface and bottom DIN decreases between the near-outfall and CCB stations, from ~9% to ~2% in surface DIN and ~53% to ~5% in bottom DIN. Surface and bottom DIN generally increase/decrease with increased/decreased nutrient load, as expected.

A secondary aspect of Table 1.1 is the very weak, but systematic, geographic pattern of increasing percent change magnitudes for surface chlorophyll, bottom DO concentration, and surface DO saturation from the near-outfall station through the west-central MB station to the CCB station. A plausible explanation is that changes to productivity are enhanced southward, which is downstream with respect to advection by prevailing currents, because phytoplankton require time to grow in response to the elevated nutrients. This rationale is most applicable to surface chlorophyll and surface DO saturation, although sub-pycnocline production must be important for it to also explain the positive sense of the bottom DO concentration changes with distance southward. Another secondary aspect of the results is an exception, at the surface at the CCB station, to the general pattern of DIN changes having the same sense as load changes. At the CCB station only, for surface DIN only, the response is weak but has the opposite sign from the load (i.e., DIN decreases/increases occur for increased/decreased load). This minor aspect of the response is not fully understood but it is considered to be an anomaly during the month of August (recall, the Table shows August-mean results only), because when averaged over the entire year the sense of the surface DIN response at the CCB station is the same as that of the load and thus consistent with the other stations.

It it interesting to note that the results of the 2X case are broadly similar to similar projections modeled for the offshore outfall by Hunt et al. (1999). That report evaluated 0X, 1X, and 2X projections for primary effluent loads discharged at the old harbor outfalls and at the offshore outfall that was then under construction. The report concluded that, even for the extreme 2X projection, impacts to water quality would be small on a bays-wide scale and concentrated in the vicinity of the discharge (Hunt et al. 1999).

In summary, the main findings from the changed nutrient load scenario experiments are that ecosystem function is relatively insensitive to variations in MWRA outfall nutrient loads, and that the system responds nearly linearly. For minor changes to outfall load (1.1X case) the changes relative to the control run are at most modest (~5% increase in DIN local to the outfall and very near the seafloor) and essentially indetectable for all other variables including chlorophyll and DO.

Even for the hypothetical upper bound of doubling the outfall load, while DIN increases notably relative to the control run near the outfall (53%) and modestly at the west-central MB and CCB stations (a maximum of 16% and 5% respectively), chlorophyll increases only by at most 7% and DO changes by less than 0.5%. These results support the conclusion that, for feasible ranges of changes to MWRA outfall nutrient loads (for example, up to the maximum 10% increase that could result from a new co-digestion program at the Deer Island Treatment Plant), effects on marine water quality will be very minor.

5. Summary

The UMass Dartmouth Marine Ecosystem Dynamic Modeling laboratory simulated hydrodynamic and water quality parameters for calendar year 2013 in the bays using the unstructured grid model MB-FVCOM/UG-RCA. The methods were as in the prior year's simulation (described in Zhao et al., 2015).

The hydrodynamic model reproduced the main features in observations of temperature and salinity and captured tidal and subtidal currents. The modeled seasonal cycle of stratification agreed well with observations.

The water quality simulation captured general patterns in seasonal variations and vertical structure of many observed fields. In general the model showed a smaller range of values, and smaller surface-bottom differences during the stratified season, when compared to observations. Well-known observed features in the seasonal cycle and vertical structure of DIN were evidenced by the model, namely the spring/summer reduction in shallow concentrations due to phytoplankton uptake and later fall replenishment due to enhanced mixing when stratification breaks down. However, modeled chlorophyll showed a springtime increase, though weaker than a typical spring bloom, which was not consistent with the low observed 2013 levels. The model did however capture the gross features of the seasonal cycle of DO, with peaks in spring when shallow values increase due to phytoplankton growth, continuous decreases through summer and early fall, and replenishment during the winter mixed period. Model DON and PON showed modest agreement with observations, while model POC did not capture well the seasonal variations nor the vertical structure of observations due mainly to a high bias at depth. In summary, model-observation agreement was generally strongest for DIN and DO, modest for DON and PON, and poor for POC.

In order to assess the potential influence of the MWRA outfall on MB system-wide ecosystem function, results of the maximal-realism simulation were compared to a scenario simulation in

which effluent from the MWRA outfall was removed. In 2013, as in simulations of previous years, the influence of the effluent was demonstrated to be confined to within about 10-20 km of the outfall, and to consist mainly of increased ammonium concentrations there. In summer the influence was more confined to the deeper water column, and minimally dispersed horizontally, in association with stronger stratification and weaker circulation due to reduced winds. Conversely the enhanced vertical mixing and stronger currents during the more windy unstratified winter conditions led the signature of the effluent to extend nearer to the surface, and be dispersed over longer ranges. However, the low light availability and low temperatures during winter mean phytoplankton growth, the most likely system attribute to potentially respond to elevated ammonium levels, remained weak. Consequently the effluent had no important effect on system-wide ecosystem functionality such as phytoplankton growth or oxygen levels.

Additional scenario simulations were completed to investigate the potential influence of hypothetical increased nutrient loads from the MWRA outfall in MB. These runs had nutrient concentrations (ammonium, nitrite, nitrate, and phosphate) in the MWRA effluent that were scaled up by 10% and 100% (doubled) relative to measured effluent concentrations. The 10% increase simulation is a conservative upper bound for estimates of the effect that a new co-digestion program under consideration for the Deer Island Treatment Plant could have on outfall nutrient load, if it were to be implemented. The 100% increase simulation is a hypothetical extreme to learn about the upper bound of potential influences. The response of the system to the 10% increase was most pronounced in DIN, for which there was a modest increase local to the outfall and near to the seafloor, but the effect on chlorophyll and DO was essentially imperceptible. The response of the system to the 100% increase was clearly detectable and resulted in substantially higher DIN (~53%) local to the outfall, modest increases (~7%) to chlorophyll, and changes of less than 0.5% in DO. Relative to the maximal-realism case, the effects of the 100% increase (doubling) were generally about equal in magnitude and opposite in sense to those of removing the outfall effluent from the simulation. This indicates that, for nutrient loads between 0 and 2 times the current load, the system is responding nearly linearly. The main conclusion is that for feasible levels of changes to nutrient loads (e.g., a 10% increase), the parameters that will be influenced (such as DIN) will respond nearly linearly and the effects on ecosystem function and water quality will be very minor.

6. References

Becker S. 1992. The seasonal distribution of nutrients in Massachusetts and Cape Cod Bays. Masters Thesis, University of New Hampshire, Durham. 127pp.

Blumberg A., Ji Z. and Ziegler C.K., 1996, Modeling outfall plume behavior using a far field model, *J. Hydraulic Engineering*, 112: 610-616.

Chen C., Tian R., Beardsley R.C., Qi J. and Xu Q. 2010. Modeling 2008 in Massachusetts Bay using an upgraded unstructured-grid Bays Eutrophication Model. Boston: Massachusetts Water Resources Authority. Report 2010-15. 127pp.

Fitzpatrick J.J. and Isleib, R.A., 2003. Post-audit analysis of the impacts of wastewater treatment plant outfall relocation on Boston Harbor, Massachusetts Bay and Cape Cod Bay water quality Proceedings of the Water Environment Federation, WEFTEC 2003, pp. 530-555.

Hunt C.D., Kropp R.K., Fitzpatrick J.J., Yodzis P., and Ulanowicz R.E**.** 1999**.** A Review of Issues Related to the Development of a Food Web Model for Important Prey of Endangered Species in Massachusetts and Cape Cod Bays. Boston: Massachusetts Water Resources Authority. Report ENQUAD 99-14. 62 pp.

HydroQual, 1995. A water quality model for Massachusetts and Cape Cod Bays: Calibration of the Bay Eutrophication Model (BEM). Boston: Massachusetts Water Resources Authority. Report 1995-08. 402pp.

HydroQual, 2000. Bays Eutrophication Model (BEM): modeling analysis for the period 1992-1994. Boston: Massachusetts Water Resources Authority. Report 2000-02. 158pp.

HydroQual, 2004. “User’s Guide for RCA, Release 3.0”, Hydroqual, Inc, New Jersey.

Jiang, M., Wallace G.T., Zhou M., Libby S., and Hunt, C.D., 2007. Summer formation of a high-nutrient low-oxygen pool in Cape Cod Bay, USA, *J. Geophys. Res*., 112, C05006, doi:10.1029/2006JC003889.

Jiang M. and Zhou M. 2006. Massachusetts Bay Eutrophication Model: 2002-2004 Simulation. Boston: Massachusetts Water Resources Authority. Report 2006-13. 126pp.

Keay K.E., Leo W.S., and Libby P.S. 2012. Comparisons of Model-Predicted and Measured Productivity in Massachusetts Bay. Boston: Massachusetts Water Resources Authority. Report 2012-03. 11 p. plus Appendix.

Libby P.S., Borkman D.G., Geyer W.R., Turner J.T., and Costa A.S. 2014. 2013 Water column monitoring results. Boston: Massachusetts Water Resources Authority. Report 2014-17. 43 pp.

Libby P.S., Gagnon C., Albro C., Mickelson M., Keller A., Borkman D., Turner J., and Oviatt C.A. 2005. Combined work/quality assurance plan for baseline water quality monitoring: 2004-2005. Boston: Massachusetts Water Resources Authority. Report ms-074 Version 1. 76 pp., plus appendices.

Menzie C.A., Cura J.J., Jr, Freshman J.S., and Potocki B. 1991. Boston Harbor: estimates of loadings. Boston: Massachusetts Water Resources Authority. Report 1991-04. 108pp.

Montoya J.P., Rathbun K.M., and Mayo C.S. 2003. Information Briefing to Outfall Monitoring Science Advisory Panel. Recent nitrogen isotope data from Massachusetts and Cape Cod Bays. January 6, 2003. 8 pp.

Tian, R.C., Chen C.S., Xu Q.C., Xue P.F., Cowles G.W., Beardsley R. and Rothschild B. 2009. Massachusetts Bay Eutrophication Model: 2006-2007 Simulation. Boston: Massachusetts Water Resources Authority. Report 2009-11. 147pp.

Tian, R.C., Chen, C., Zhao, L.Z., Xue, P., Leo, W.S., Mickelson M.J. 2010. Modeling 2009 in Massachusetts Bay using the unstructured-grid Bays Eutrophication Model. Boston: Massachusetts Water Resources Authority. Report 2010-22. 100pp.

Tucker J., and Giblin A.E.. 2002. Stable isotope analyses of sediment and invertebrate samples from Boston Harbor and Massachusetts Bay. Boston: Massachusetts Water Resources Authority. Report 2002-21. 24 p.

Tucker J., Giblin A.E., Hopkinson C.S., Jr, and Vasiliou D. 2000. Benthic nutrient cycling in Boston Harbor and Massachusetts Bay: 1999 annual report. Boston: Massachusetts Water Resources Authority. Report 2000-11. 63 p.

Tucker J., Kelsey S., and Giblin A.E. 2010. 2009 benthic nutrient flux annual report. Boston: Massachusetts Water Resources Authority. Report 2010-10. 27 p.

Xue, P., Chen C., Qi J., Beardsley R.C., Tian R., Zhao L., and Lin H., 2014. Mechanism studies of seasonal variability of dissolved oxygen in Mass Bay: A multi-scale FVCOM/UG-RCA application. *Journal of Marine Systems*. 131, 102-119.

Zhao, L.Z., Chen, C., Leo, W.S. and Mickelson M.J. 2012. Modeling 2011 in Massachusetts Bay using the unstructured-grid Bays Eutrophication Model. Boston: Massachusetts Water Resources Authority. Report 2011-13. 135pp.

Zhao L., Tian R., Xue P., Chen C., Leo W.S., and Mickelson M.J. 2011. Modeling 2010 in Massachusetts Bay using the unstructured grid Bay Eutrophication Model. Boston: Massachusetts Water Resources Authority. Report 2011-09. 118 p.

Zhao L., Chen C., Beardsley R.C., Codiga D.L., Leo W.S., and Mickelson M.J. 2015. Modeling 2012 in Massachusetts Bay Using the Unstructured-Grid Bays Eutrophication Model. Boston: Massachusetts Water Resources Authority. Report 2015-02. 102p.

Table 1.1 Scenario simulations with outfall loading changes. Average conditions over month of August 2013.

The control simulation includes outfall load of NO_2^-, NO_3^-, NH_4^+, and PO_4^{3-} based on observations. The 0X, 1.1X, and 2X runs are identical to the control except for scaling up these concentrations by the indicated factor. The Δ% column indicates the percent change relative to the control run.

		Surface Chlorophyll		Surface DIN		Bottom DIN		Bottom DO Concentration		Surface DO Saturation	
		[μg L^{-1}]	**Δ%**	[μM]	**Δ%**	[μM]	**Δ%**	[mg L^{-1}]	**Δ%**	[%]	**Δ%**
Station N18: Near outfall	0X	0.7276	**-6.98**	2.2595	**-8.96**	4.3995	**-52.45**	7.6166	**0.01**	102.9043	**-0.17**
	Control	0.7822		2.4819		9.2525		7.6162		103.0830	
	1.1X	0.7870	**+0.61**	2.5053	**+0.94**	9.7430	**+5.30**	7.6162	**+0.00**	103.0862	**+0.00**
	2X	0.8361	**+6.89**	2.7102	**+9.20**	14.1677	**+53.12**	7.6179	**+0.02**	103.2532	**+0.17**
Station F06: West-central MB	0X	0.9088	**-7.05**	1.2654	**-8.47**	3.3116	**-15.76**	7.4791	**-0.12**	102.1782	**-0.27**
	Control	0.9777		1.3825		3.9310		7.4879		102.4529	
	1.1X	0.9843	**+0.68**	1.3948	**+0.89**	3.9941	**+1.61**	7.4894	**+0.02**	102.4711	**+0.02**
	2X	1.0465	**+7.04**	1.5045	**+8.82**	4.5634	**+16.09**	7.4982	**+0.14**	102.7259	**+0.27**
Station F02: Cape Cod Bay	0X	1.0674	**-7.24**	0.6375	**+2.13**	2.3169	**-5.20**	7.3222	**-0.19**	101.6662	**-0.35**
	Control	1.1507		0.6242		2.4439		7.3365		102.0234	
	1.1X	1.1589	**+0.71**	0.6230	**-0.19**	2.4558	**+0.49**	7.3394	**+0.04**	102.0482	**+0.02**
	2X	1.2353	**+7.35**	0.6121	**-1.94**	2.5728	**+5.27**	7.3535	**+0.23**	102.3806	**+0.35**

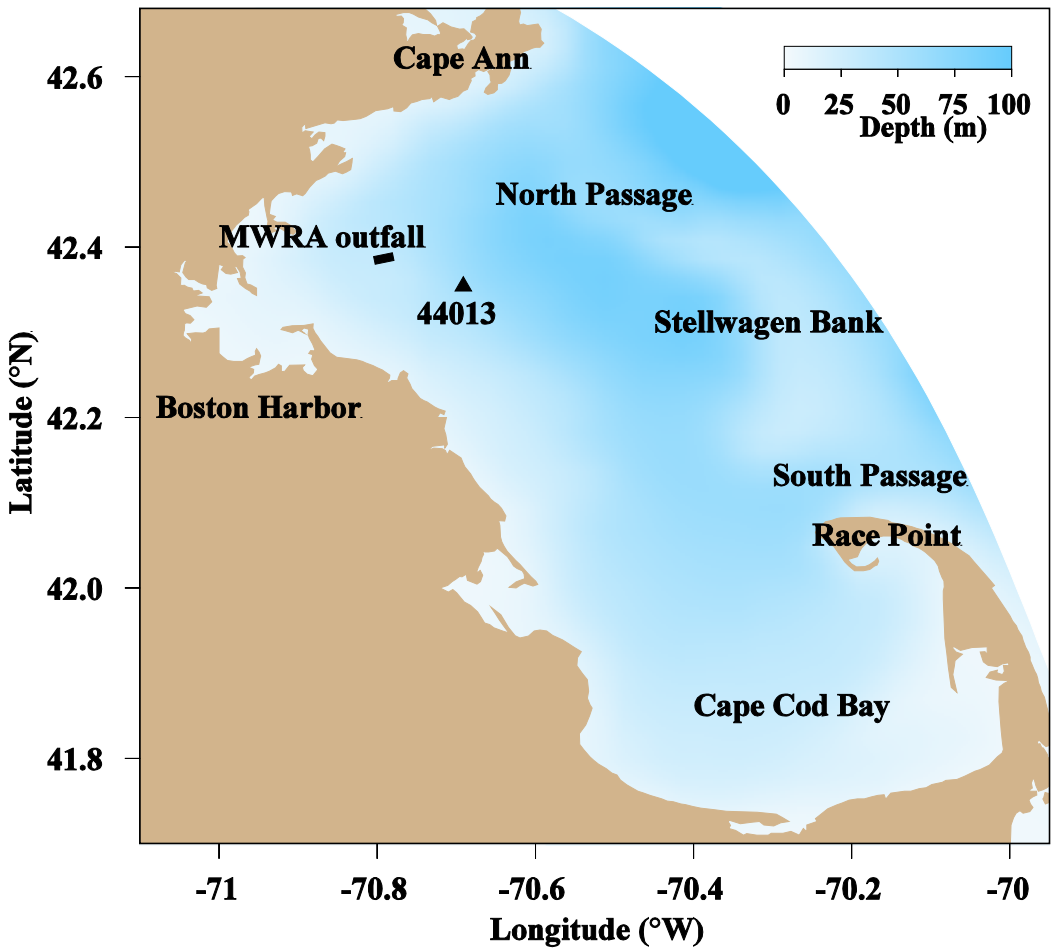

Figure 1.1 Geographic features, bathymetry, MWRA outfall location, and site of meteorological station 44013.

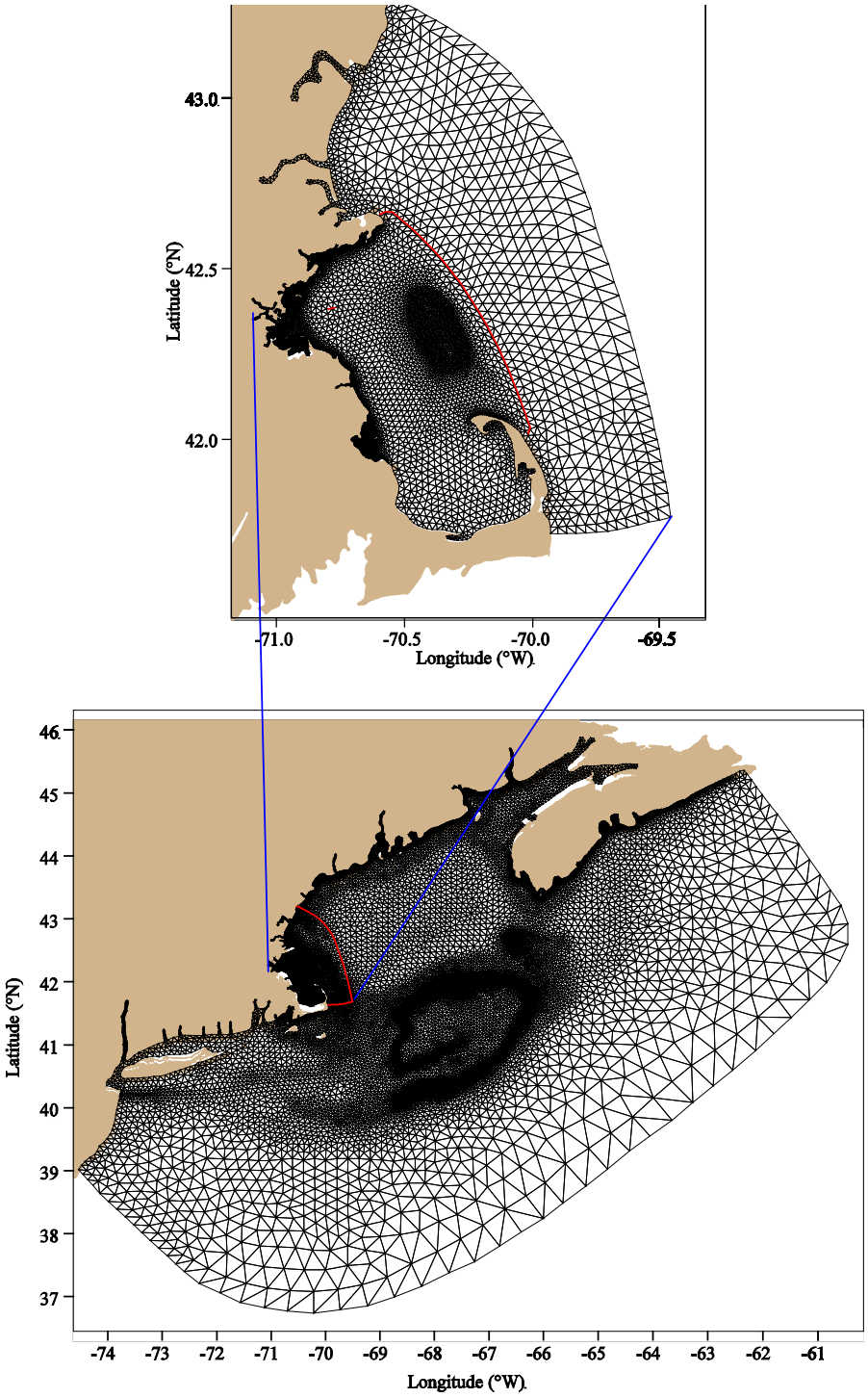

Figure 2.1 Model grids.

Lower panel: Gulf-of-Maine FVCOM grid; the red line shows the nested domain of Massachusetts Bay FVCOM. Upper panel: higher-resolution grid for MB-FVCOM; the red line shows the domain of the water quality model UG-RCA, which does not extend as far east as the MB-FVCOM grid.

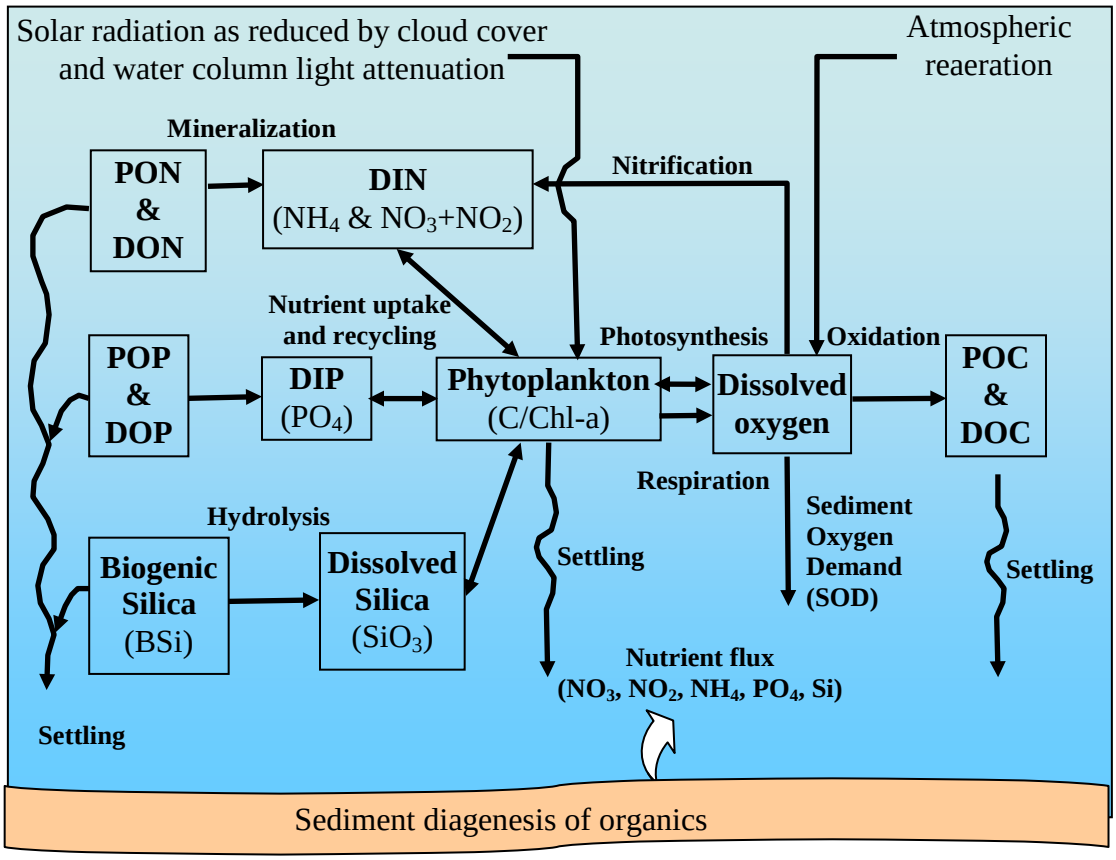

Figure 2.2 Schematic of water quality model (reproduced from Hydroqual, 2004).

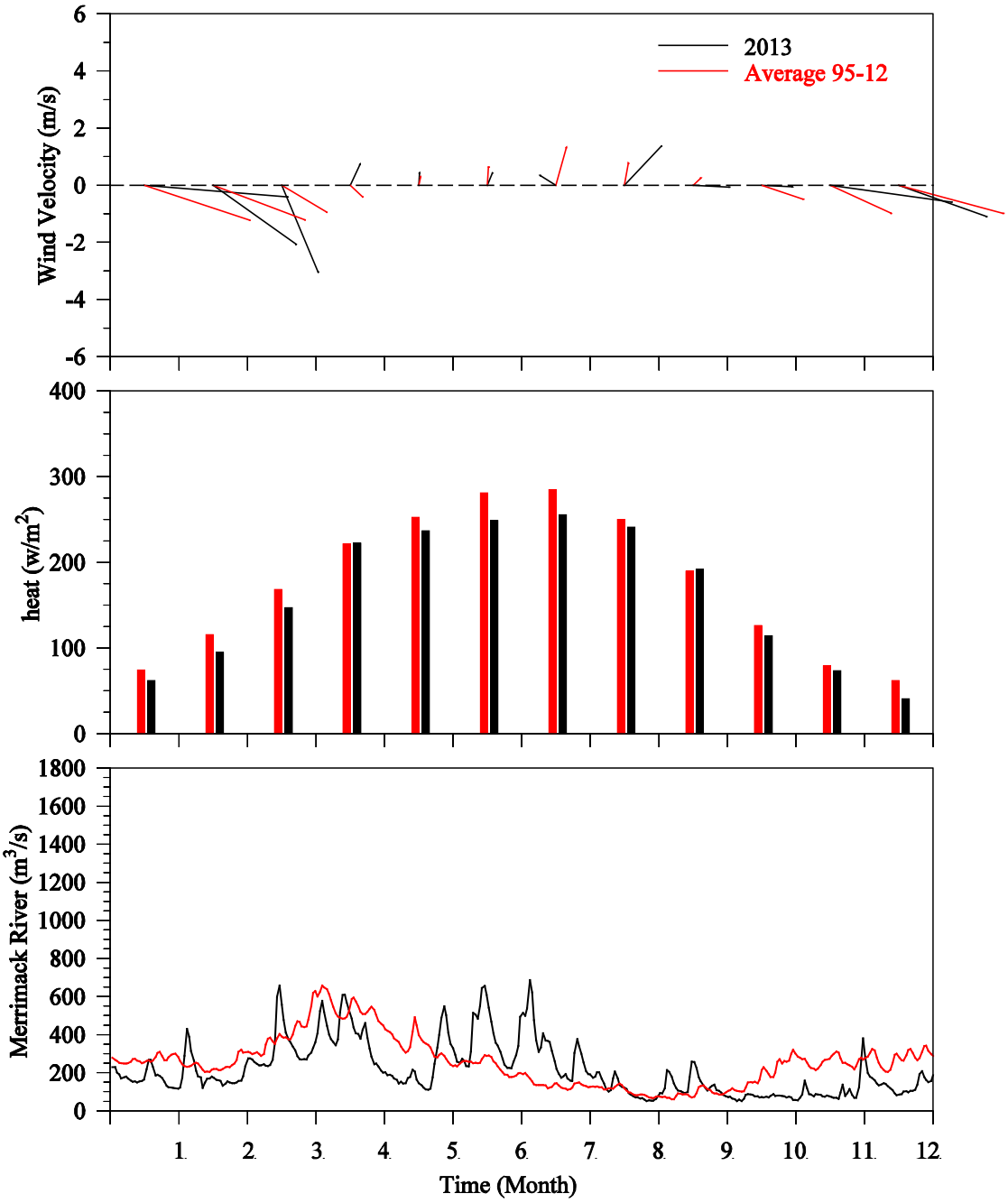

Figure 3.1 Monthly-averaged wind (upper panel) and heat flux (mid panel) and daily-averaged discharge from Merrimack River in 2013 (black) and the 18-year (1995-2012) average (red).

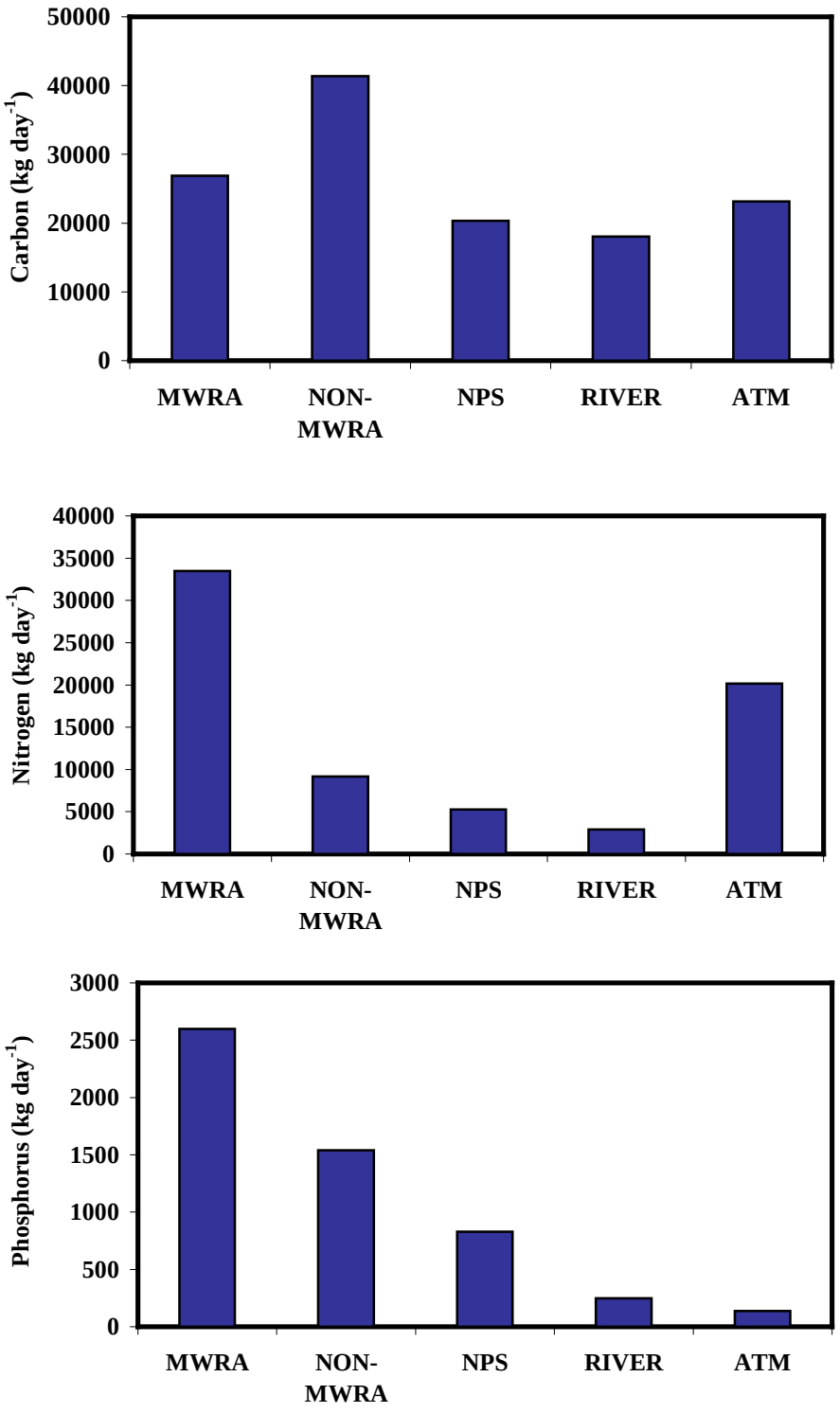

Figure 3.2 Mean daily loads of carbon, nitrogen and phosphorus from non-oceanic sources in 2013.

MWRA = MWRA outfall; NON-MWRA = Non MWRA point sources; NPS = Non-point sources; RIVER: River loadings; ATM: Atmospheric deposition.

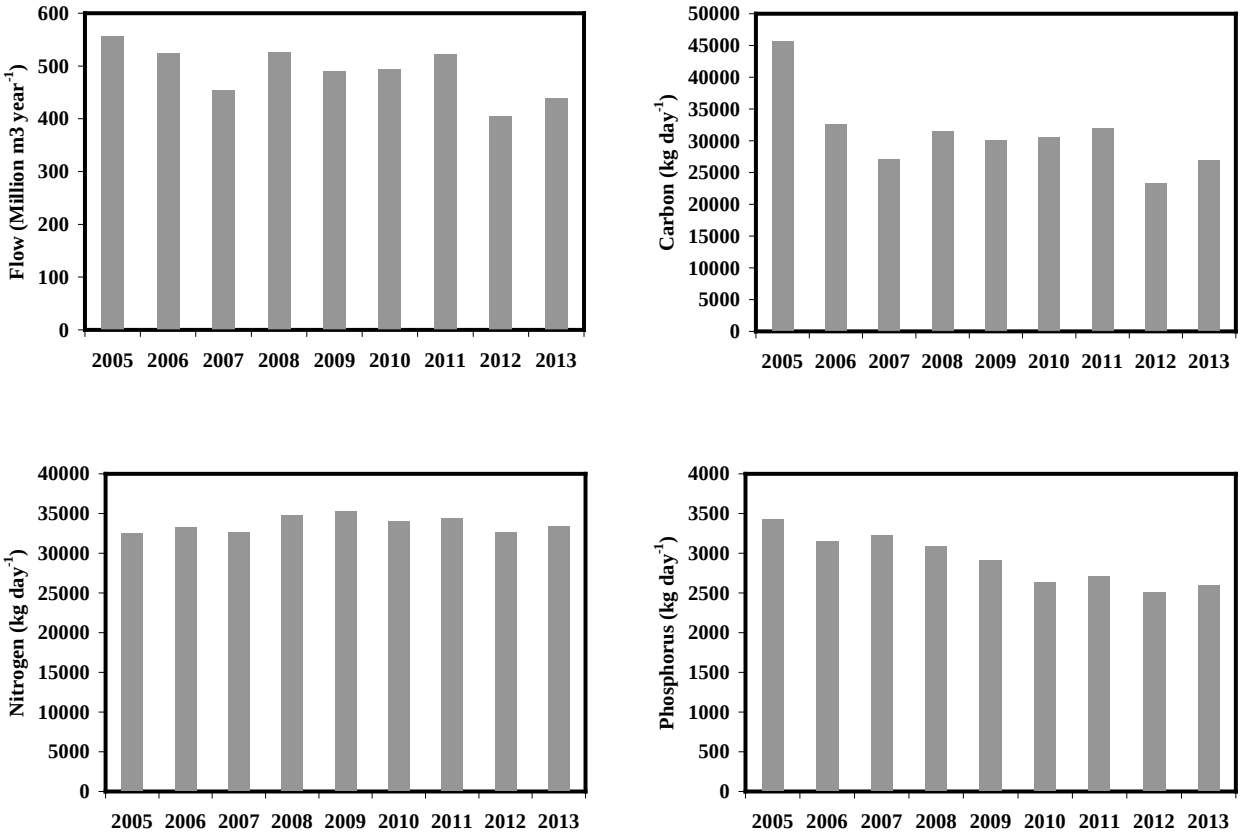

Figure 3.3 MWRA outfall mean annual flow and daily carbon, nitrogen and phosphorus loads 2005-2013.

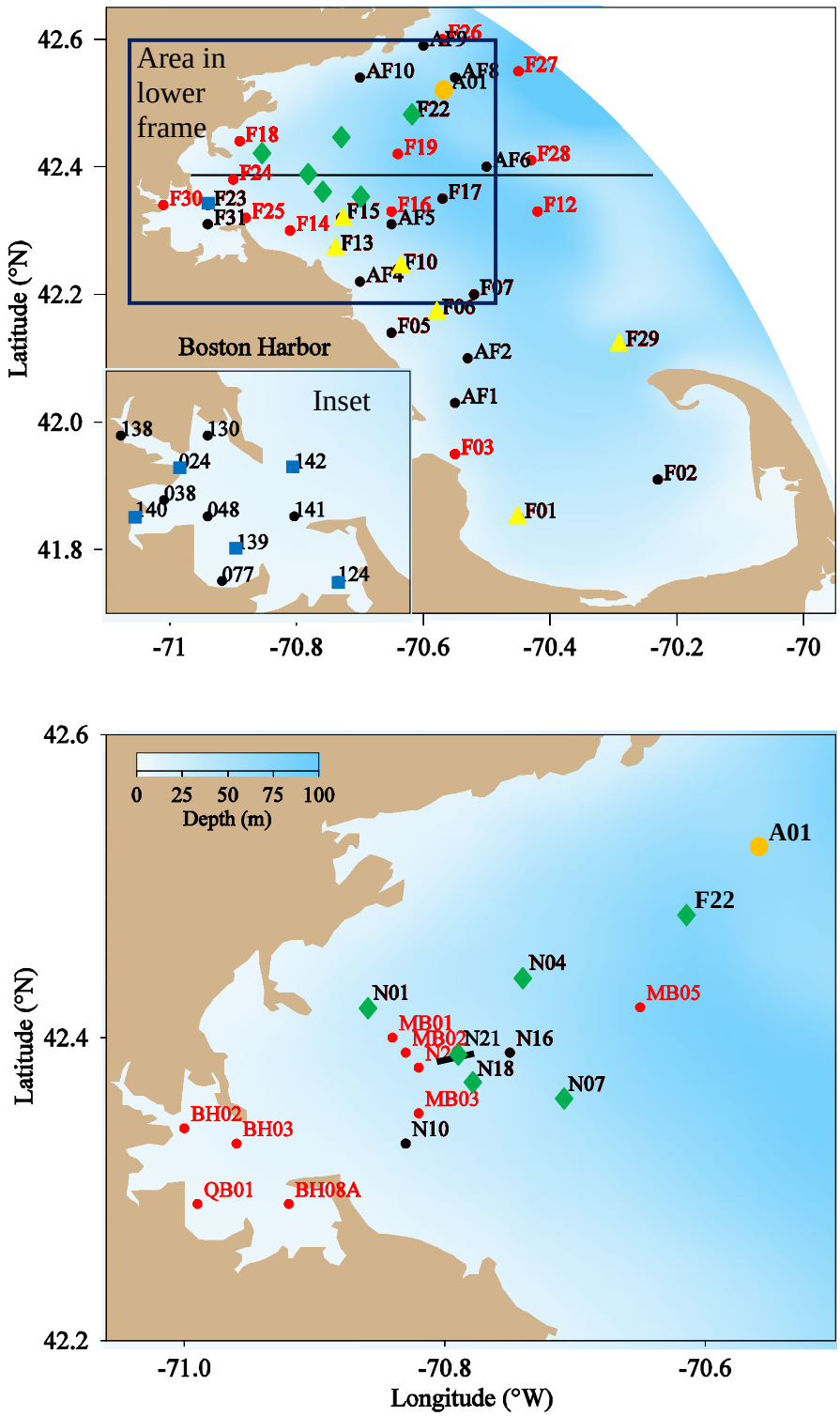

Figure 3.4 Stations. Subsets grouped together in later plots: northern (green), southern (yellow), harbor (blue).

Red stations were sampled in past years, not 2013. **Upper frame:** Farfield (prefix F) and Alexandrium Rapid Response Study (prefix AF) stations; lower left inset, Boston Harbor stations (numeric names). Black west-east line: vertical section in later plots. **Lower frame:** Nearfield (N) stations and sediment flux study stations (prefixes BH for Boston Harbor, MB for Massachusetts Bay, and QB for Quincy Bay). NERACOOS mooring site is A01 (orange).

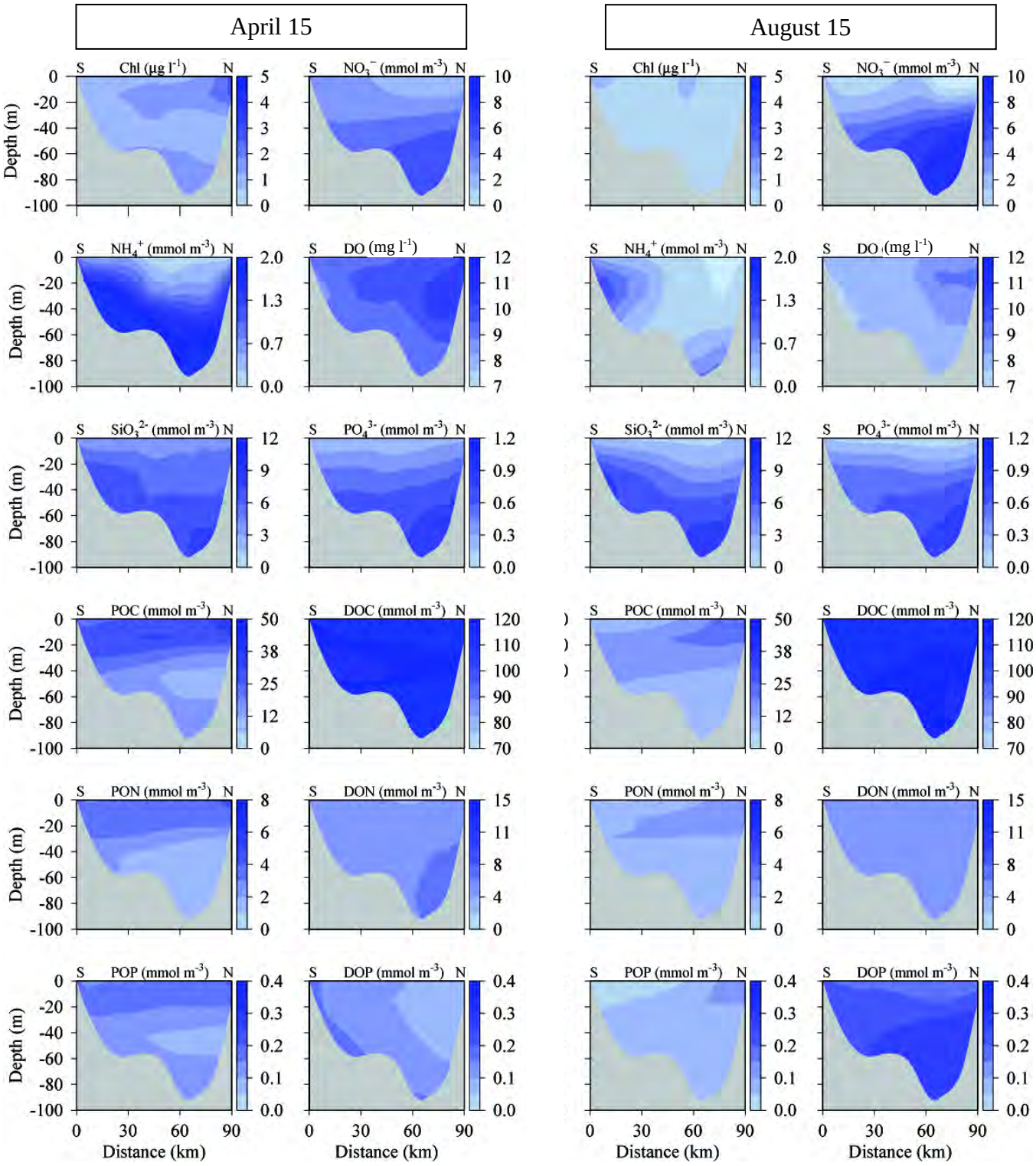

Figure 3.5 Open boundary chlorophyll, nutrients, DO and organics concentrations.

April 15 (left 2 columns) and August 15 (right 2 columns), 2013. Horizontal axis is distance along transect from Cape Cod (south S) to Cape Ann (north N).

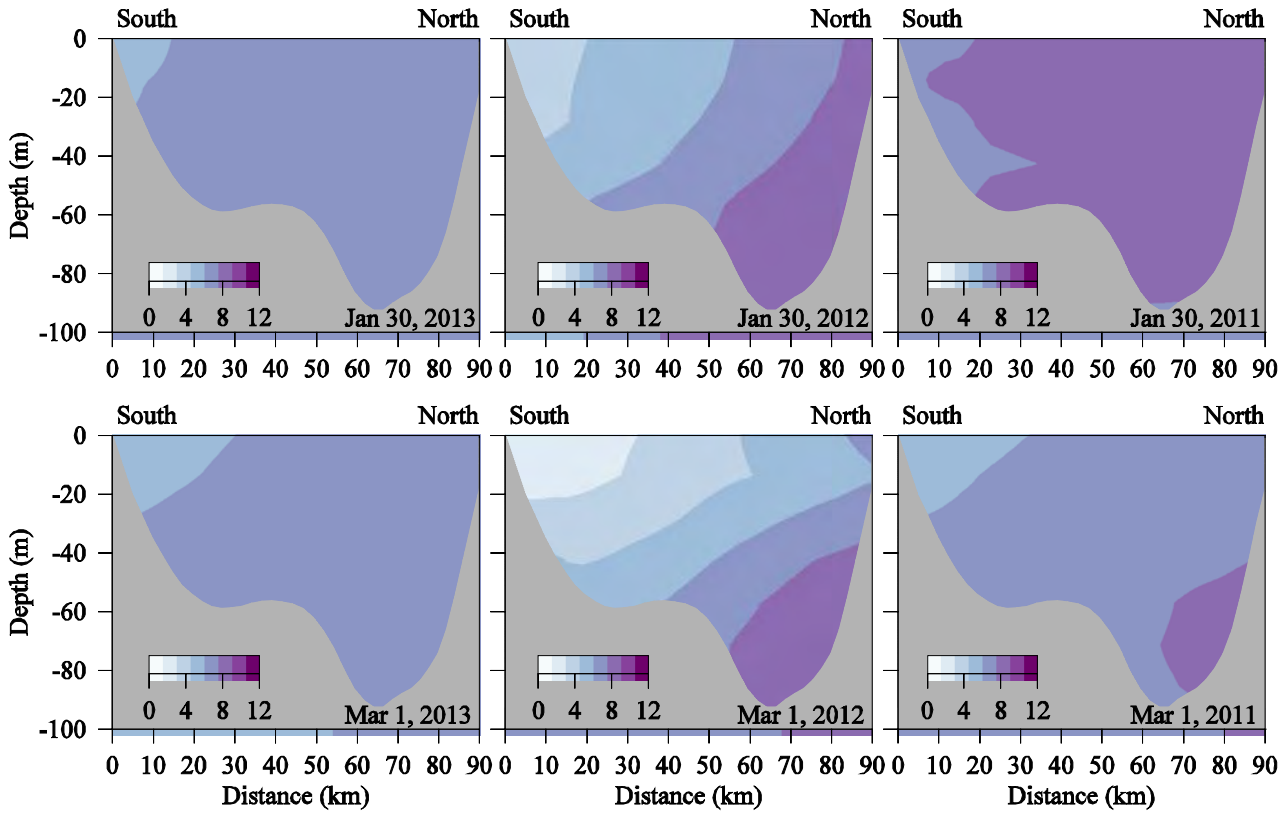

Figure 3.6 Inter-annual variations in open boundary nitrate (μM). 2013 (left), 2012 (middle) and 2011 (right) in winter. January 30 (upper) and March 1 (lower).

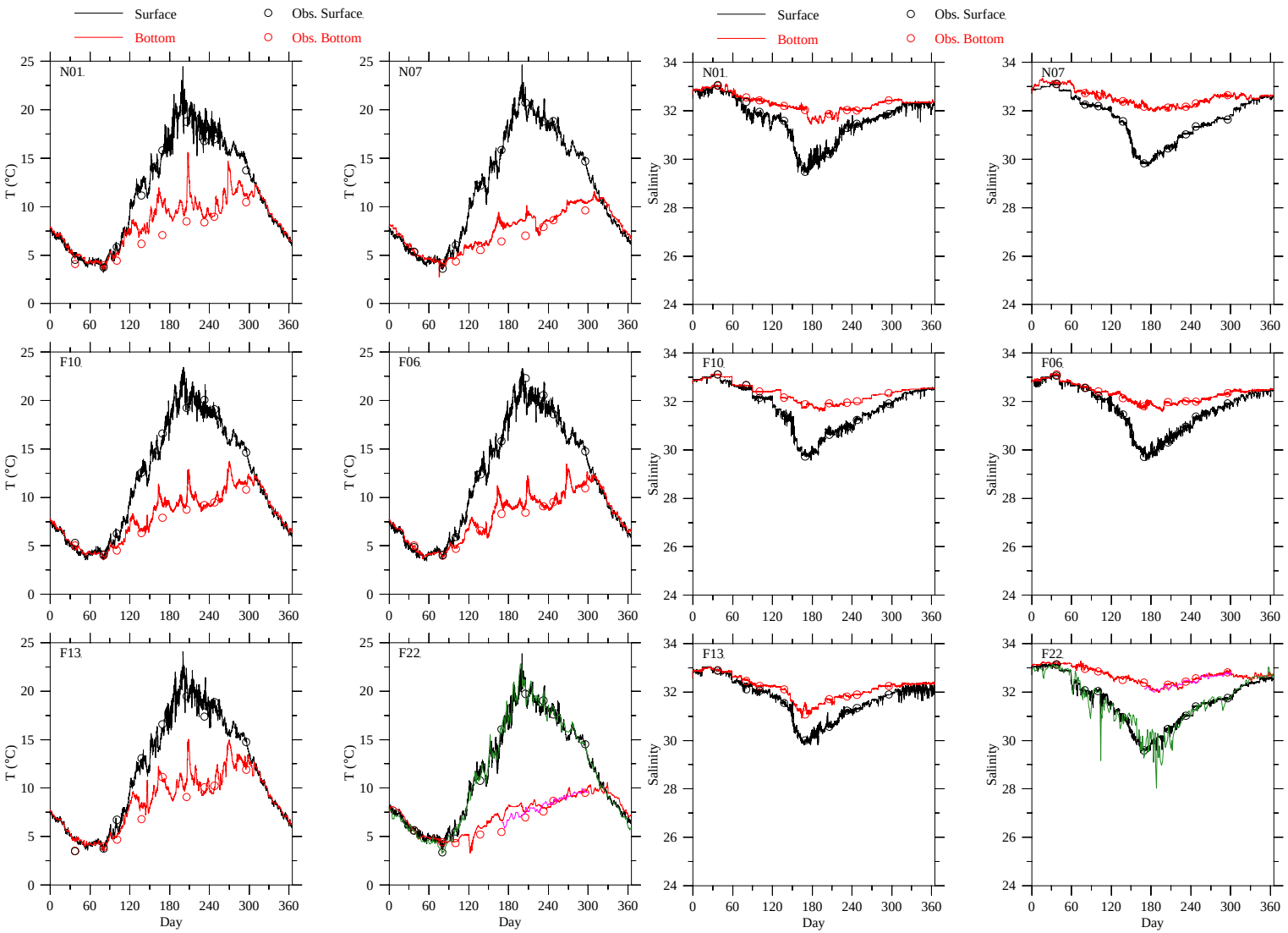

Figure 3.7 Temperature and salinity: vessel-survey observations (circles) and model output (line) at select northern/southern subset stations in 2013. Mooring A01 observations are green (near-surface) and pink (near-bottom) lines in F22 panels.

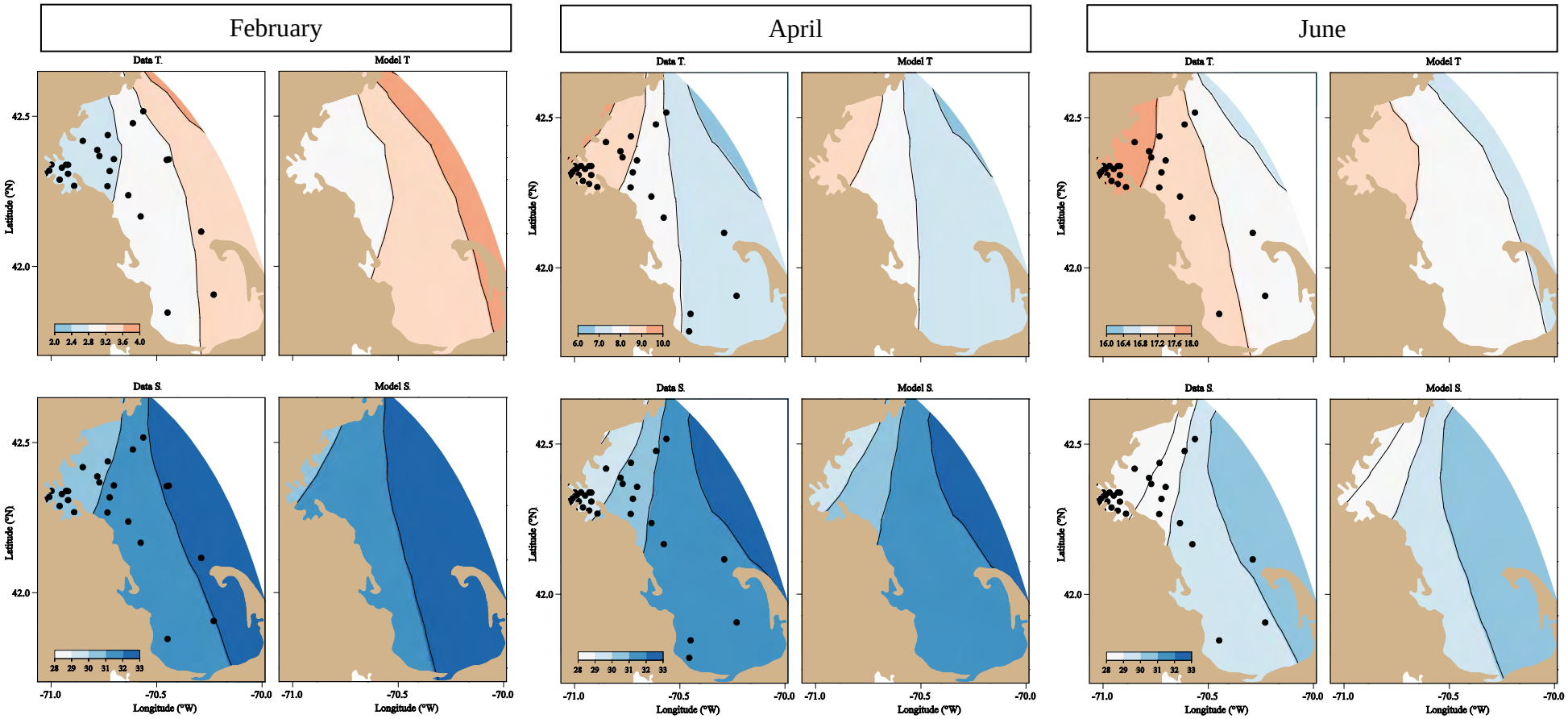

Figure 3.8 Near-surface temperature (upper, ^{o}C) and salinity (lower, PSS), Feb (left group), Apr (middle group), and Jun (right group). Observed (left in each pair) and model (right in each pair). Note differences in temperature colorscales.

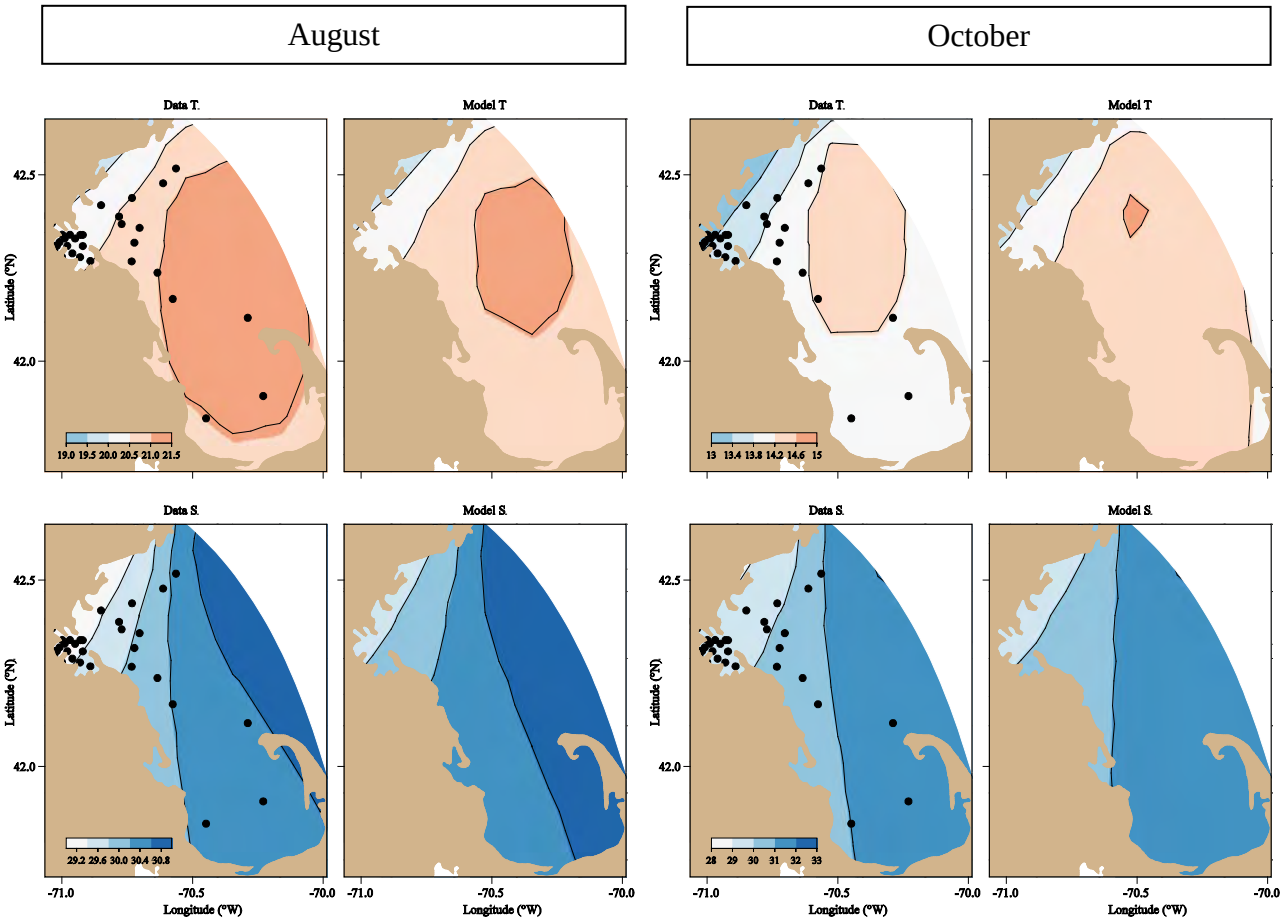

Figure 3.9 Near-surface temperature (upper, ^{o}C) and salinity (lower, PSS), Aug (left group), and Oct (right group). Observed (left in each pair) and model (right in each pair). Note differences in temperature colorscales.

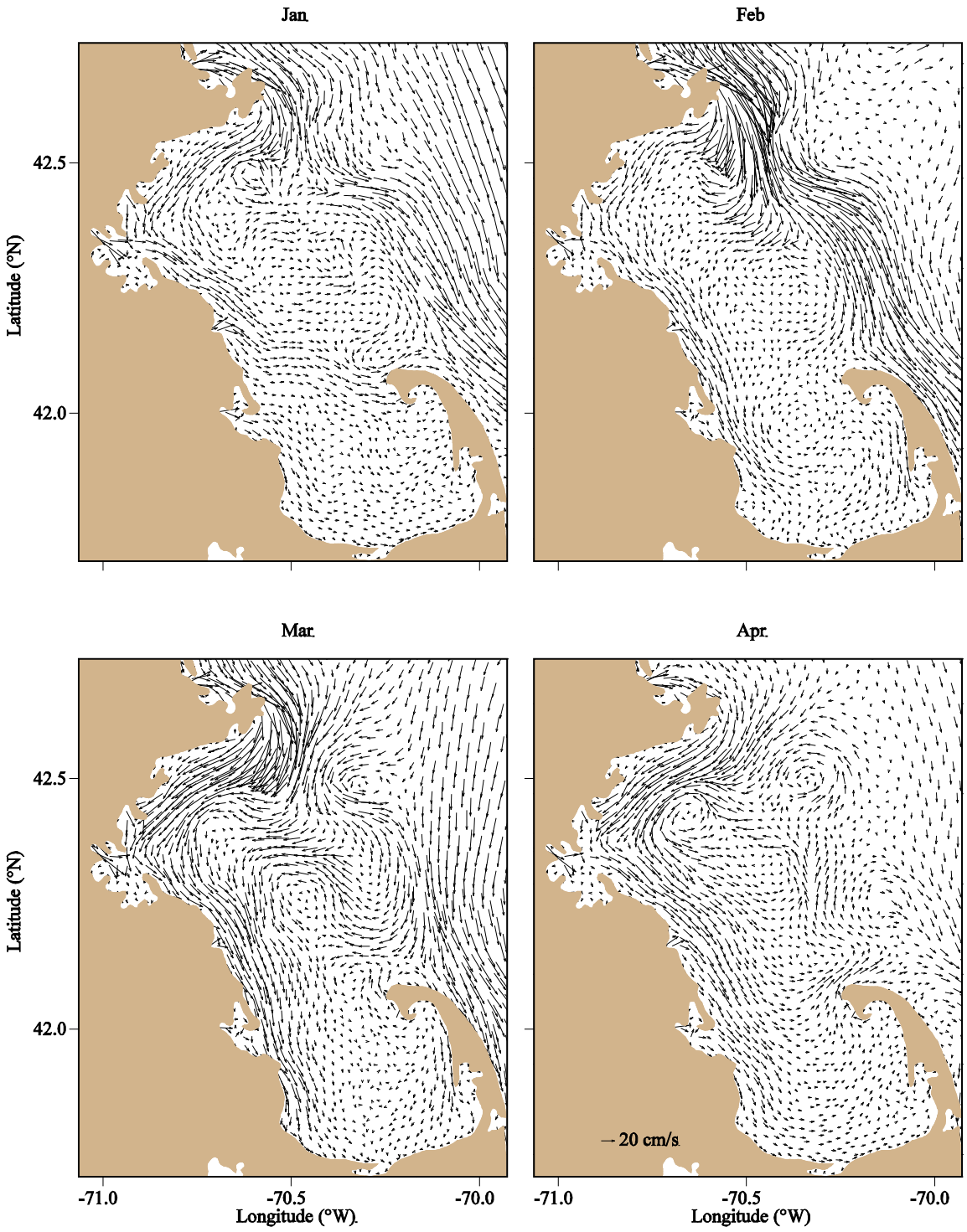

Figure 3.10 Monthly-mean model surface currents: Jan to Apr 2013.

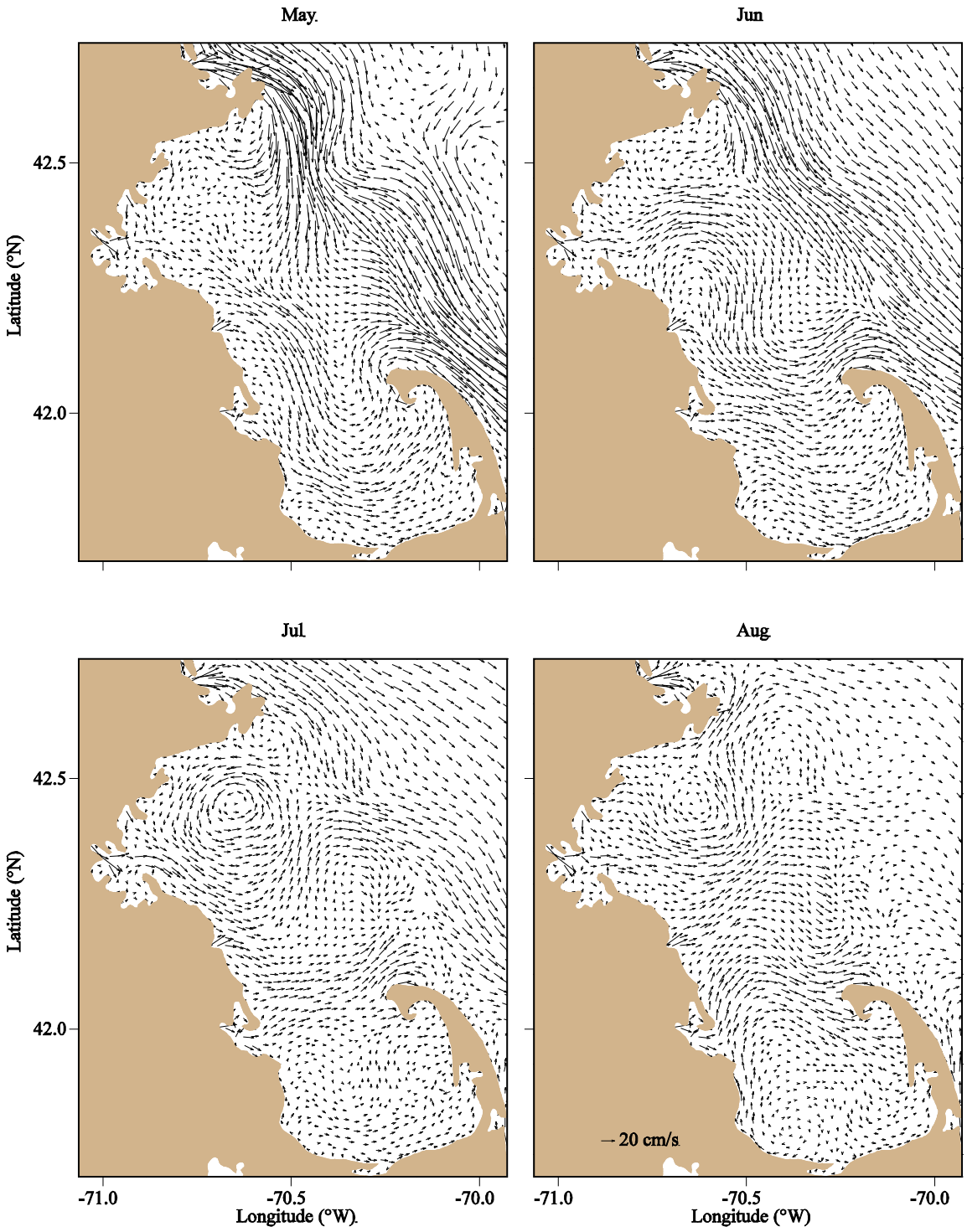

Figure 3.11 Monthly-mean model surface currents: May to Aug 2013.

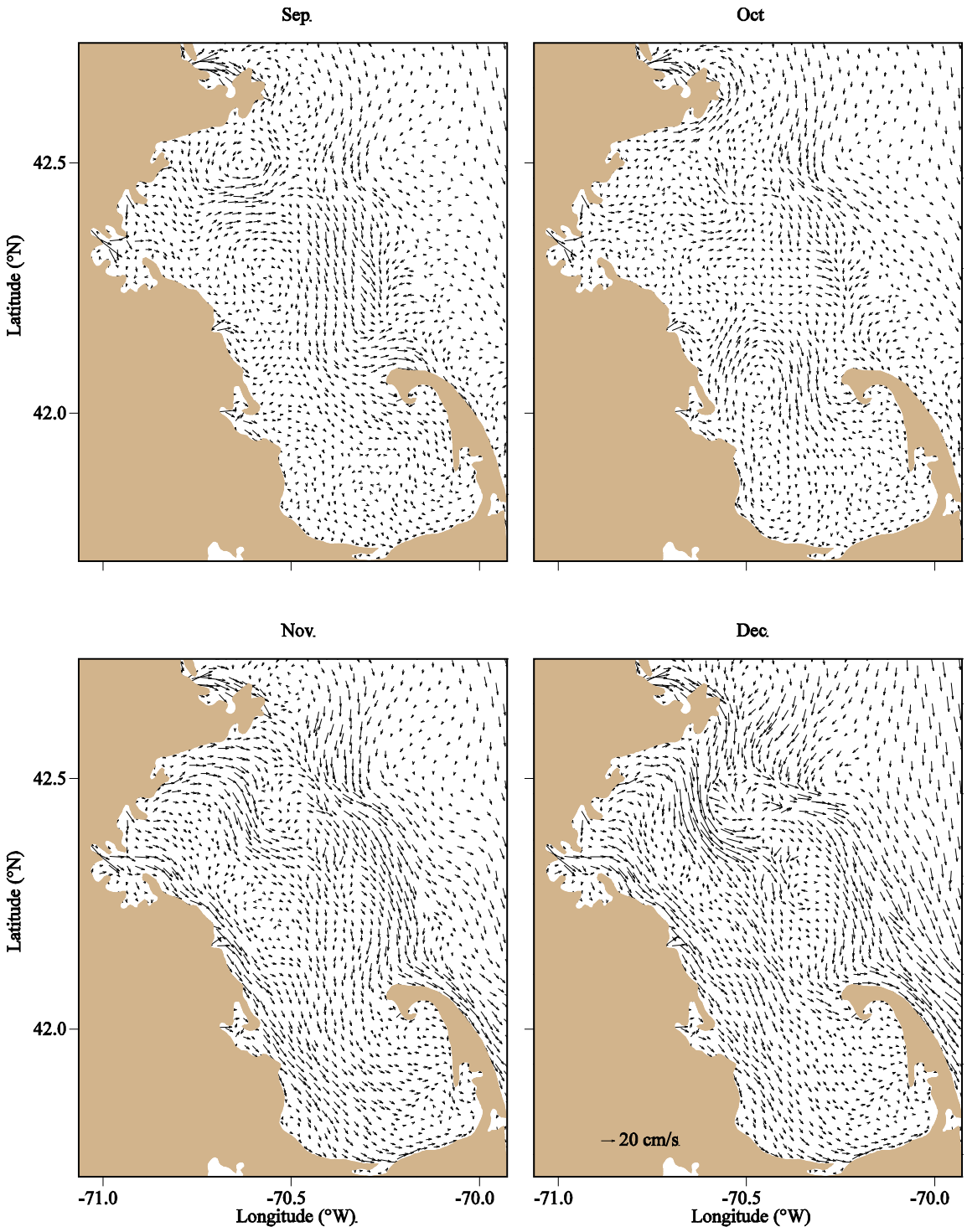

Figure 3.12 Monthly-mean model surface currents: Sep to Dec 2013.

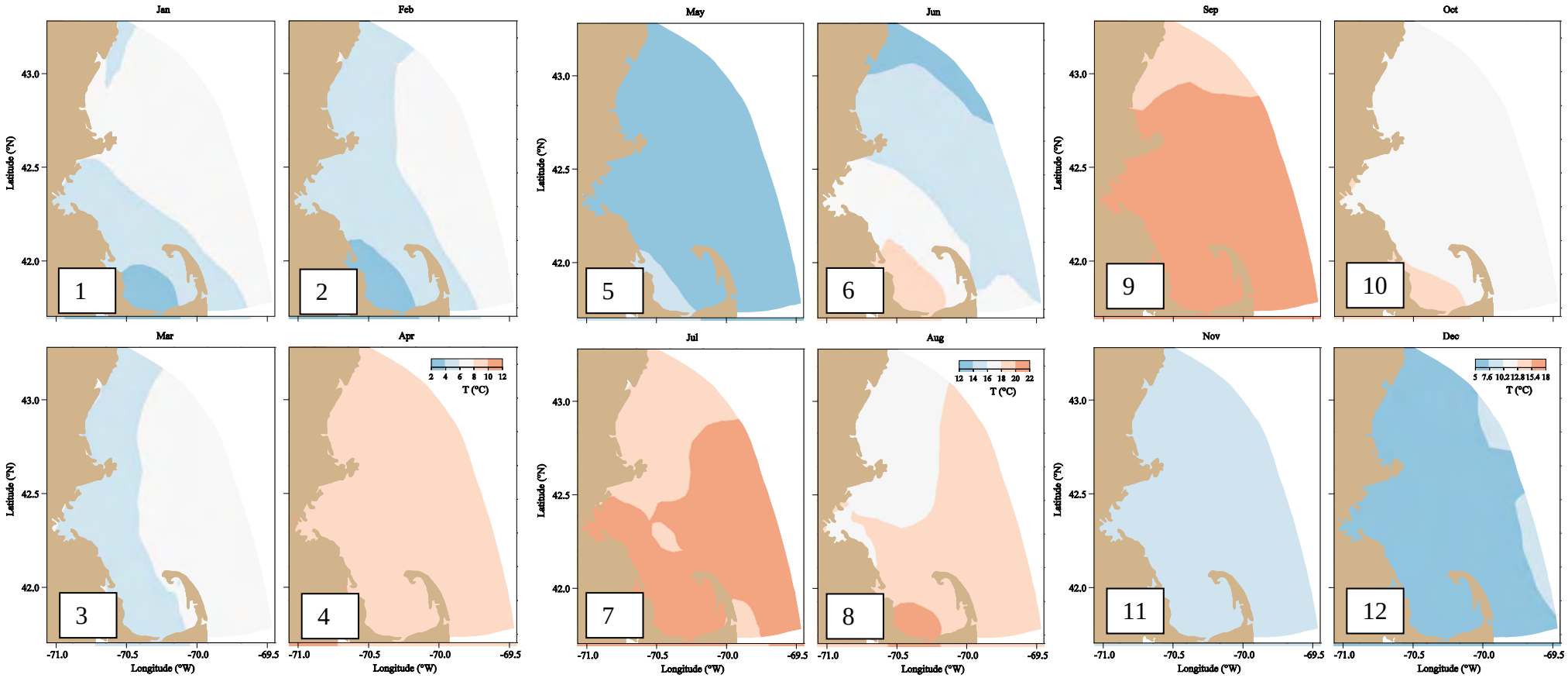

Figure 3.13 Model surface temperature at the end of each month of 2013. Note differences in temperature colorscales.

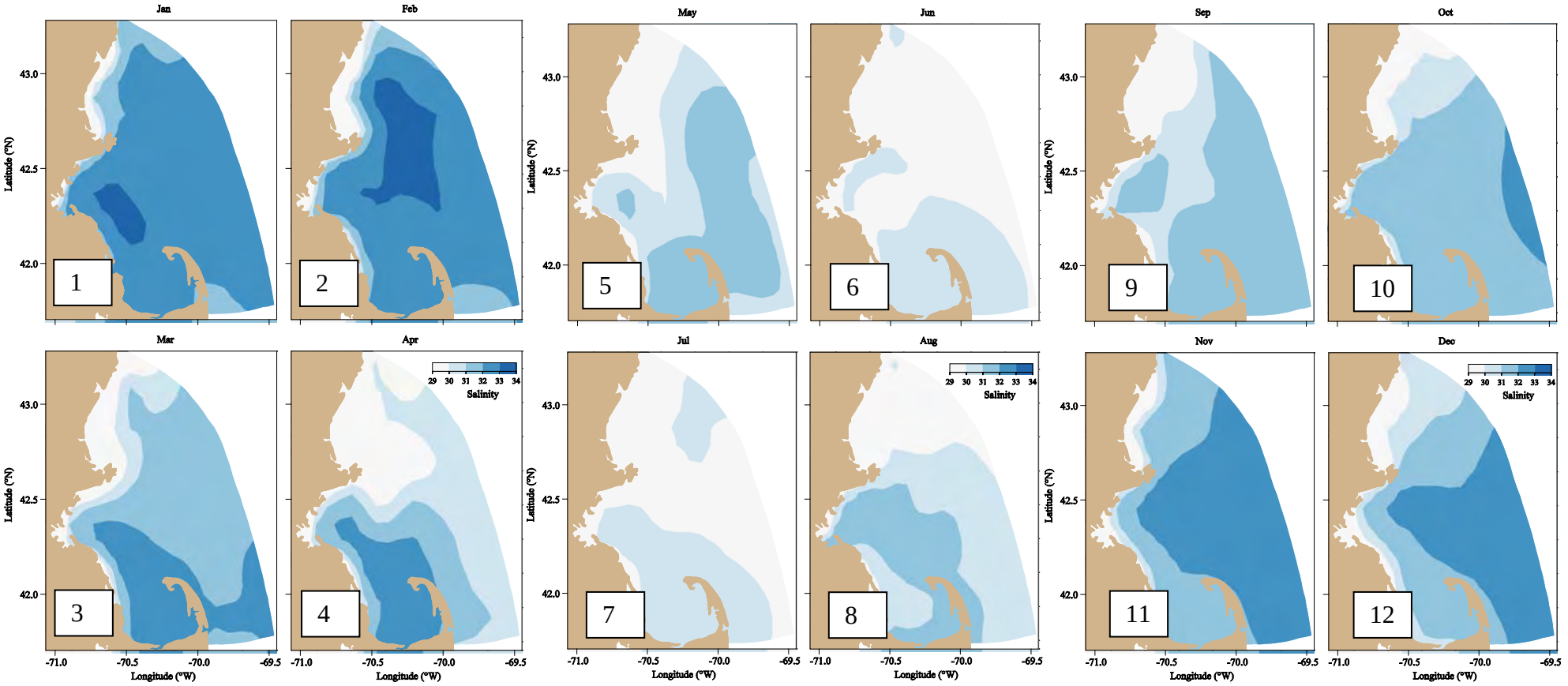

Figure 3.14 Model surface salinity at the end of each month of 2013.

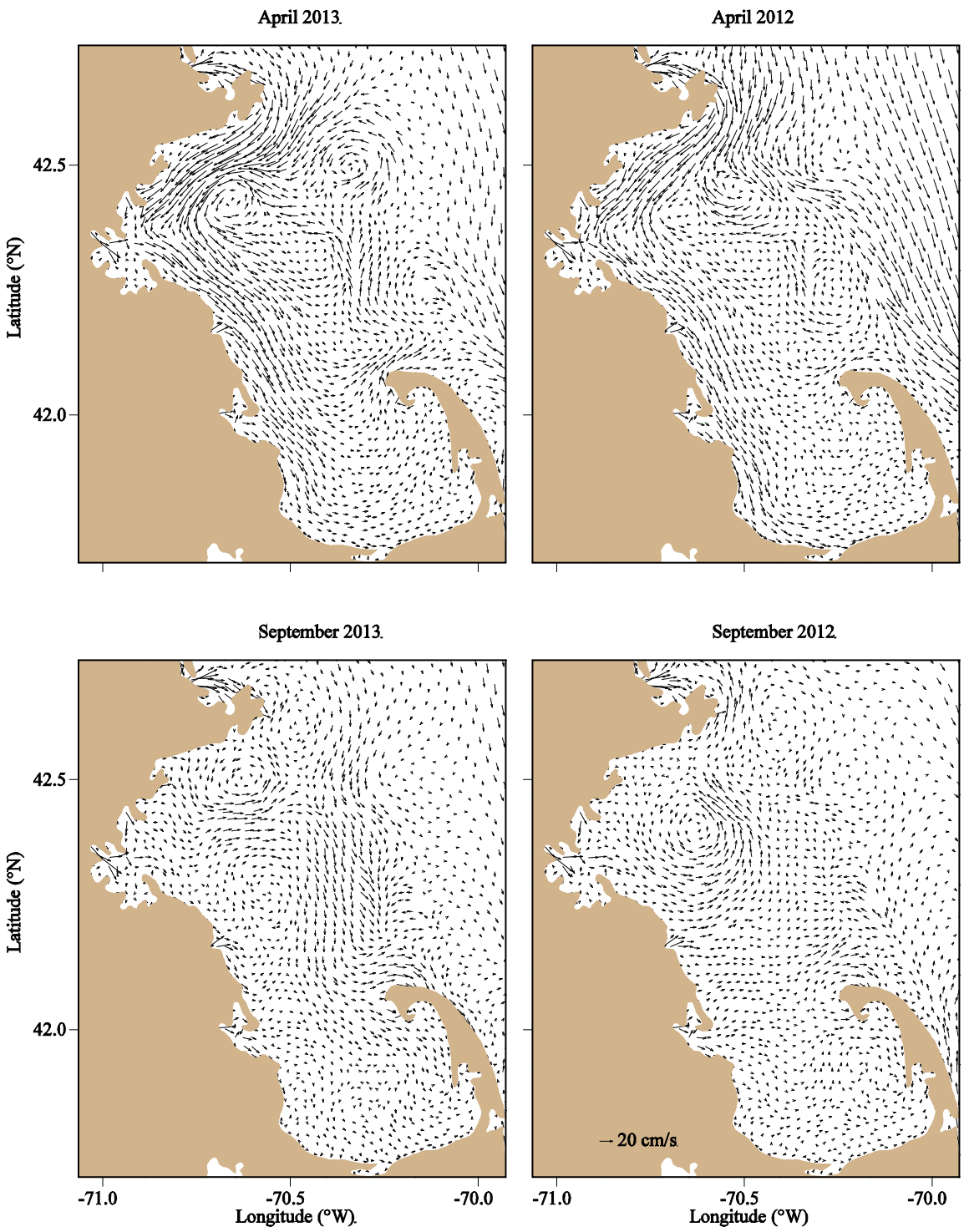

Figure 3.15 Inter-annual variation in monthly-mean surface currents: Apr (upper) and Sep (lower) during 2013 (left) and 2012 (right).

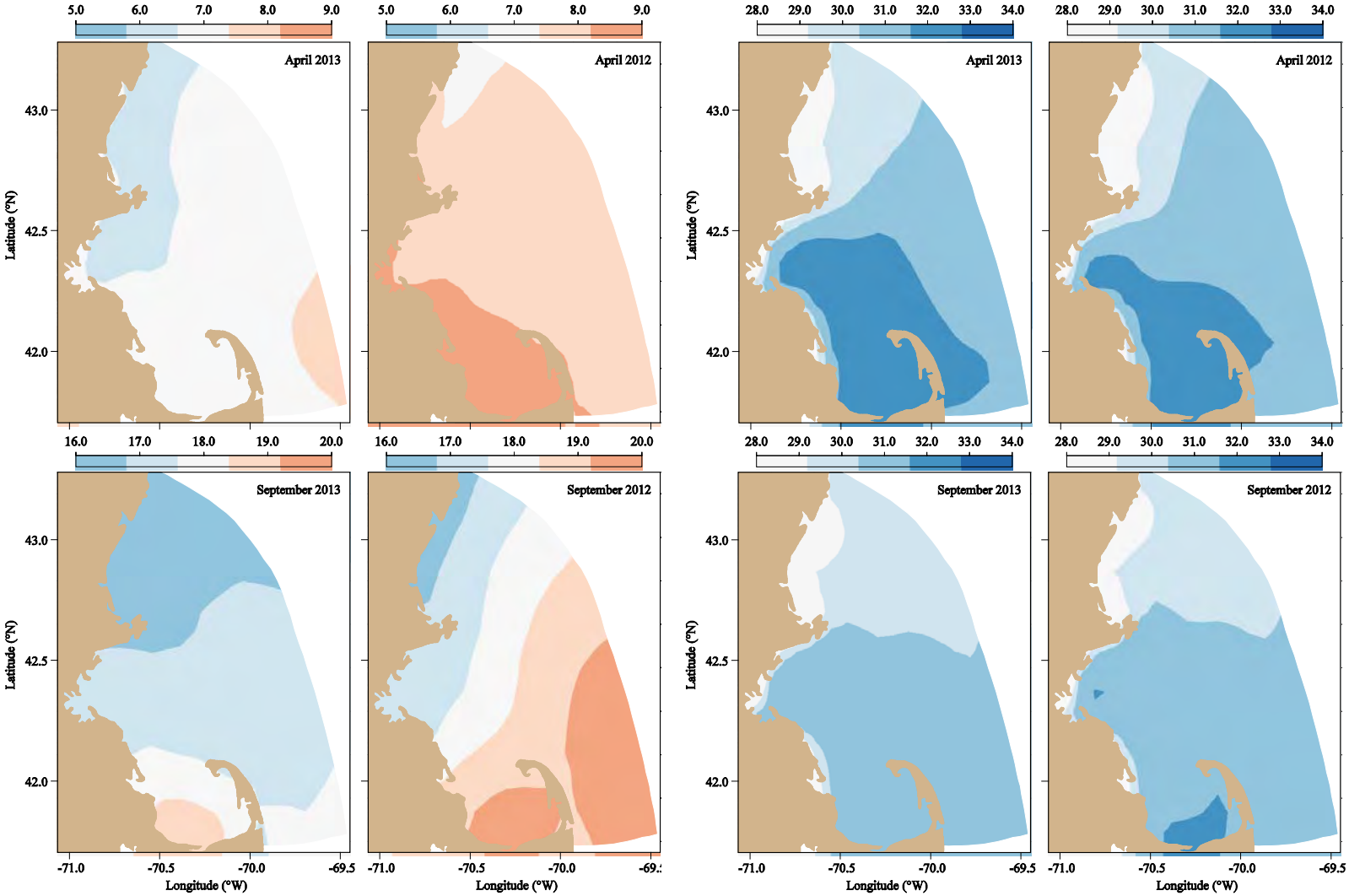

Figure 3.16 Inter-annual variation in monthly-mean surface temperatures (left group, ^{o}C) and salinities (right group, PSS): Apr (upper) and Sep (lower) during 2013 (left) and 2012 (right).

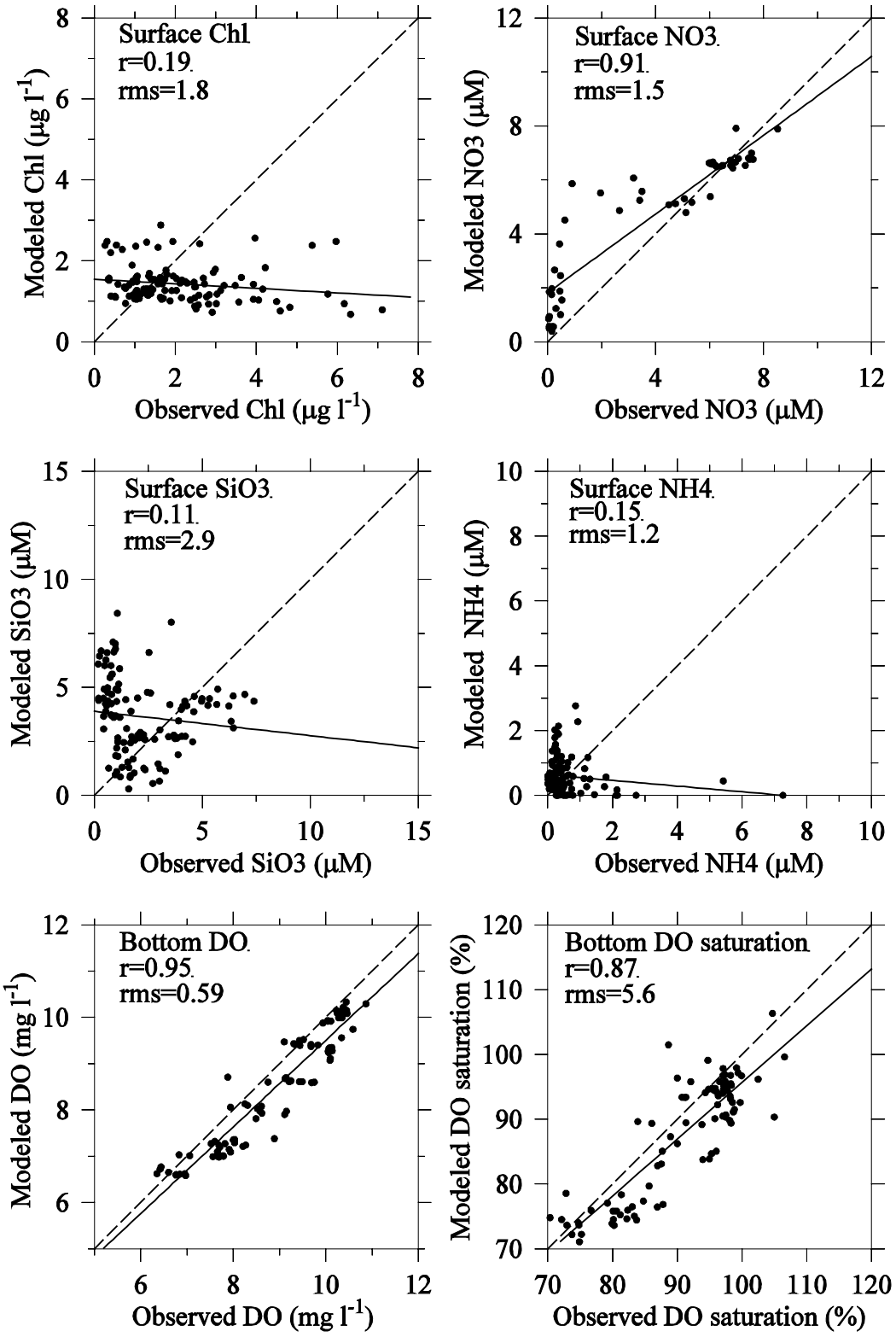

Figure 3.17 Model-observation correlations and regressions (solid lines) of key parameters, all stations outside BH, 2013.

Dashed lines indicate equality between observed and modeled results.

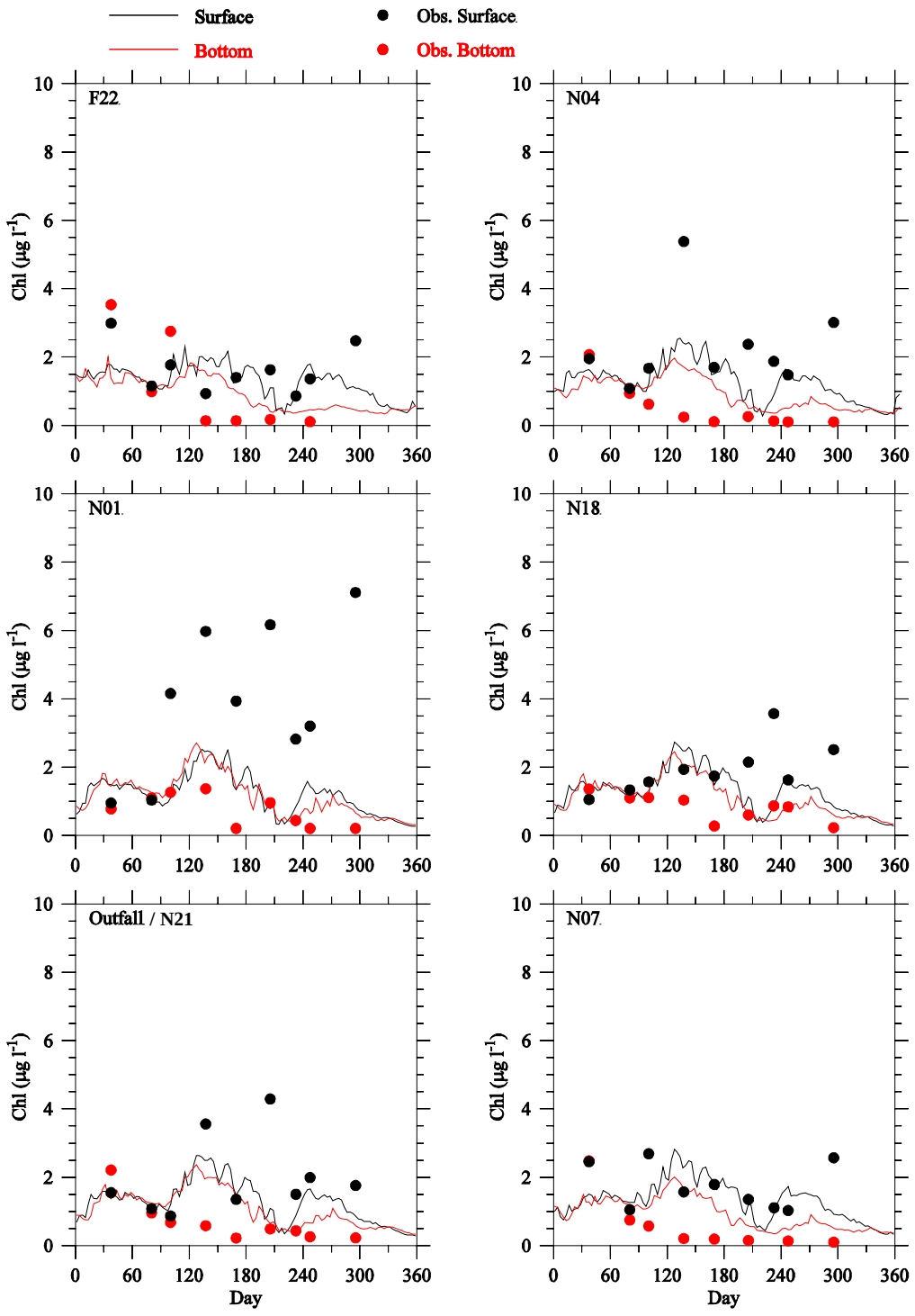

Figure 3.18 Chlorophyll: observed (dots) and modeled (lines) at northern subset stations in 2013.

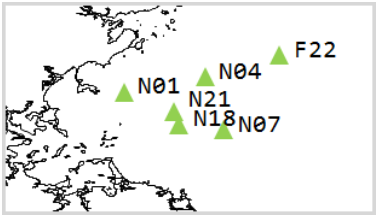

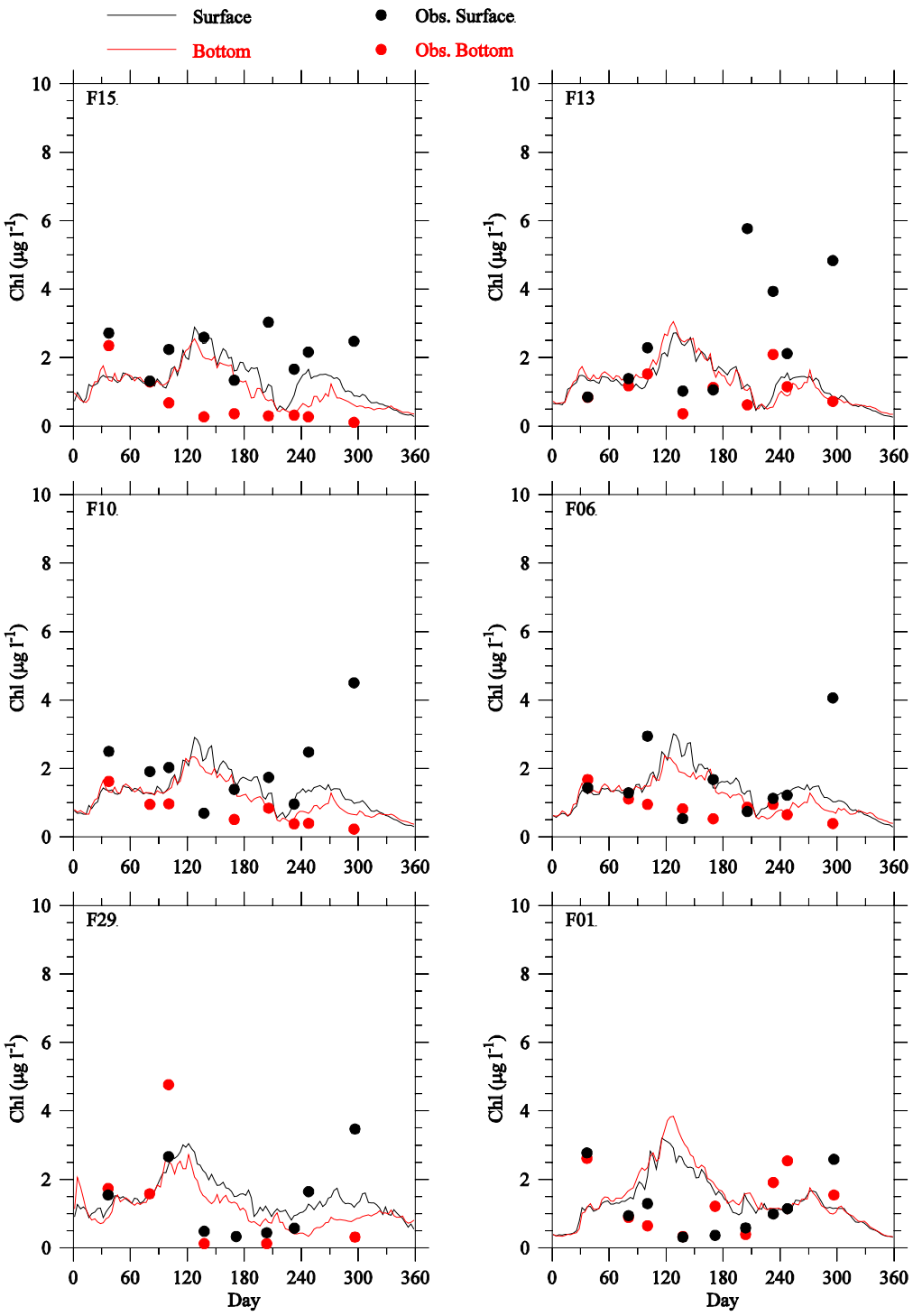

Figure 3.19 Chlorophyll: observed (dots) and modeled (lines) at southern subset stations in 2013.

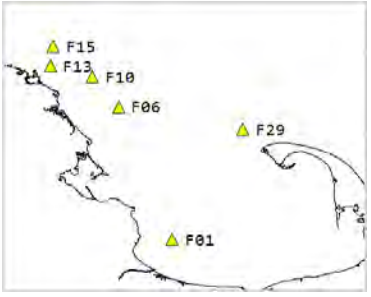

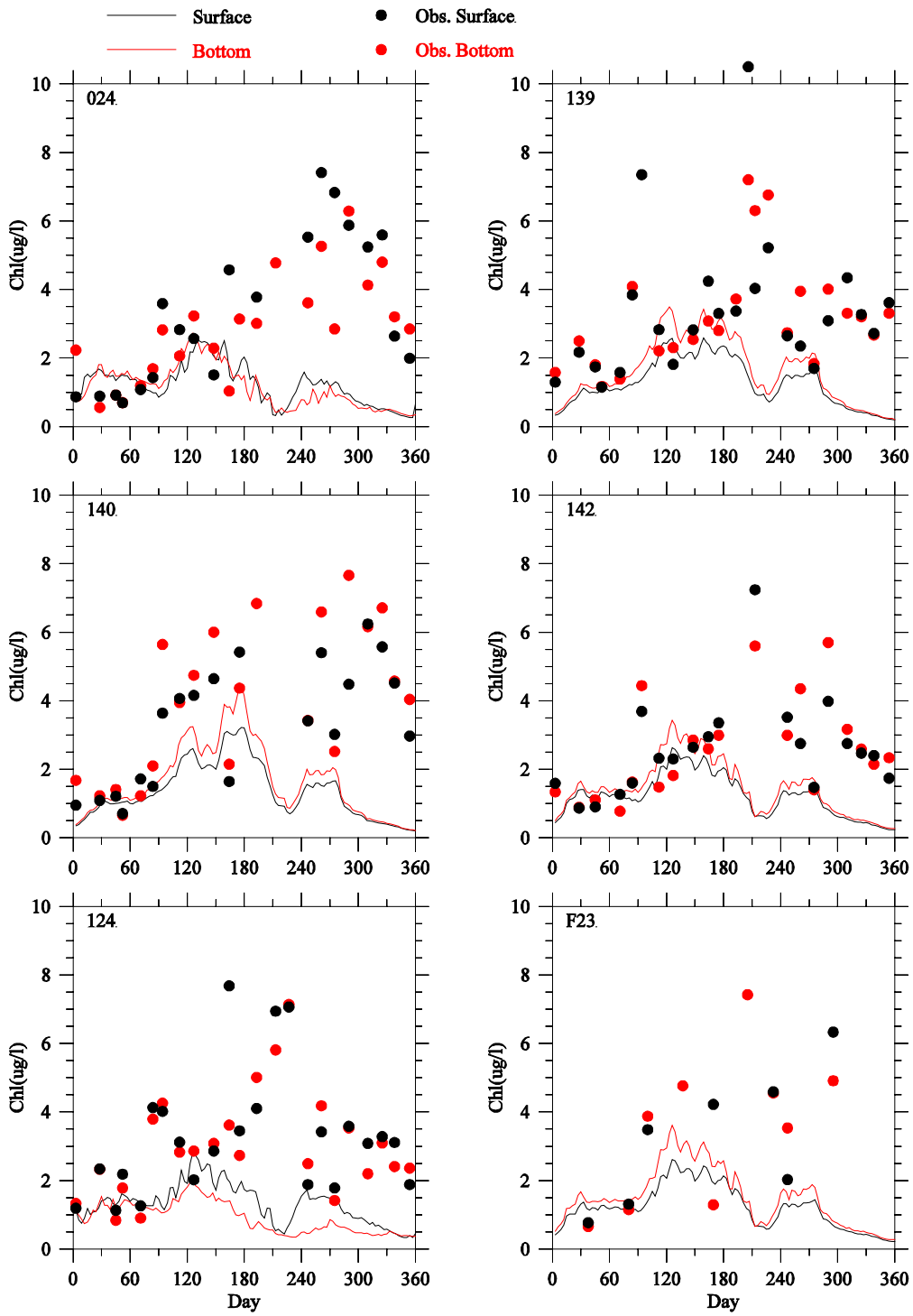

Figure 3.20 Chlorophyll: observed (dots) and modeled (lines) at harbor subset stations in 2012.

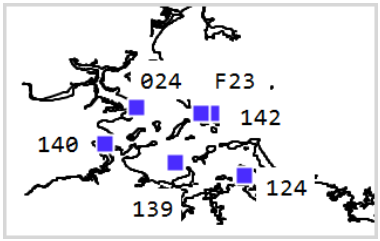

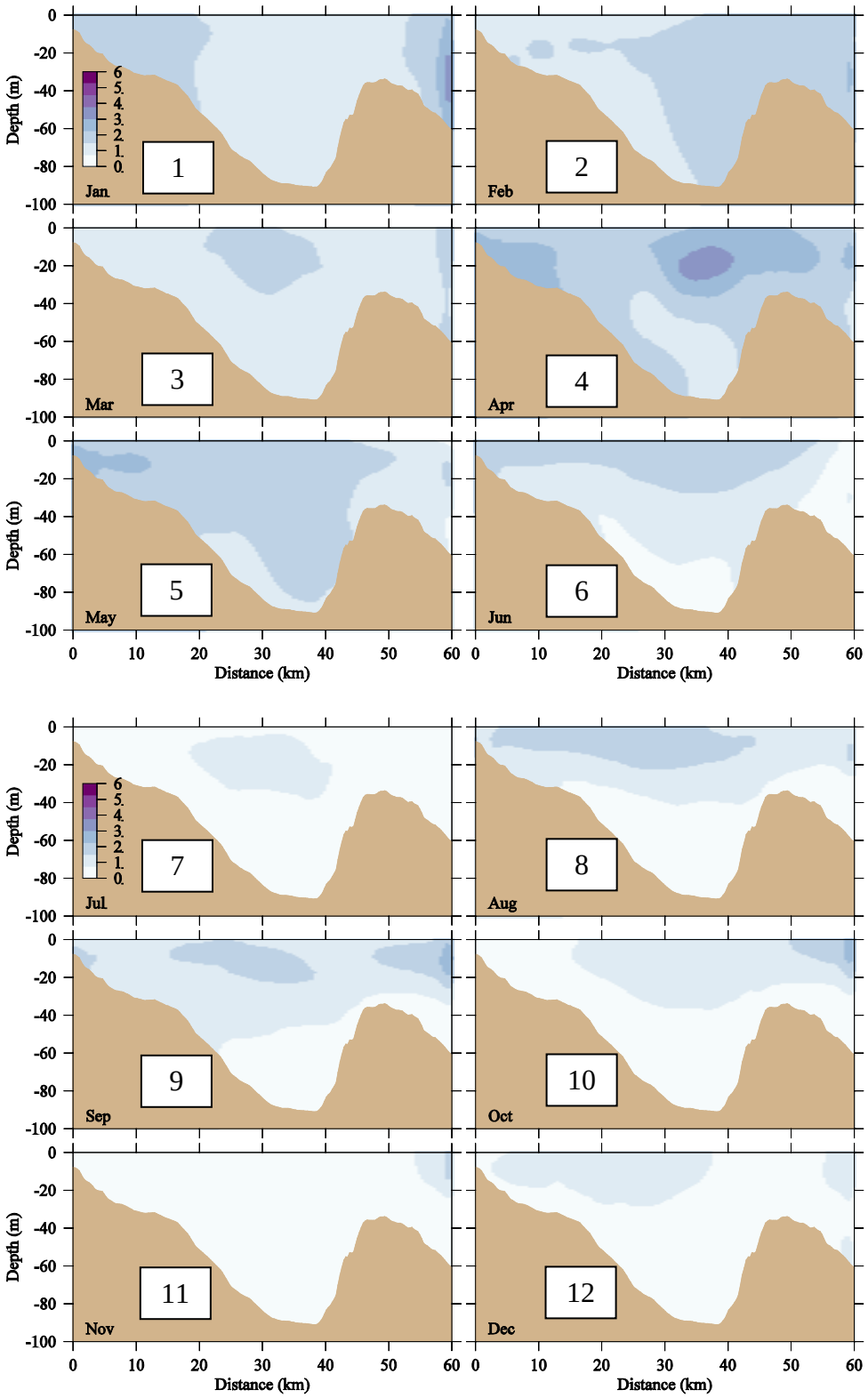

Figure 3.21 Model chlorophyll (μg L^{-1}): west-east transect through MWRA outfall, end of each month, 2013.

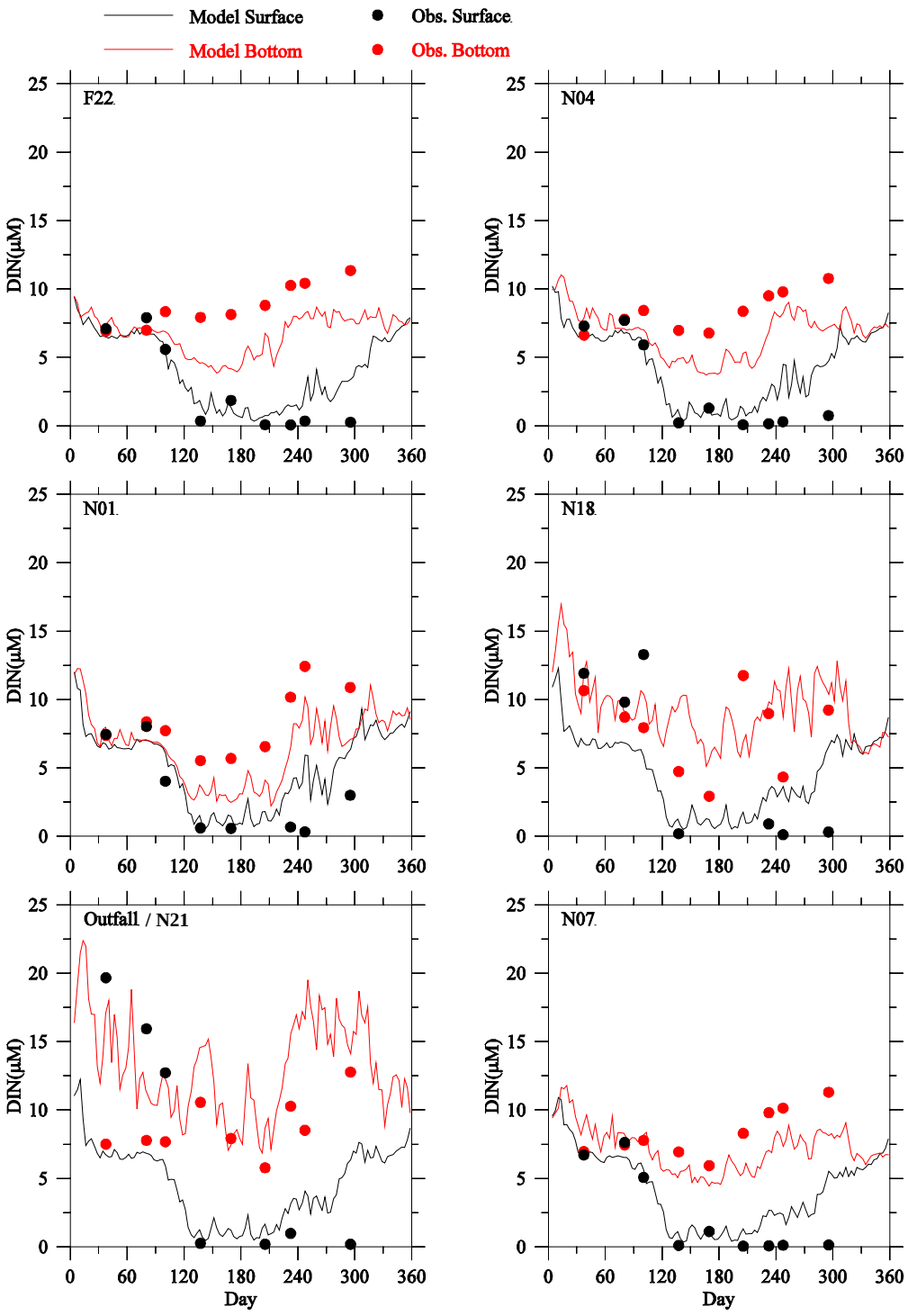

Figure 3.22 DIN: observed (dots) and modeled (lines) at northern subset stations in 2013.

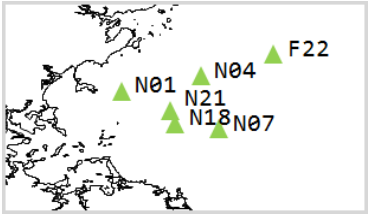

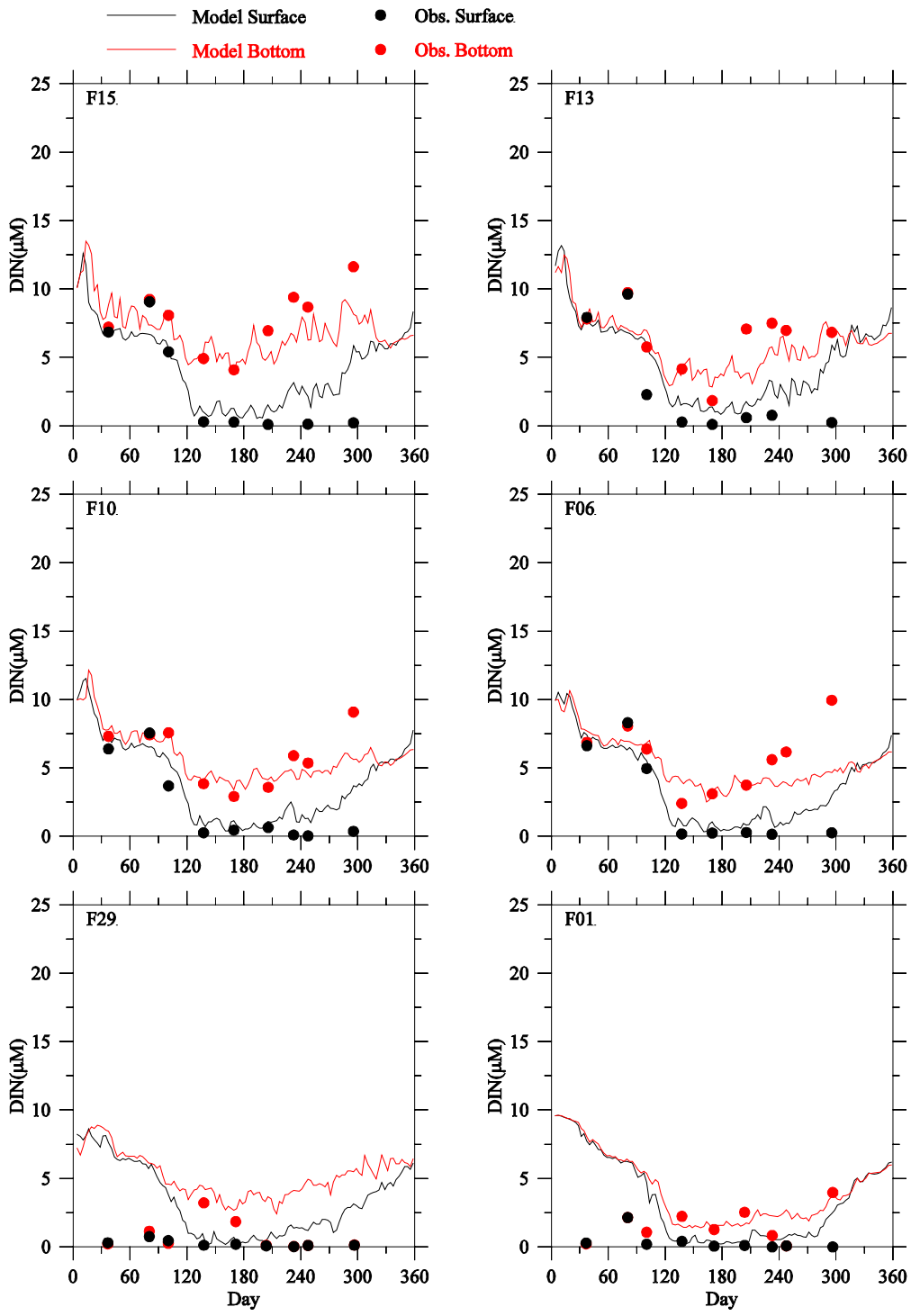

Figure 3.23 DIN: Observed (dots) and modeled (lines) at southern subset stations in 2013.

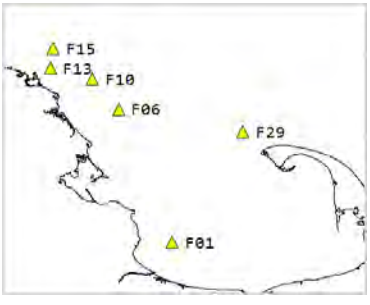

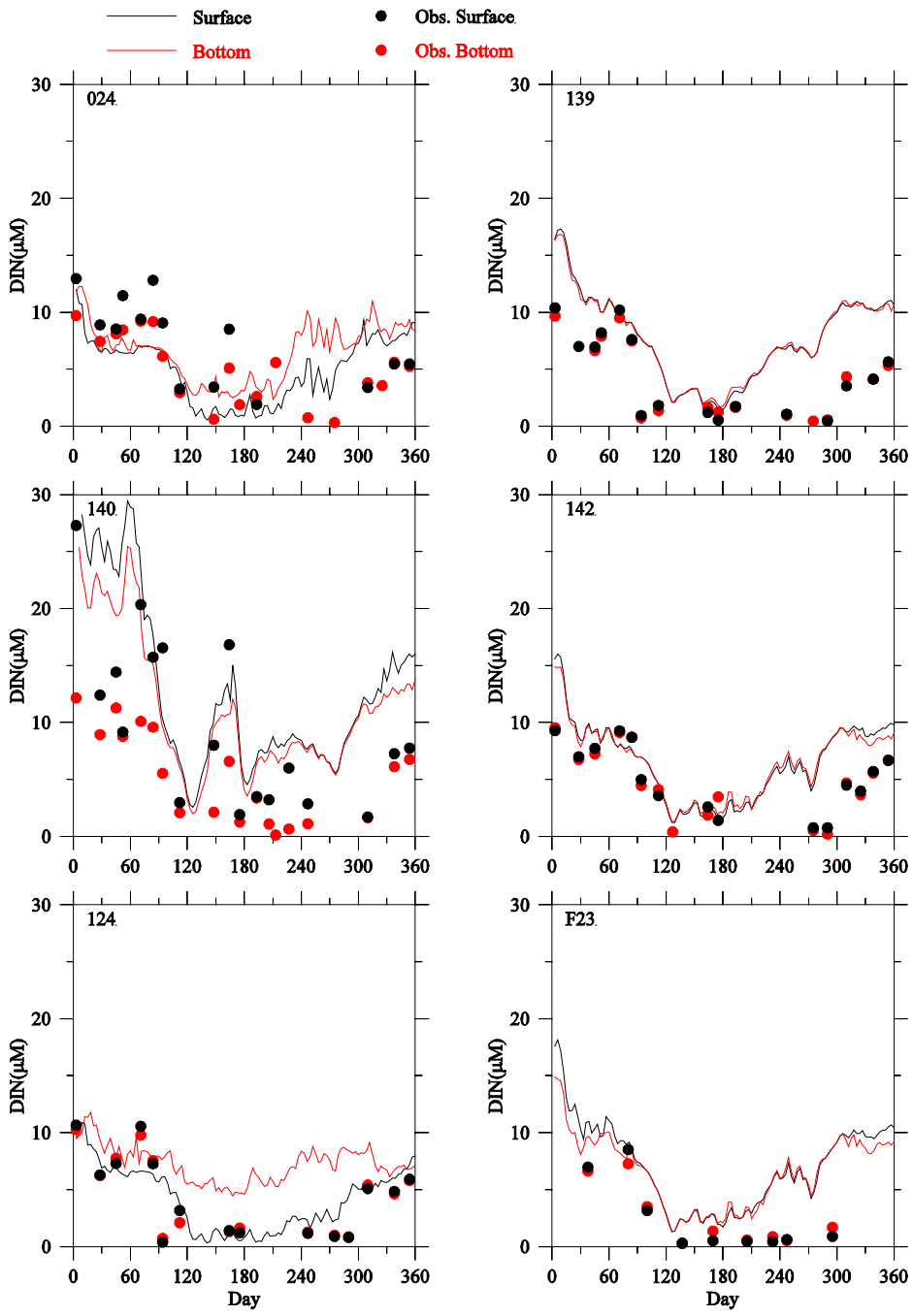

Figure 3.24 DIN: observed (dots) and modeled (lines) at harbor subset stations in 2013.

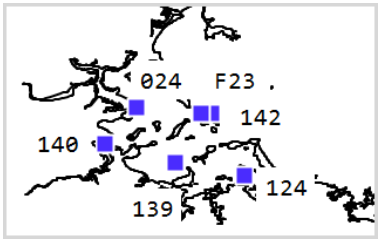

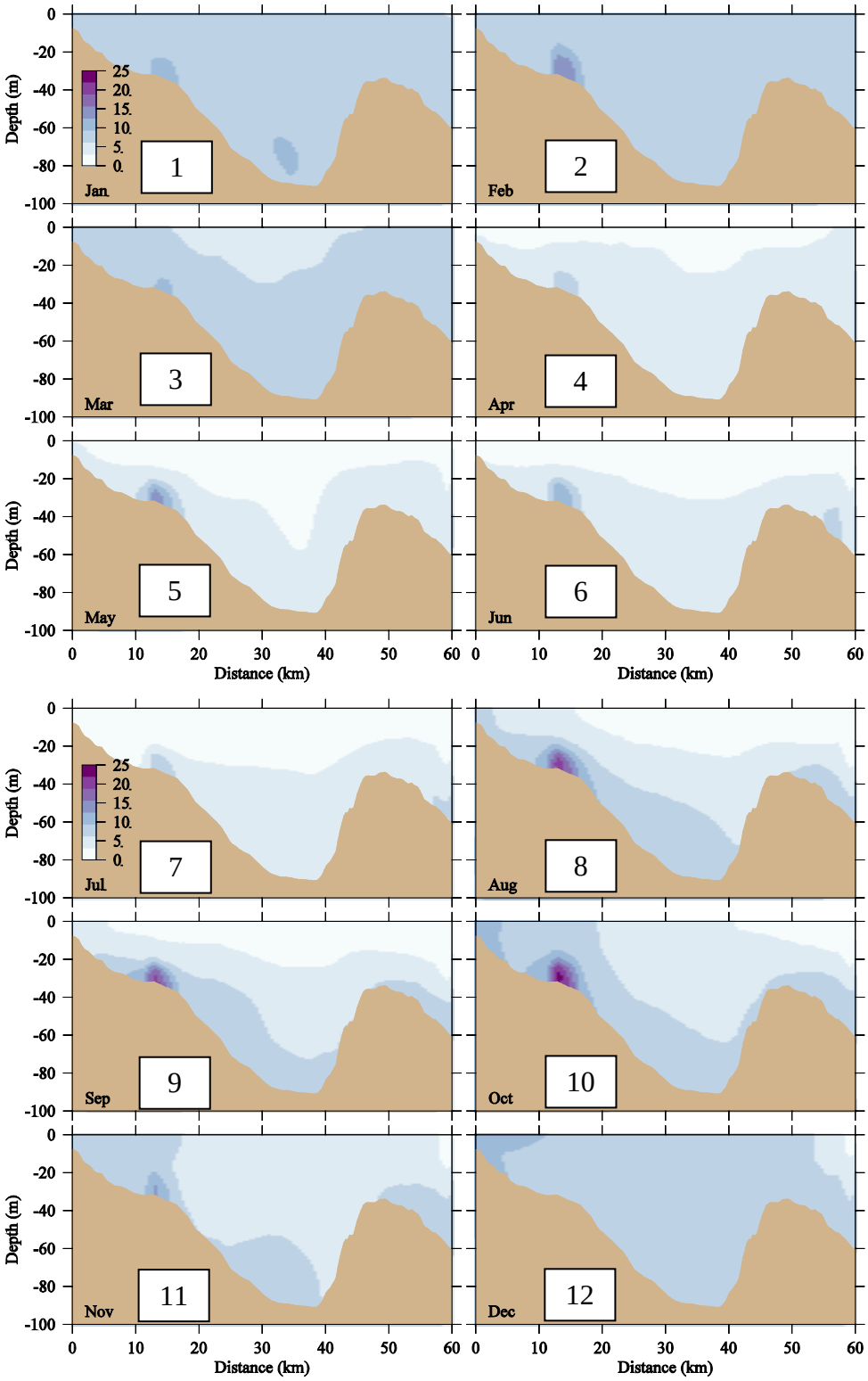

Figure 3.25 Model DIN (μM): west-east transect through MWRA outfall, end of each month, 2013.

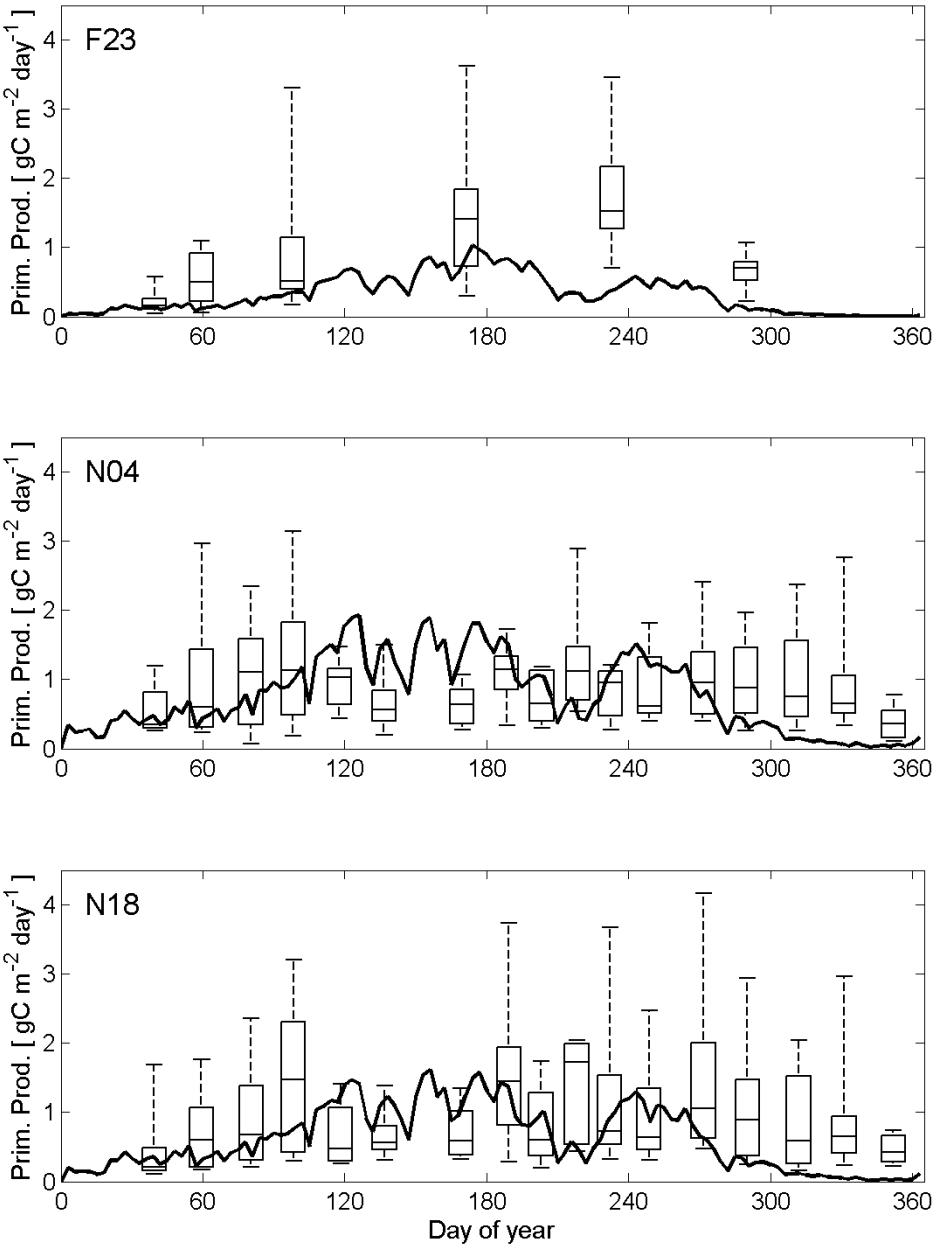

Figure 3.26 Model vertically-integrated primary production in 2013 (heavy line), with 1995-2010 observations (box-whiskers), at select MB stations.

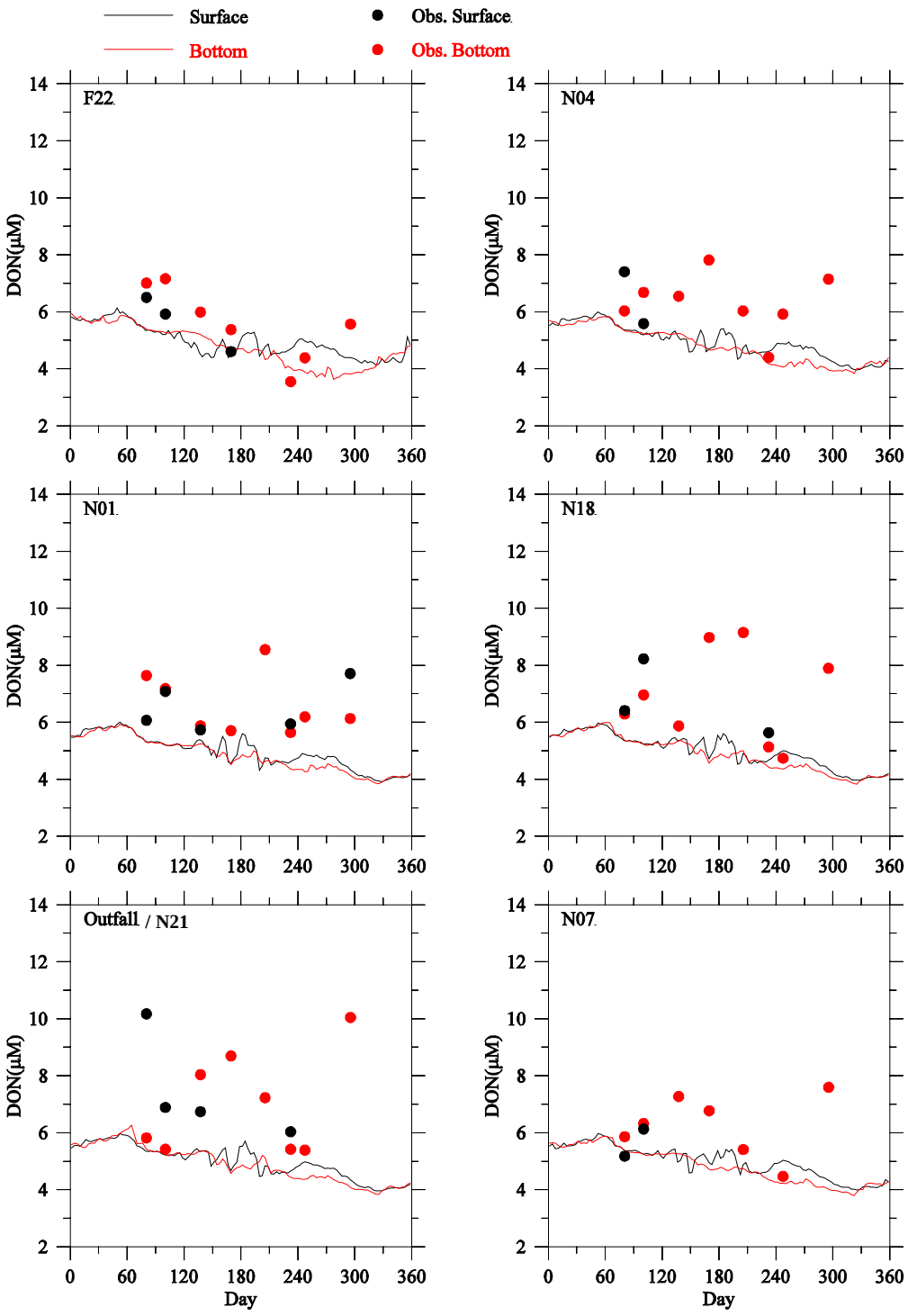

Figure 3.27 DON: observed (dots) and modeled (lines) at northern subset stations in 2013.

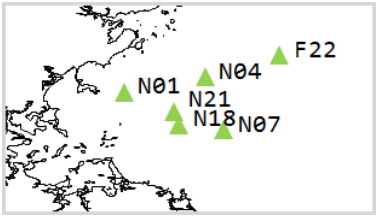

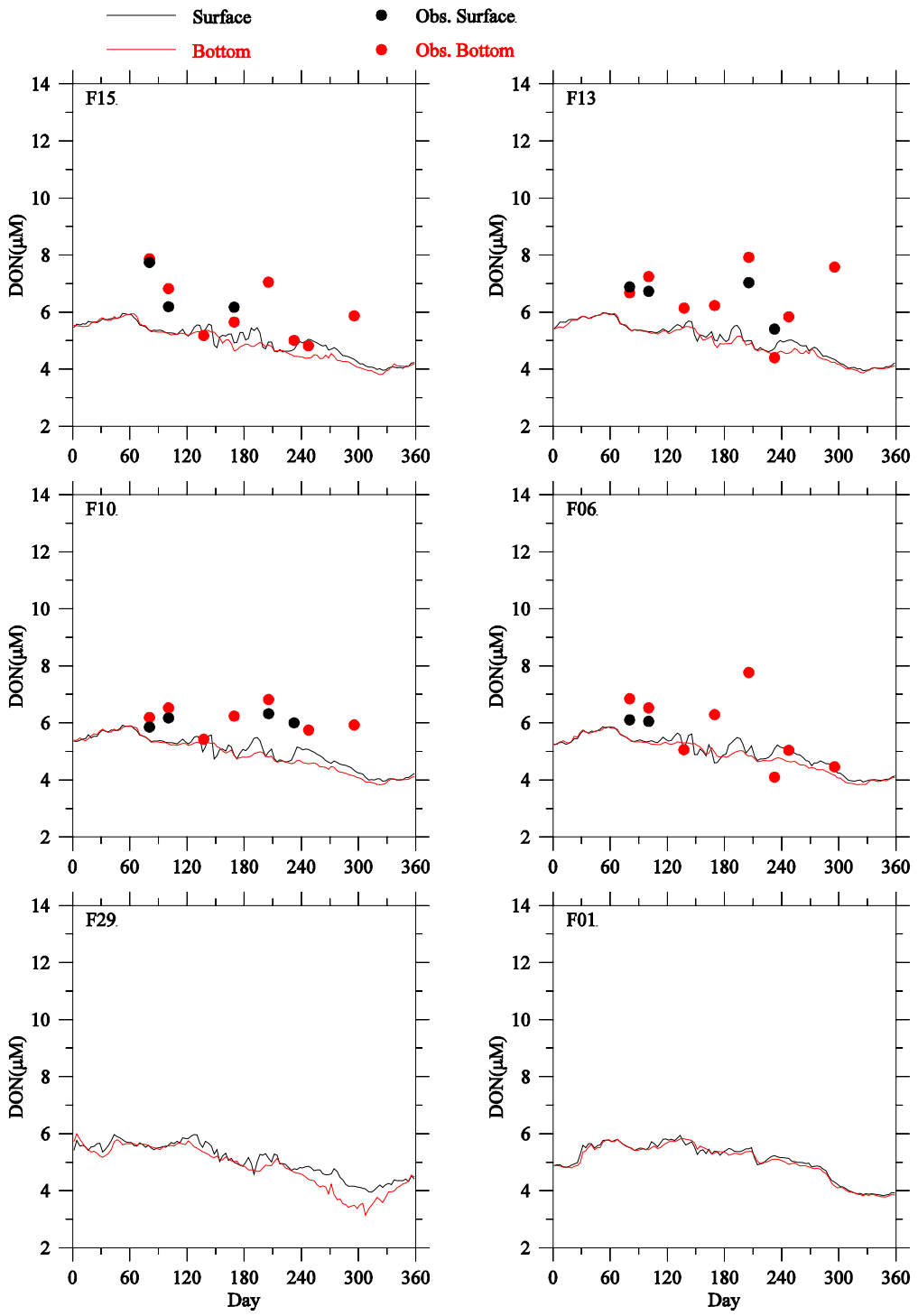

Figure 3.28 DON: observed (dots) and modeled (lines) at southern subset stations in 2013.

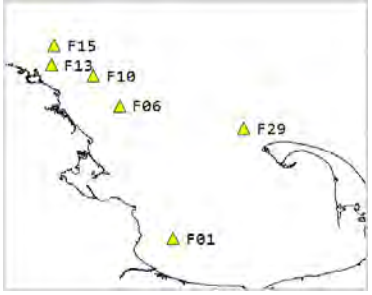

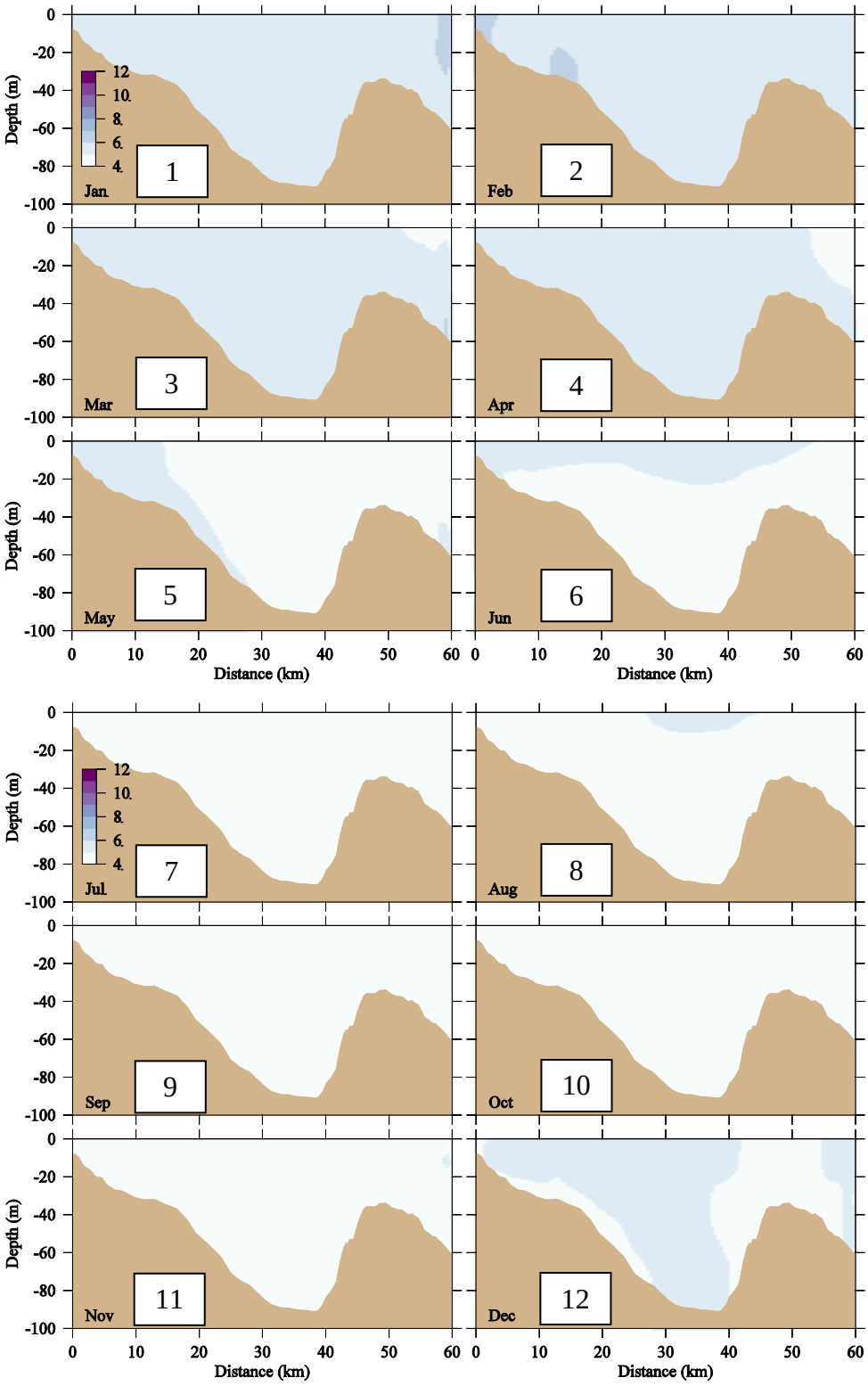

Figure 3.29 Model DON (μM): west-east transect through MWRA outfall, end of each month, 2013.

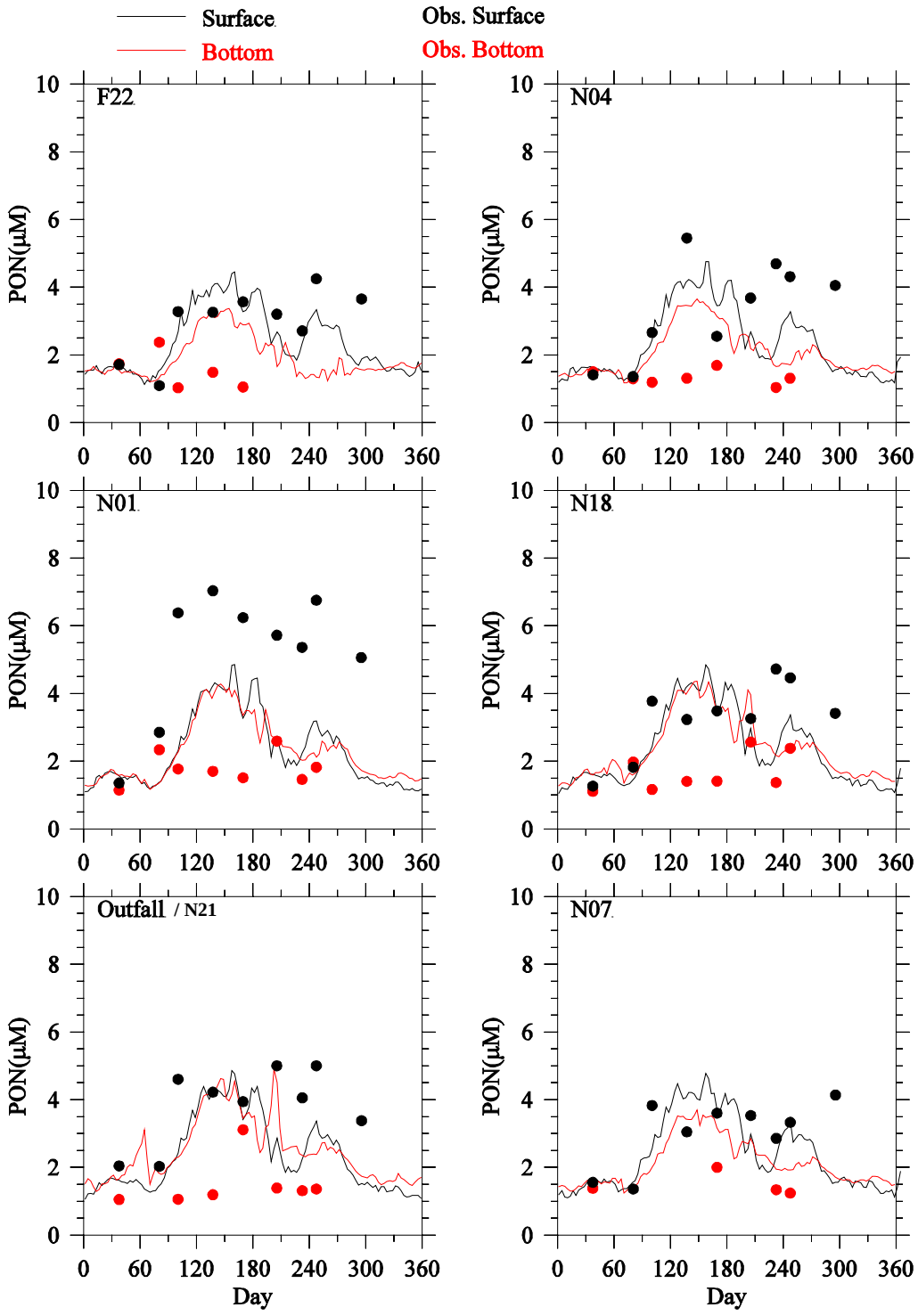

Figure 3.30 PON: observed (dots) and modeled (lines) at northern subset stations in 2013.

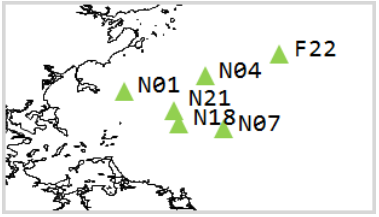

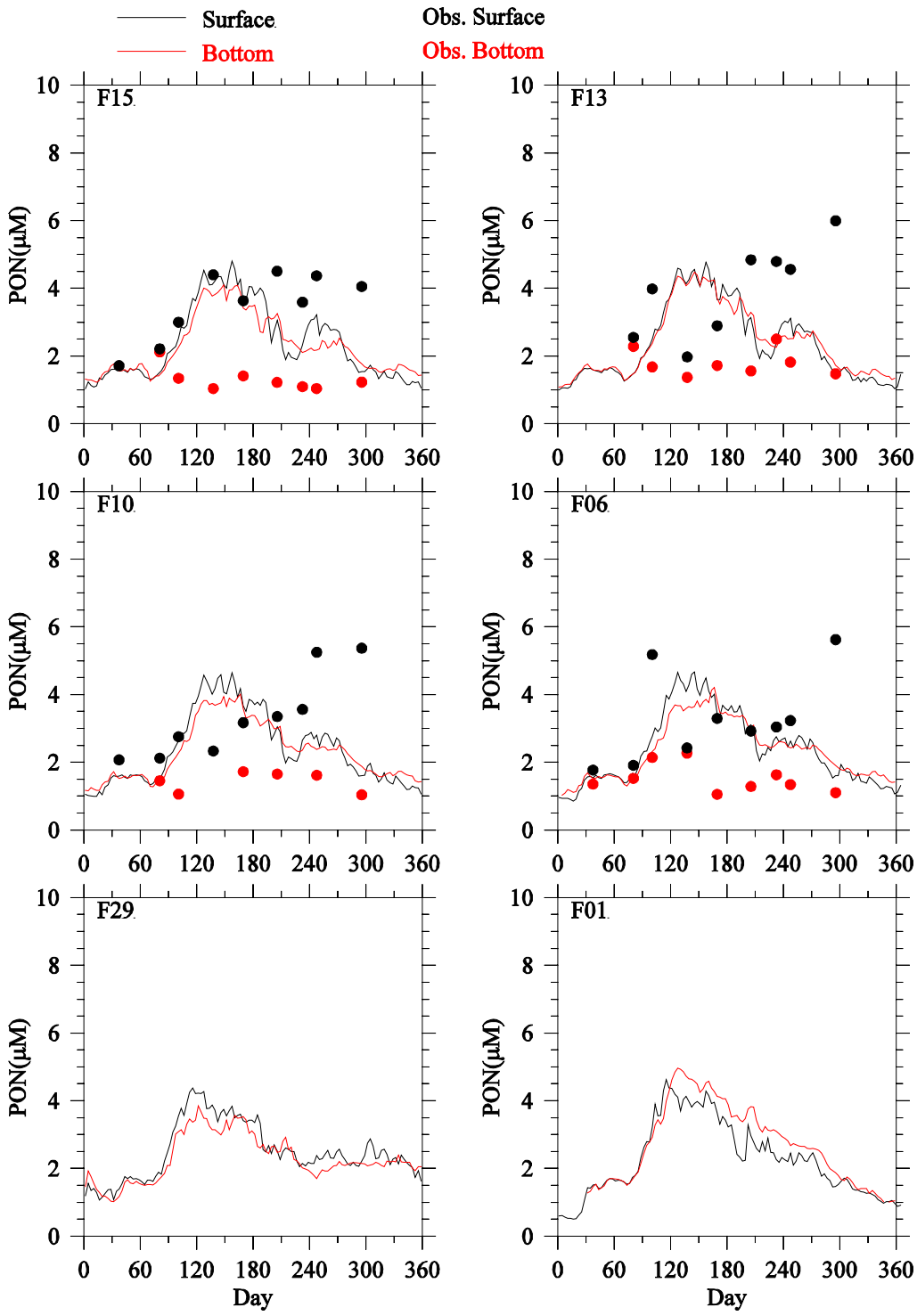

Figure 3.31 PON: observed (dots) and modeled (lines) at southern subset stations in 2013.

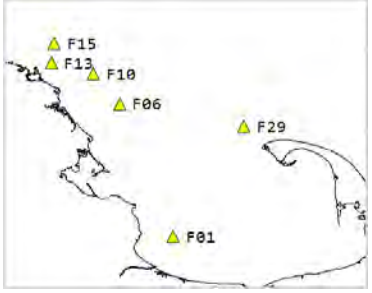

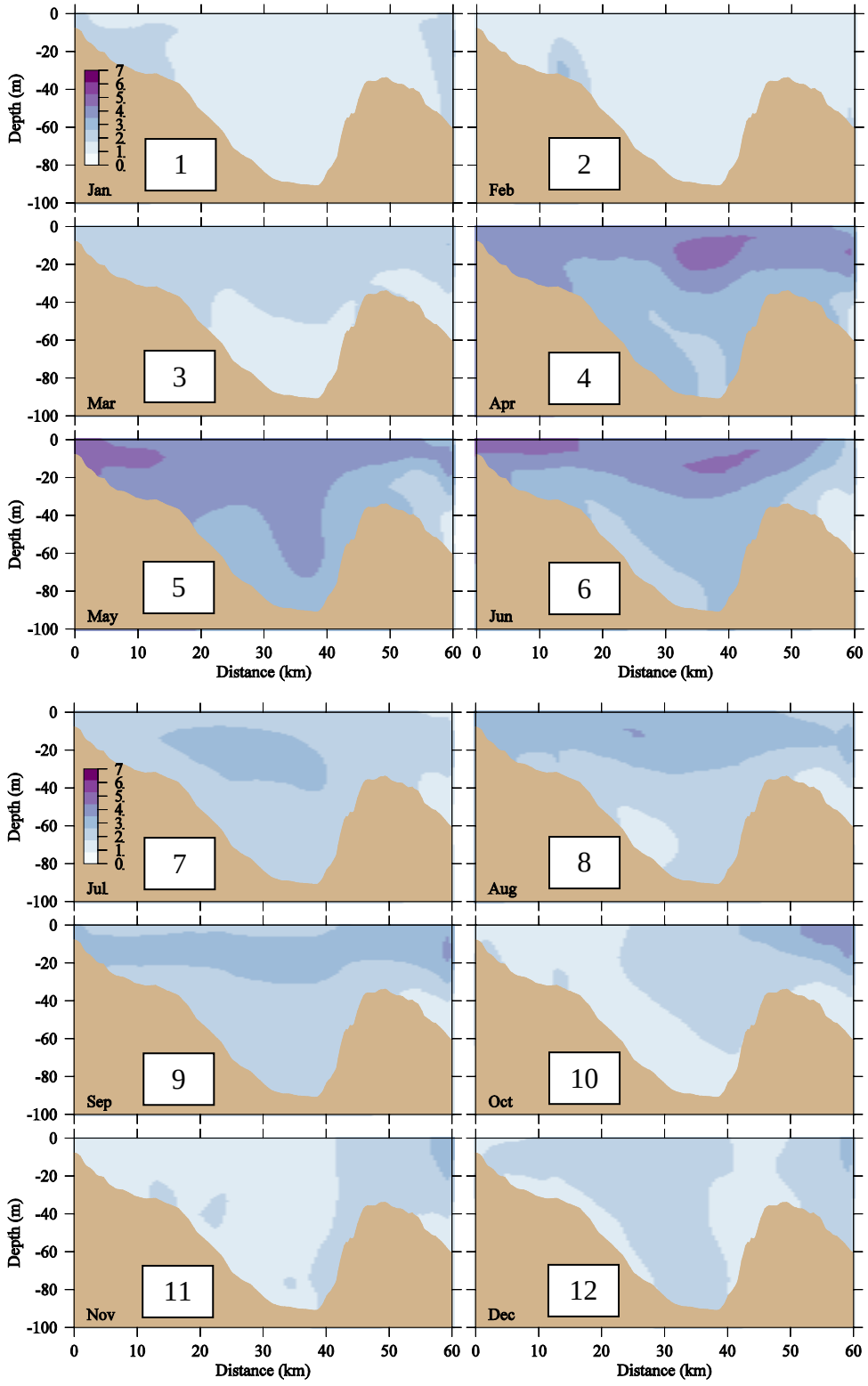

Figure 3.32 Model PON (μM): west-east transect through MWRA outfall, end of each month, 2013.

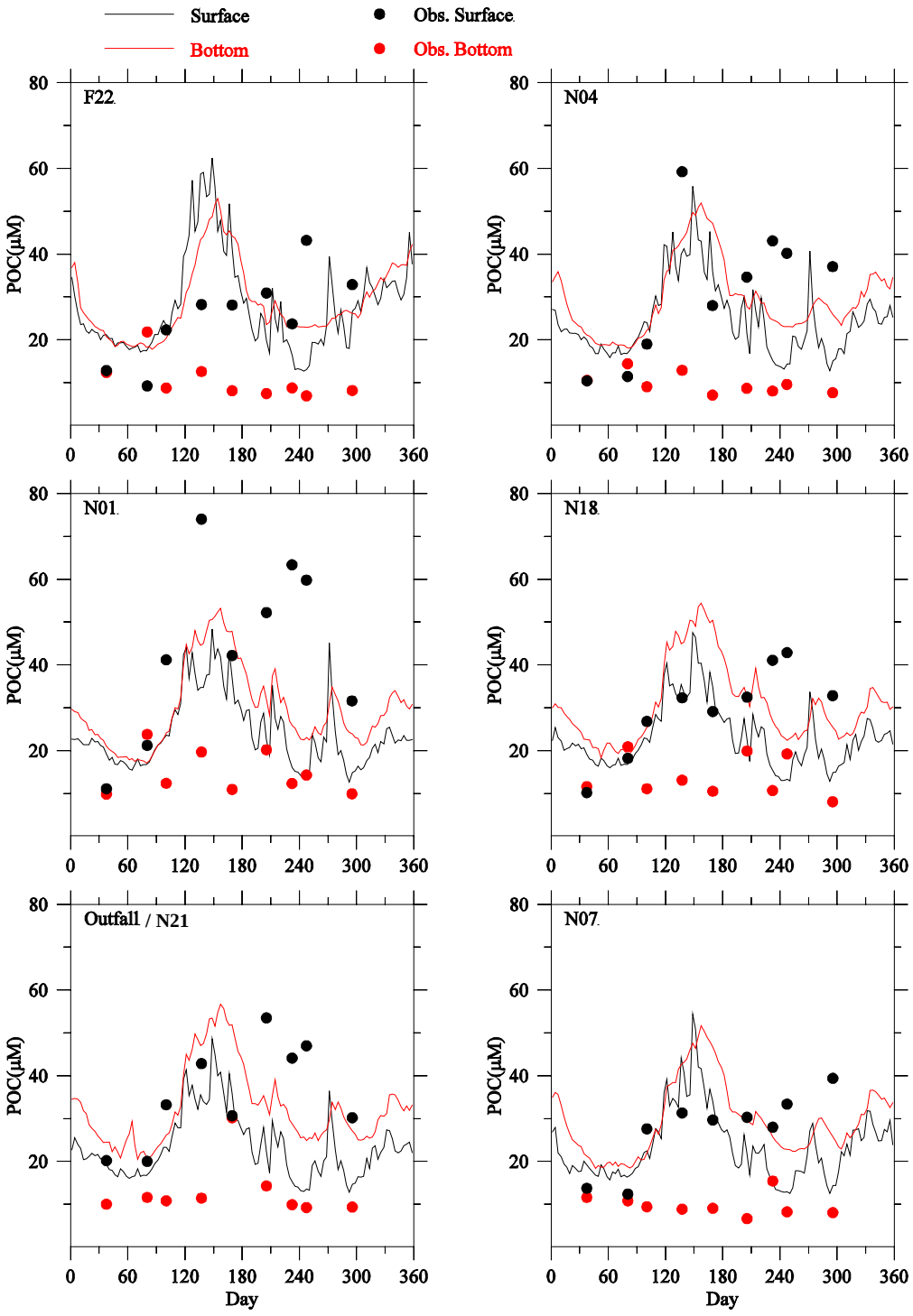

Figure 3.33 POC: observed (dots) and modeled (lines) at northern subset stations in 2013.

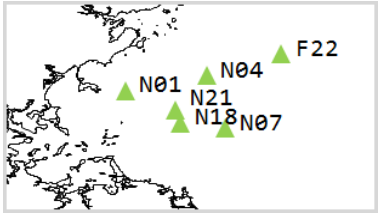

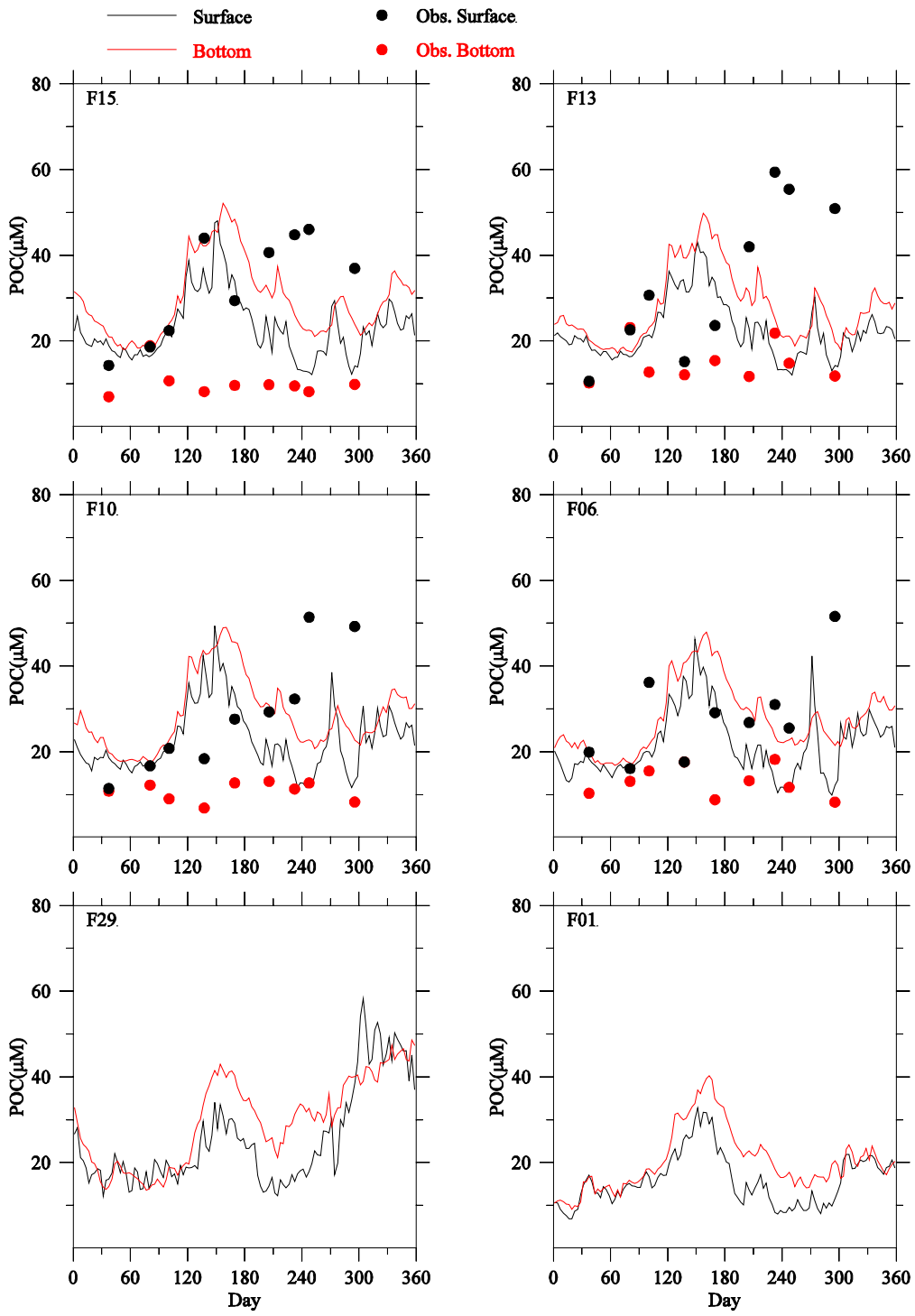

Figure 3.34 POC: observed (dots) and modeled (lines) at southern subset stations in 2013.

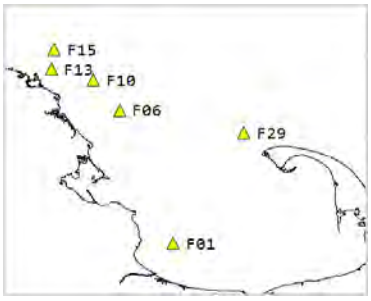

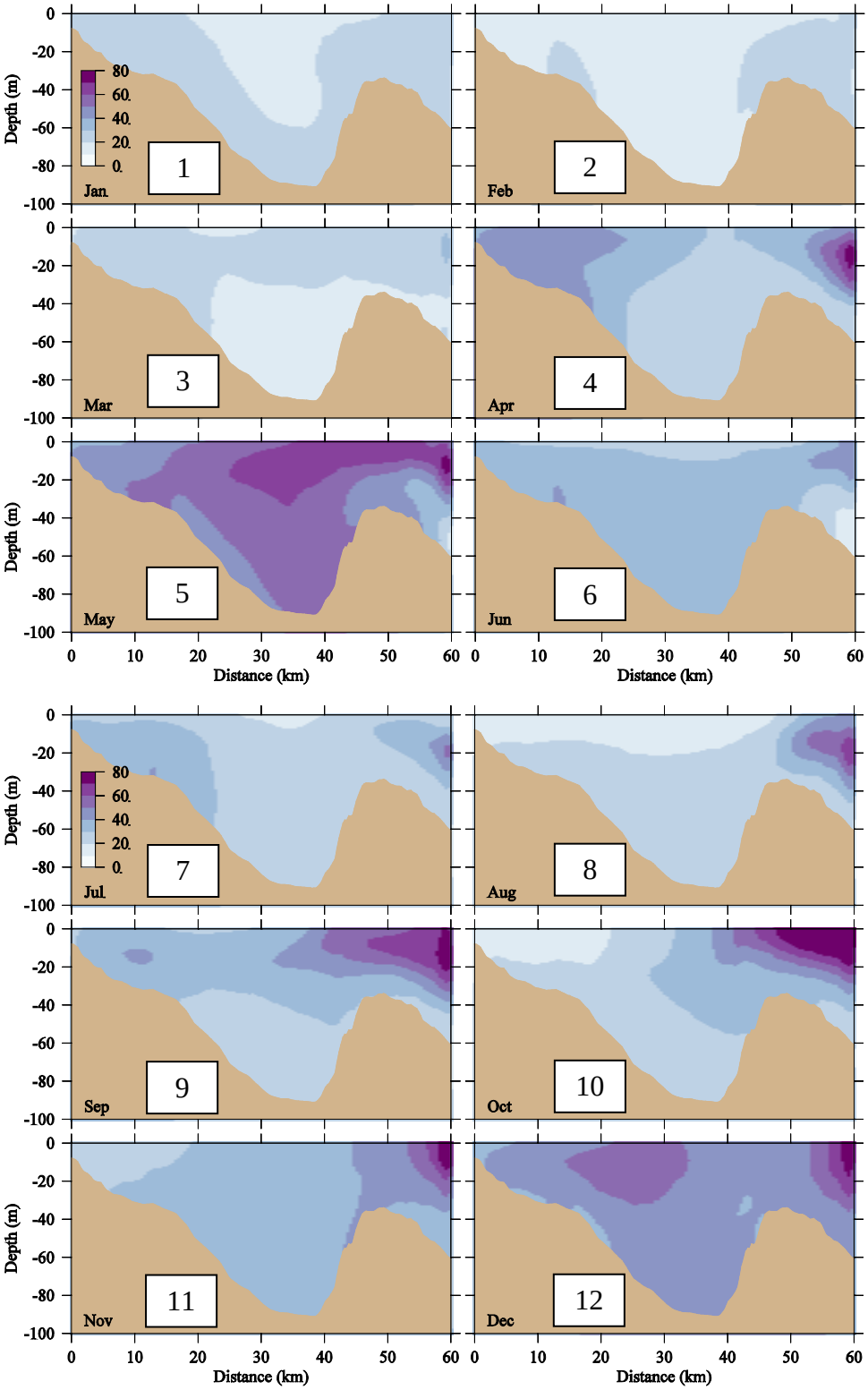

Figure 3.35 Model POC (μM): west-east transect through MWRA outfall, end of each month, 2013.

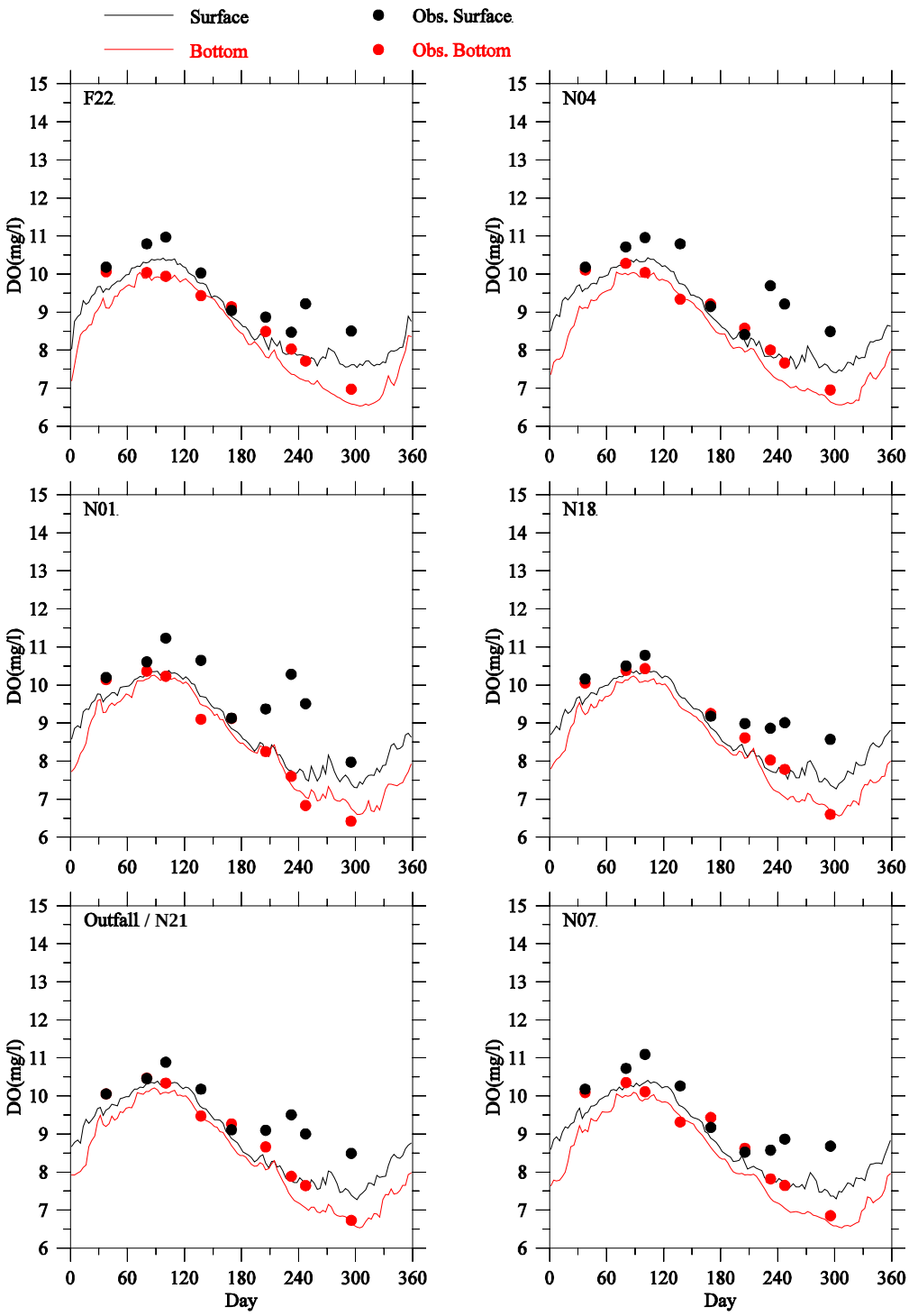

Figure 3.36 DO (mg L^{-1}): observed (dots) and modeled (lines) at northern subset stations in 2013.

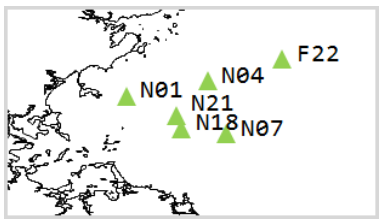

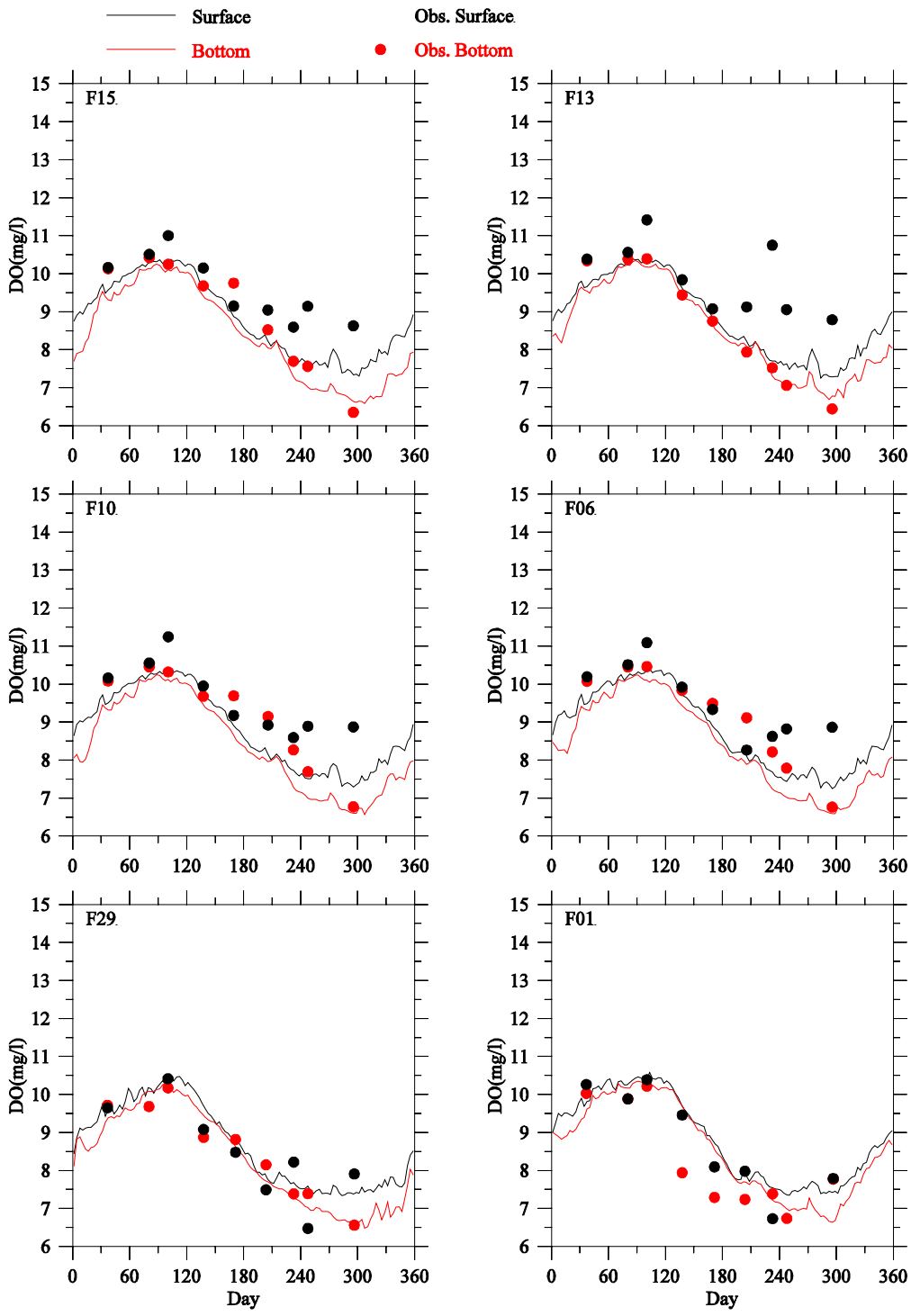

Figure 3.37 DO (mg L^{-1}): observed (dots) and modeled (lines) at southern subset stations in 2013.

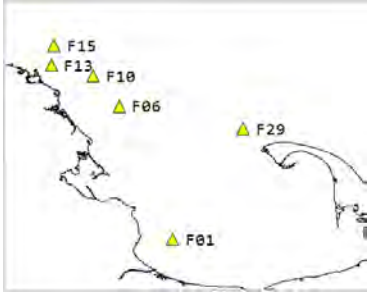

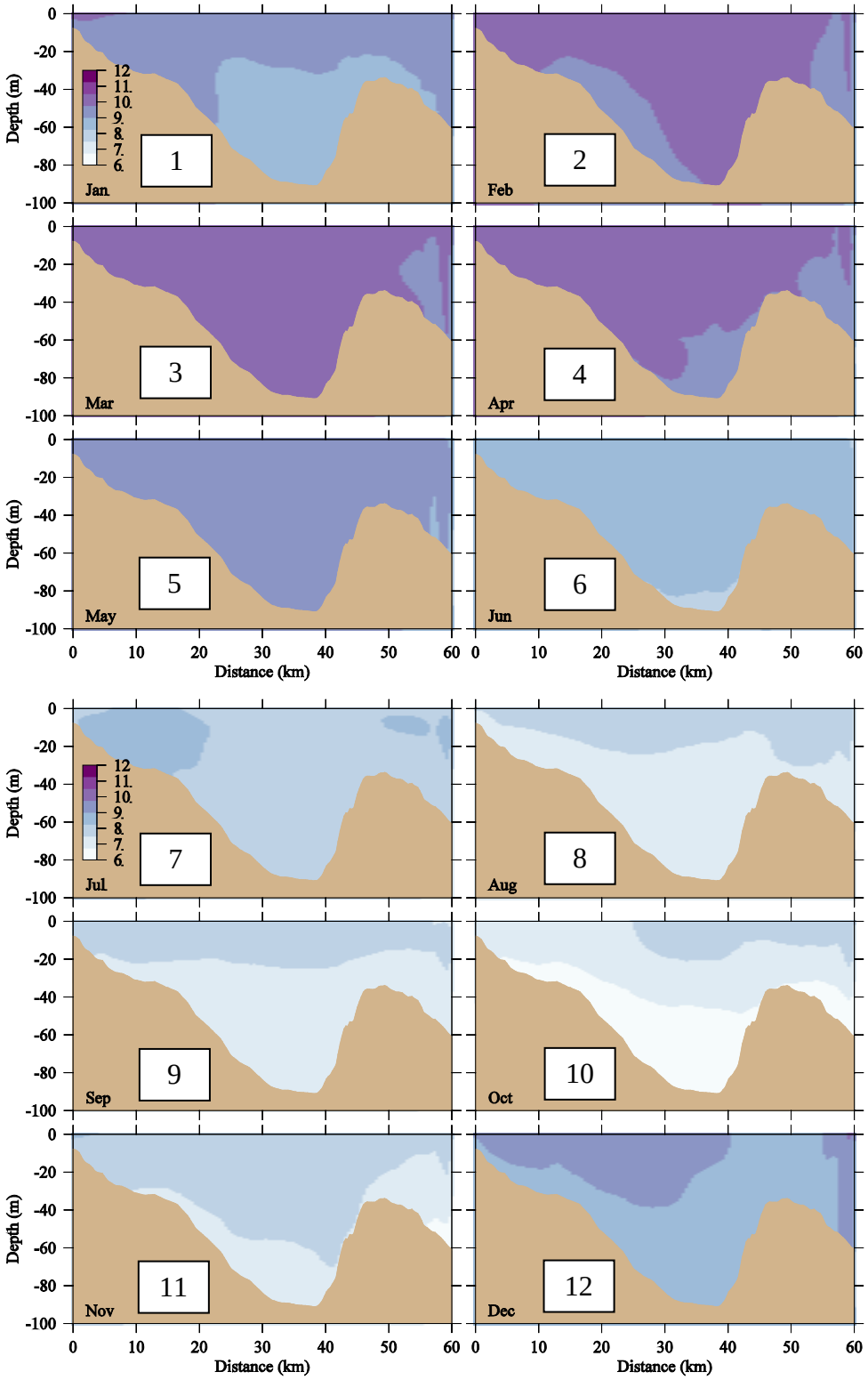

Figure 3.38 Model DO (mg L^{-1}): west-east transect through MWRA outfall, end of each month, 2013.

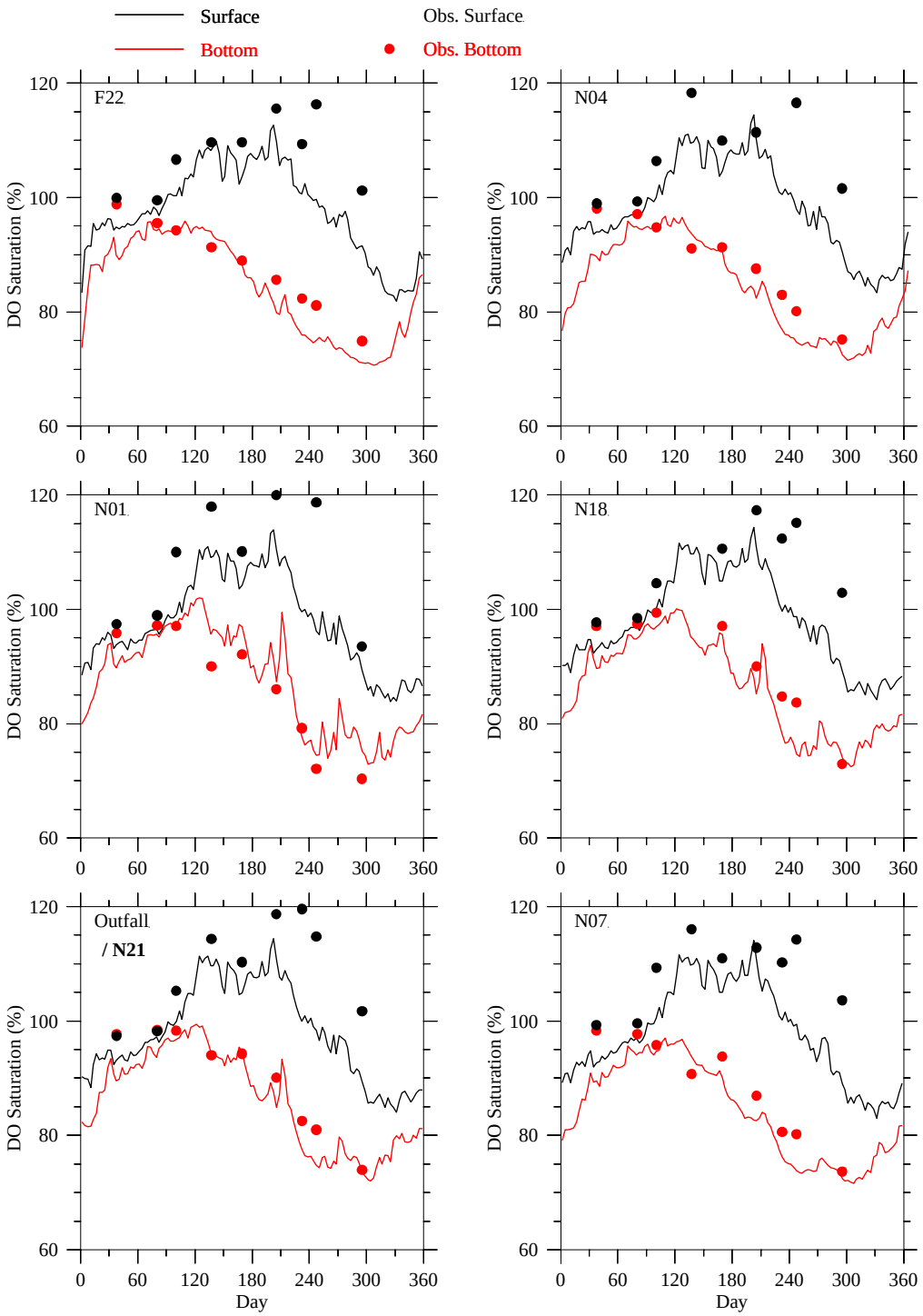

Figure 3.39 DO saturation (%): observed (dots) and modeled (lines) at northern subset stations in 2013.

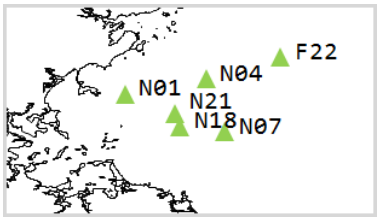

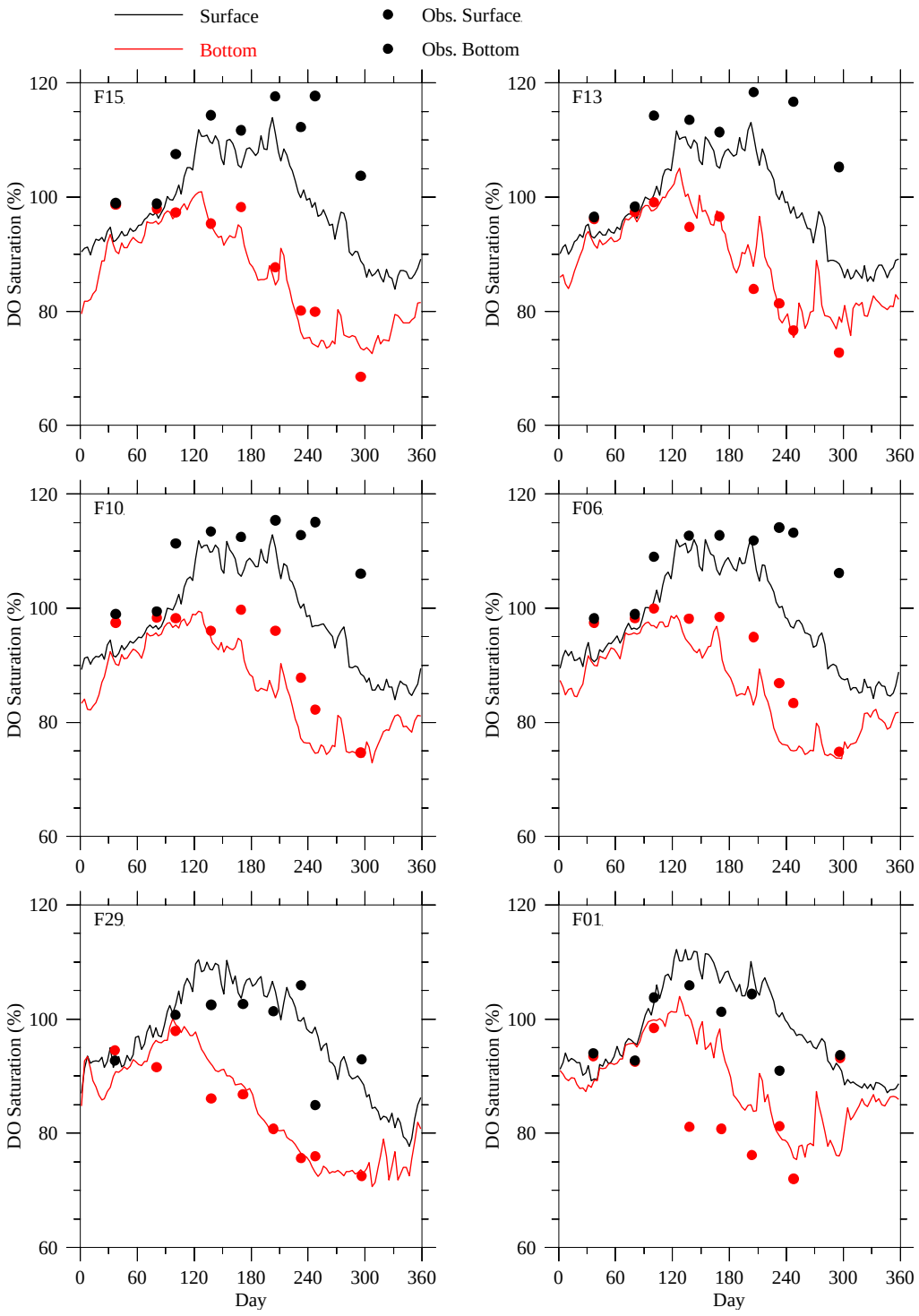

Figure 3.40 DO saturation (%): observed (dots) and modeled (lines) at southern subset stations in 2013.

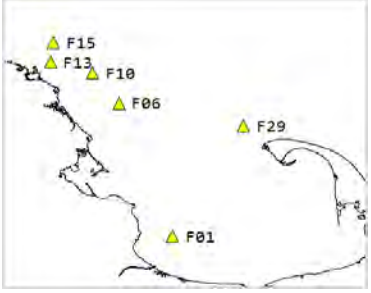

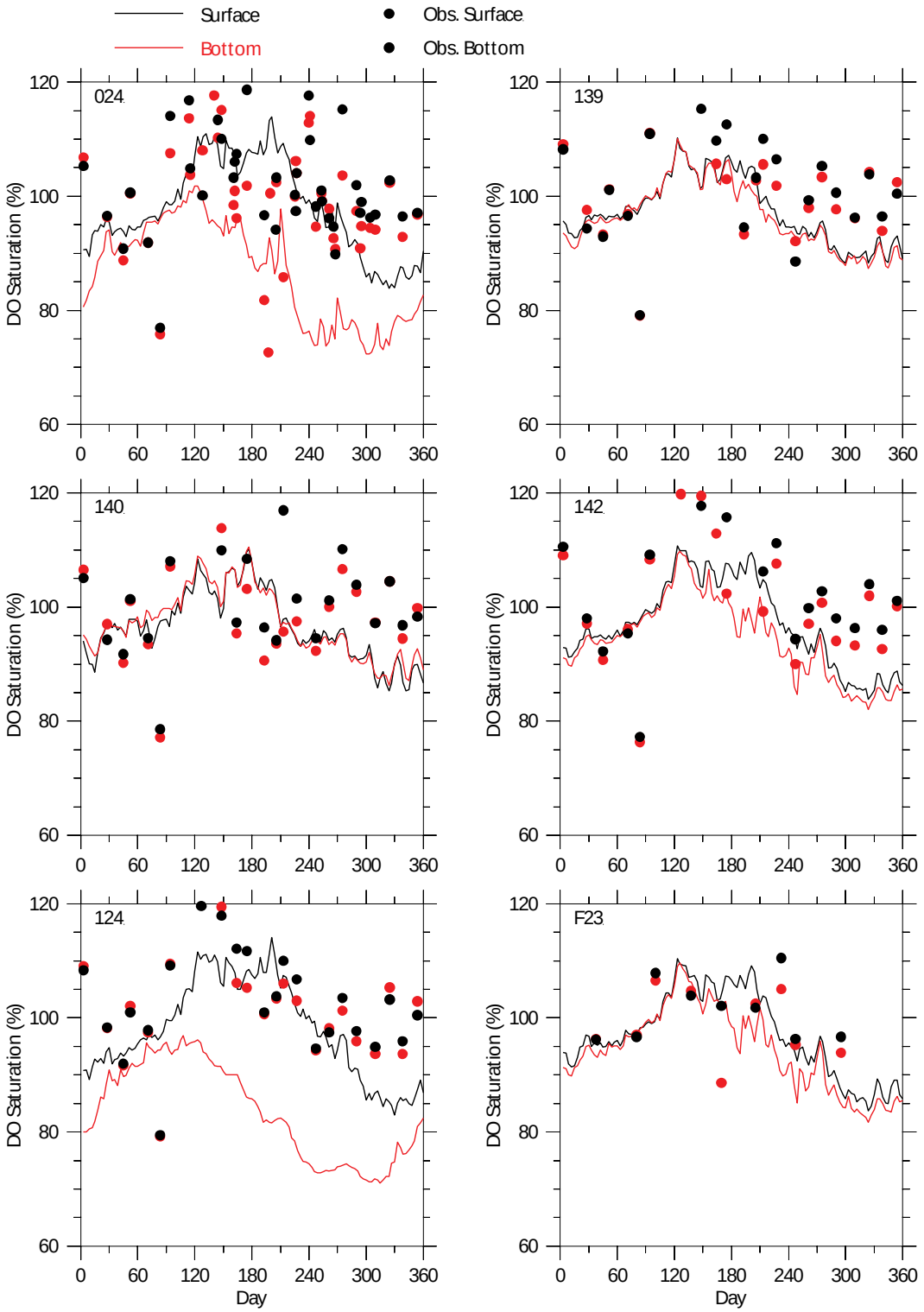

Figure 3.41 DO saturation (%): observed (dots) and modeled (lines) at harbor subset stations in 2013.

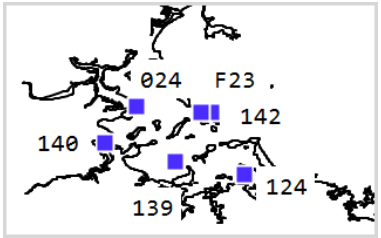

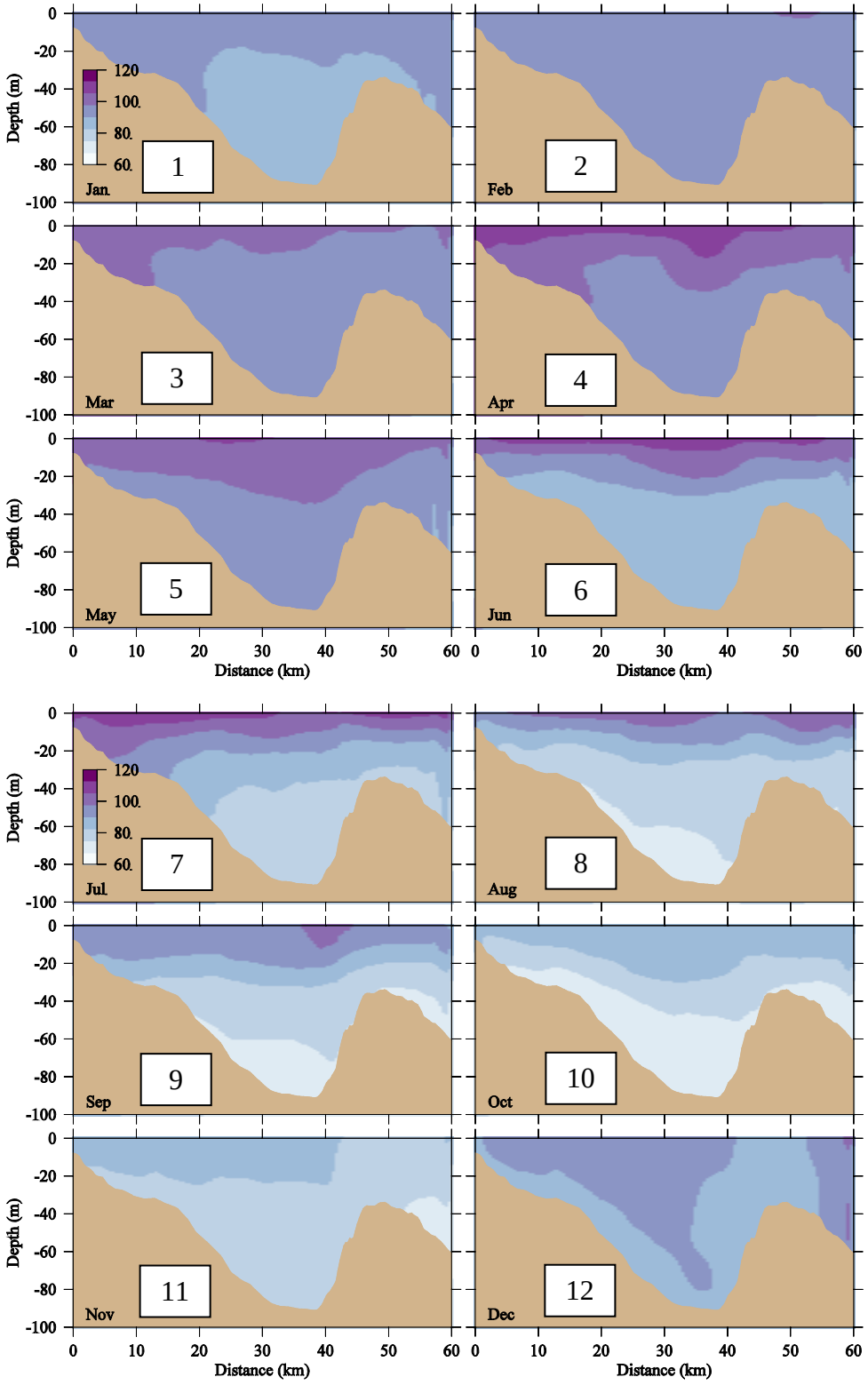

Figure 3.42 Model DO saturation (%): west-east transect through MWRA outfall, end of each month, 2013.

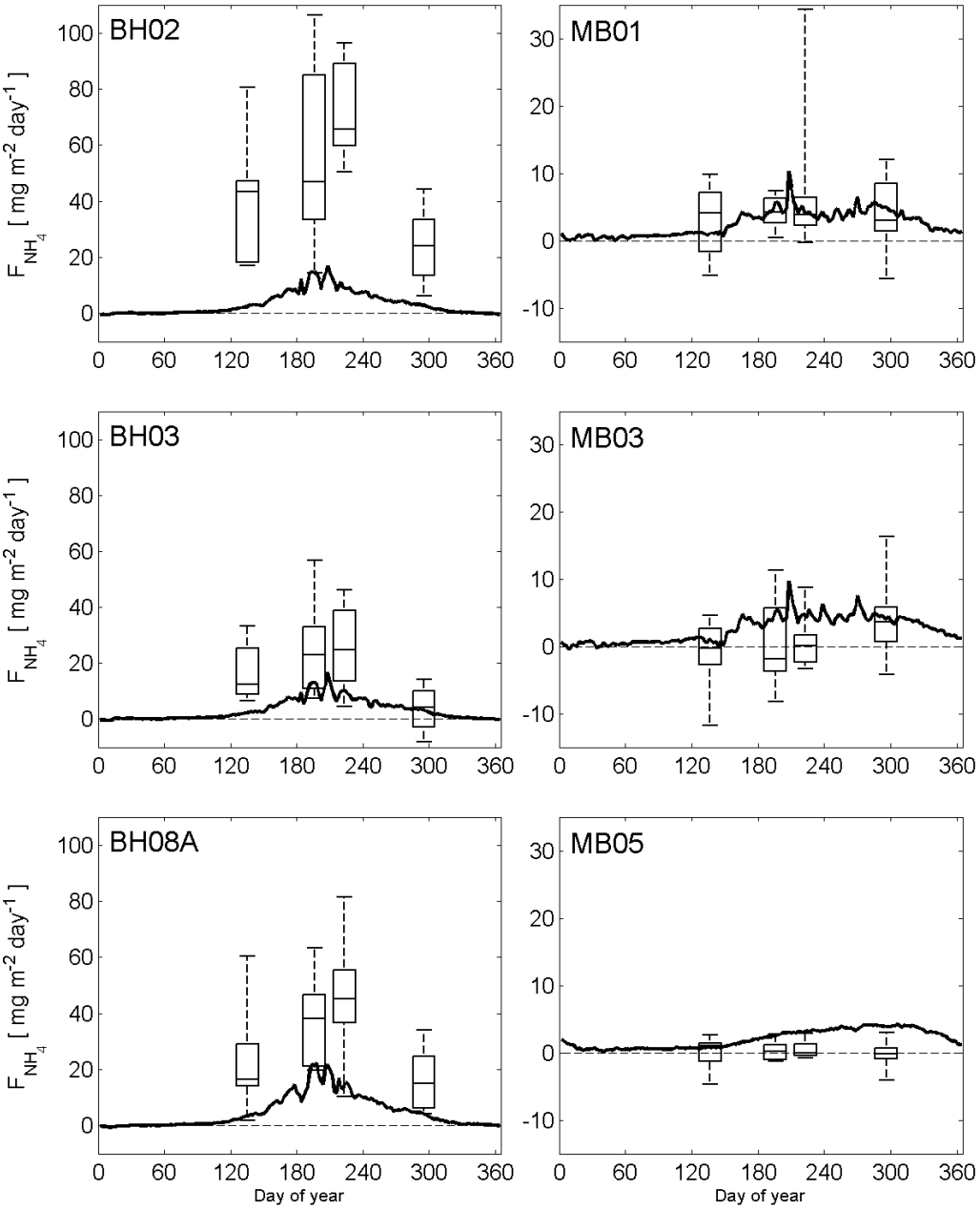

Figure 3.43 Model sediment NH_4^+ flux in 2013 (heavy line), with 2001-2010 observations (box-whiskers), at select sediment flux study stations.

Note scale change between BH stations (left column) and MB stations (right column).

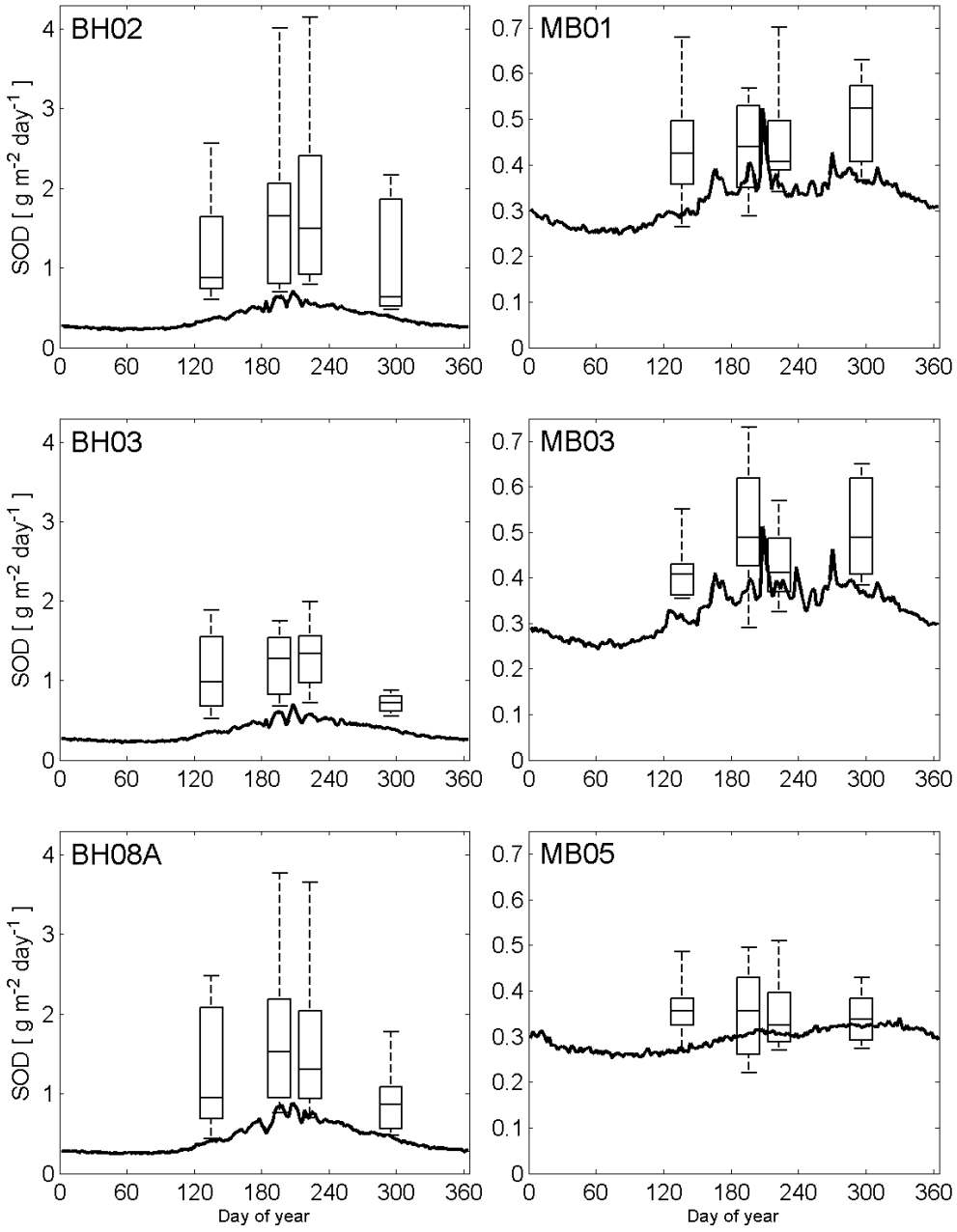

Figure 3.44 Model sediment oxygen demand in 2013 (heavy line), with 2001-2010 observations (box-whiskers), at select sediment flux study stations.

Note scale change between BH stations (left column) and MB stations (right column).

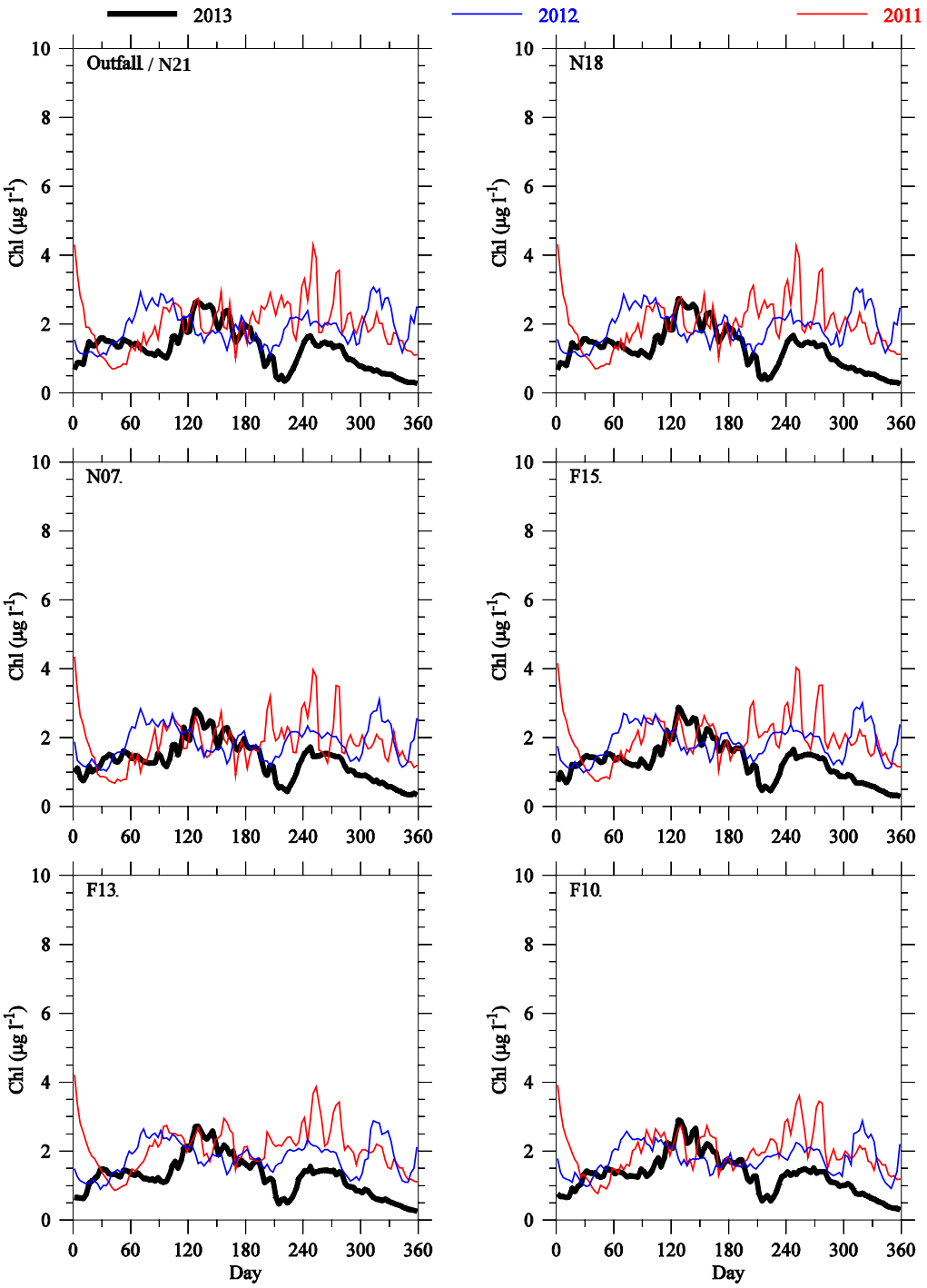

Figure 3.45 Seasonal and interannual variations, model surface chlorophyll, select MB stations: 2011 (red lines), 2012 (blue lines), and 2013 (black lines).

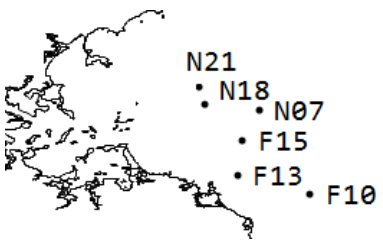

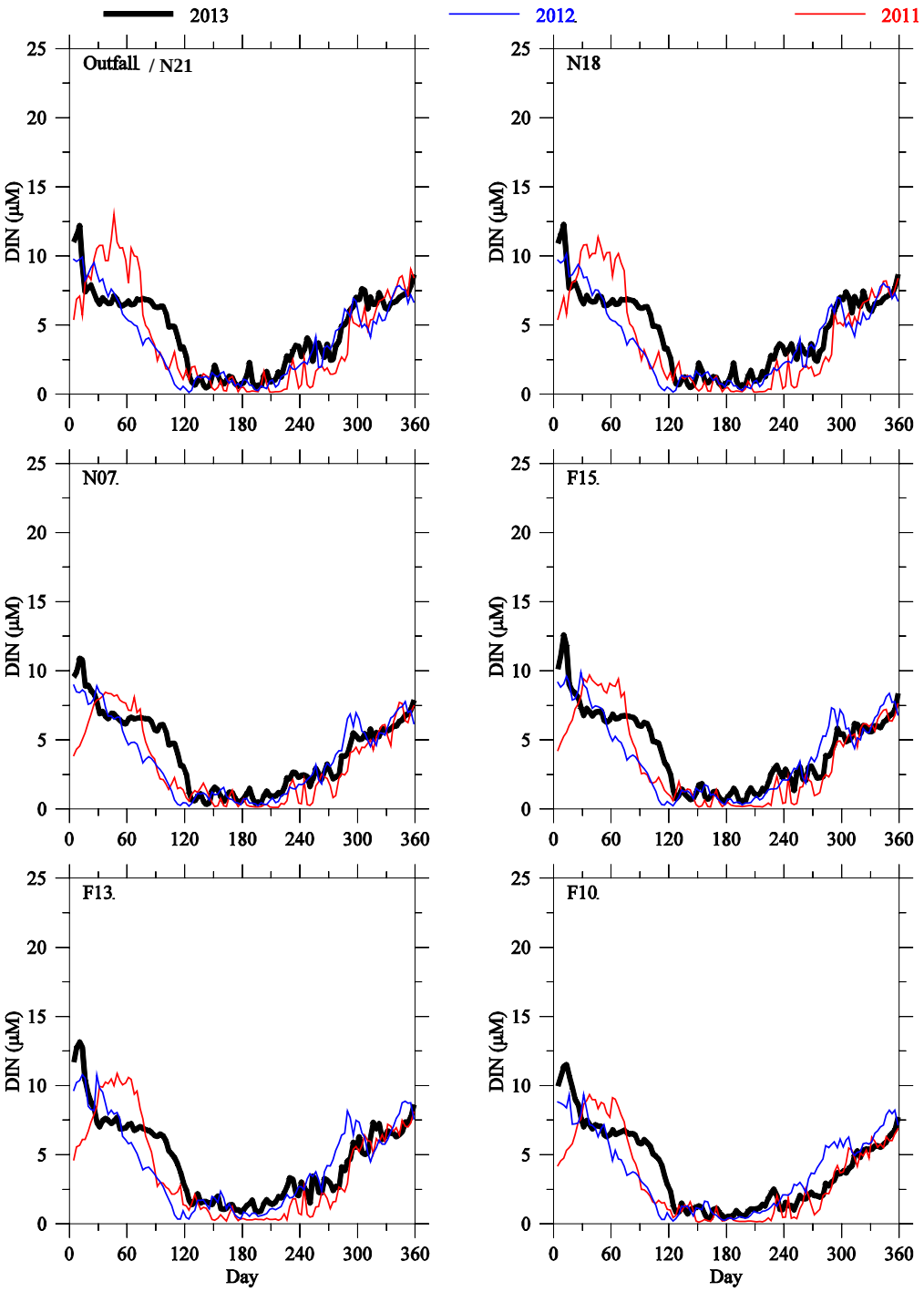

Figure 3.46 Seasonal and interannual variations, model surface DIN at select MB stations: 2011 (red lines), 2012 (blue lines), and 2013 (black lines).

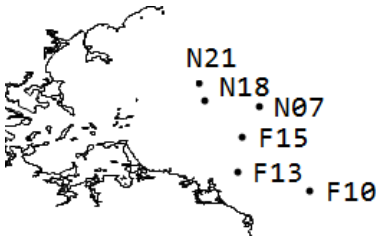

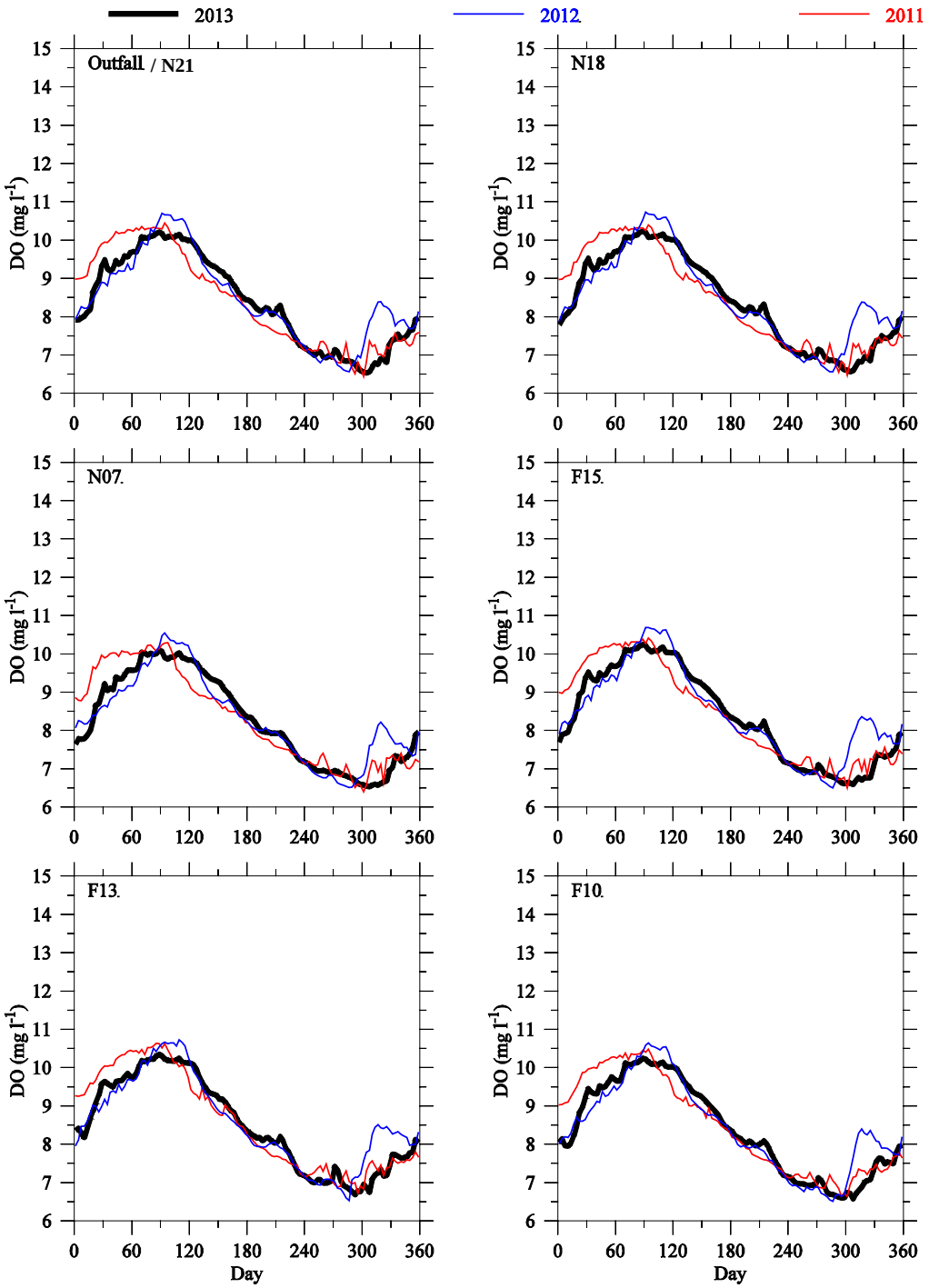

Figure 3.47 Seasonal and interannual variations, model bottom DO (mg L^{-1}) at select MB stations: 2011 (red lines), 2012 (blue lines), and 2013 (black lines).

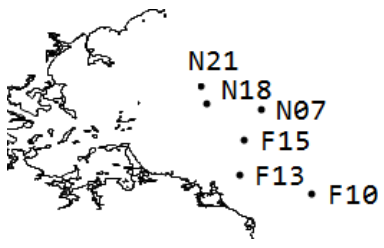

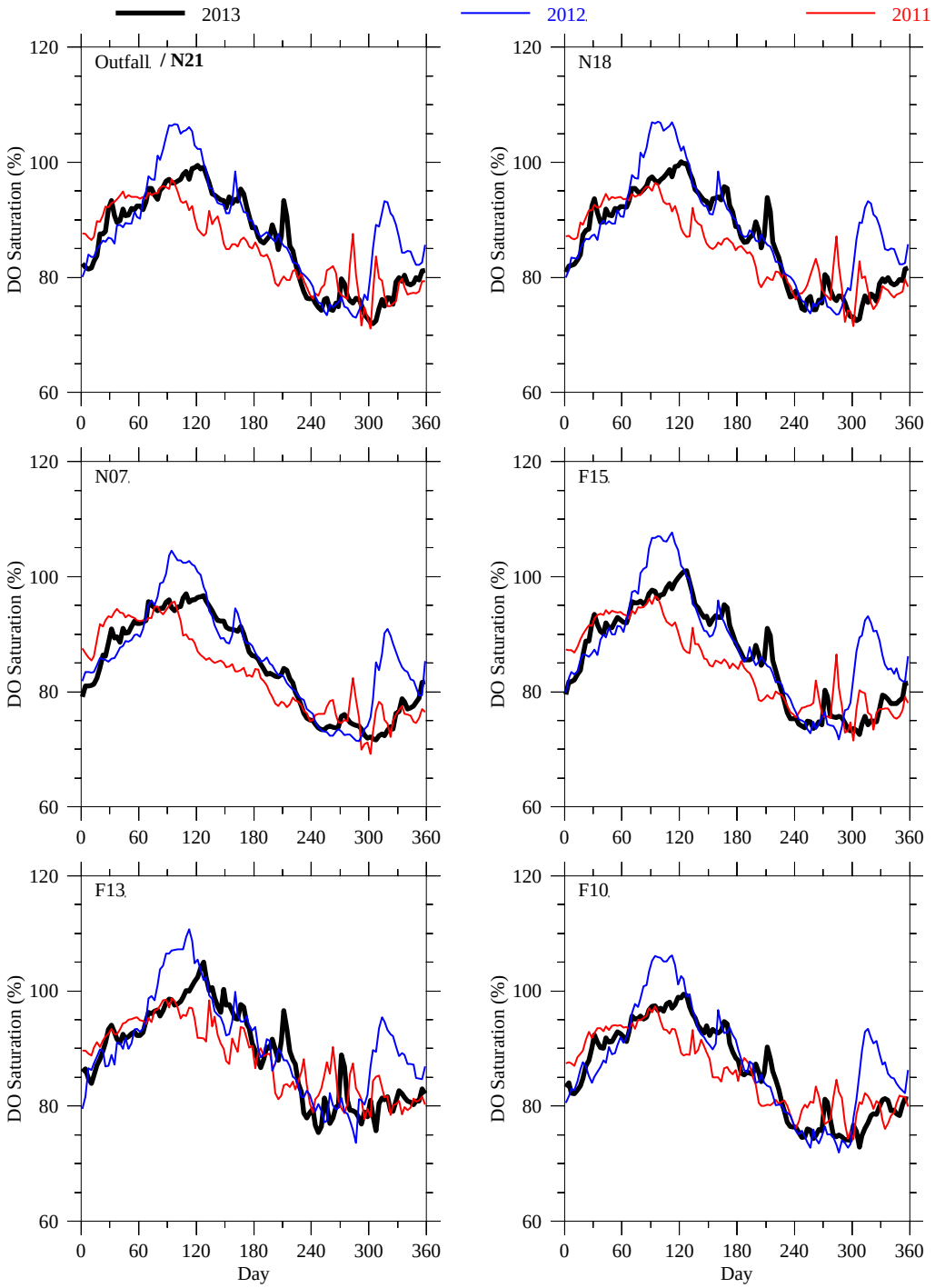

Figure 3.48 Seasonal and interannual variations, model bottom DO saturation (%) at select MB stations: 2011 (red lines), 2012 (blue lines), and 2013 (black lines).

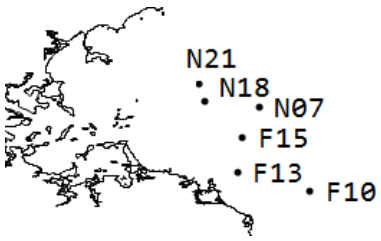

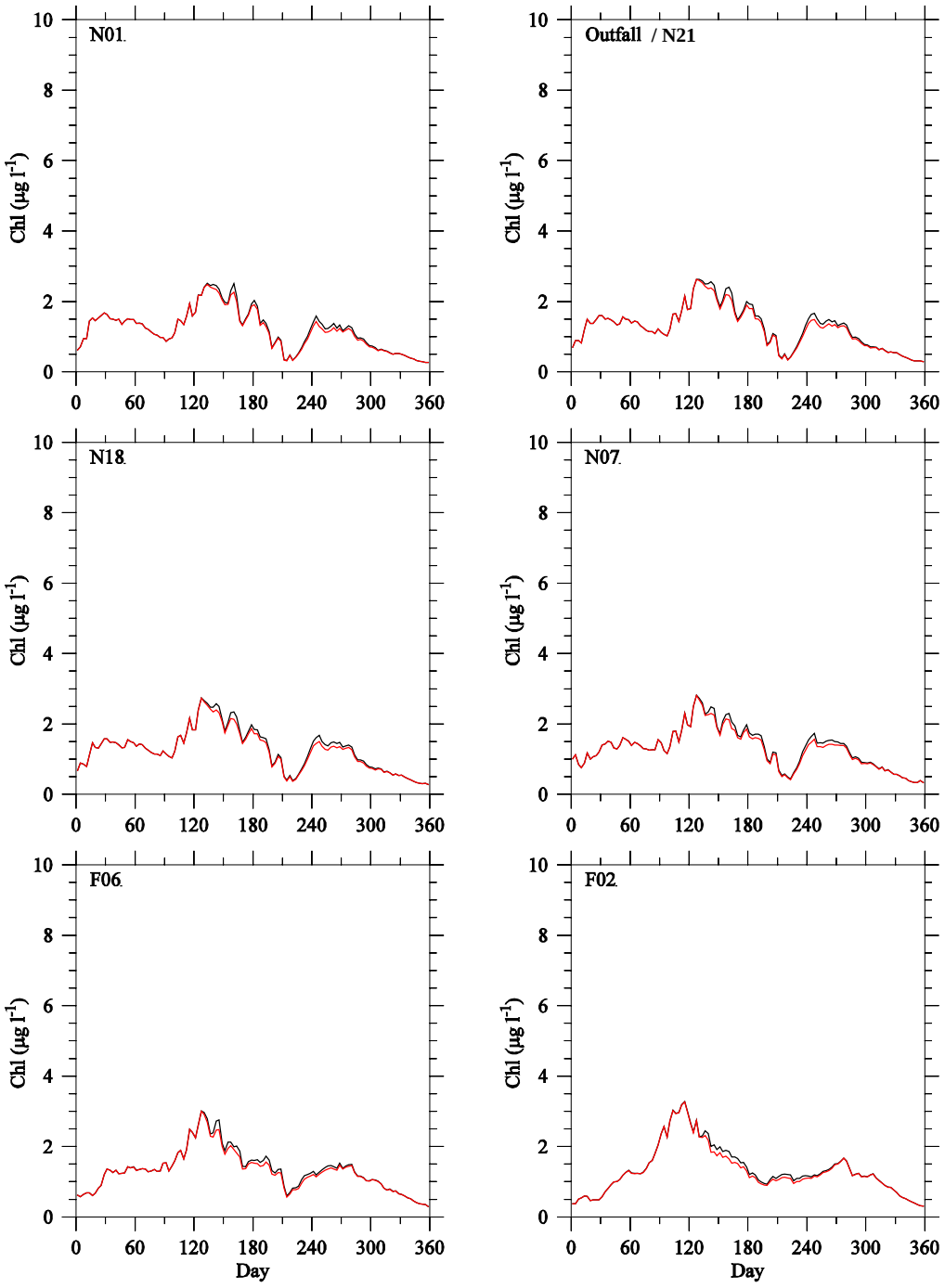

Figure 4.1 Scenario experiment surface chlorophyll: control run (black line) and non-sewage (red line) at select MB stations in 2013.

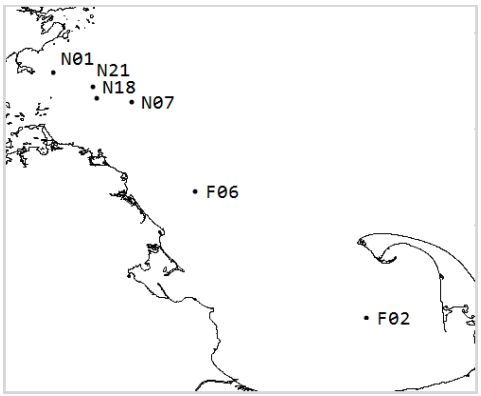

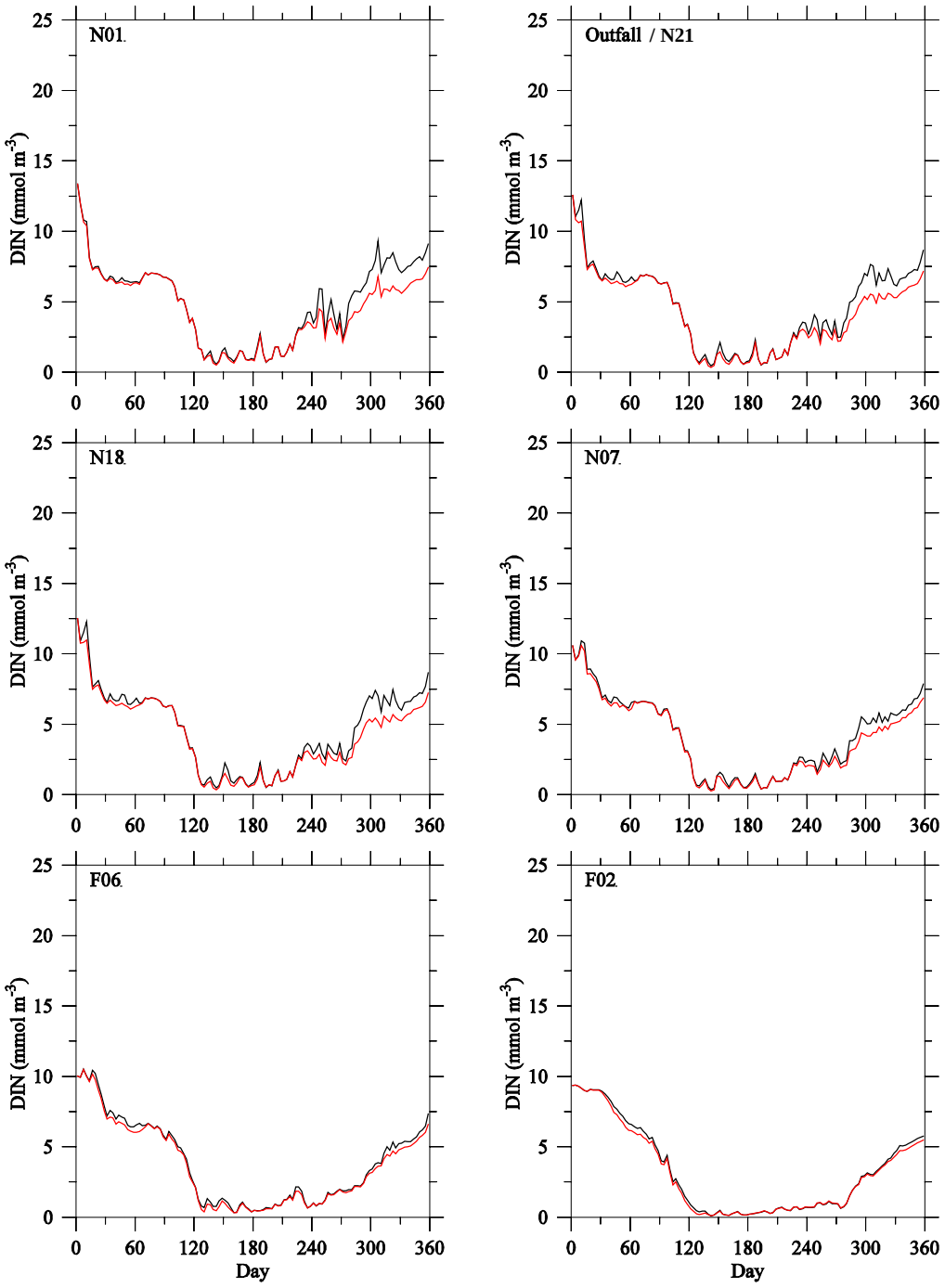

Figure 4.2 Scenario experiment surface DIN: control run (black line) and non-sewage (red line) at select MB stations in 2013.

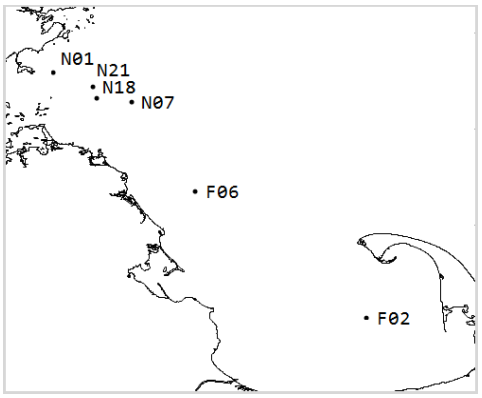

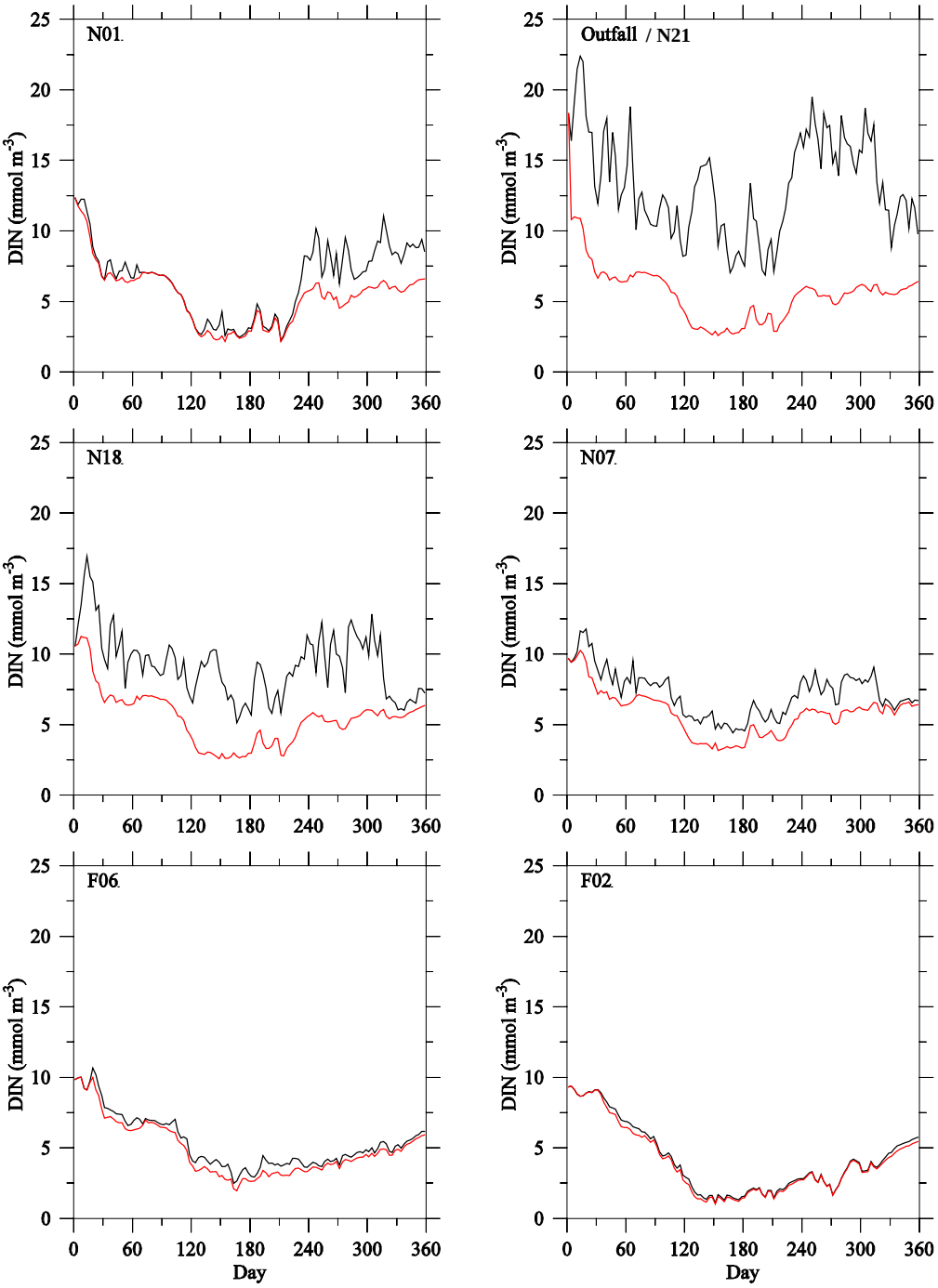

Figure 4.3 Scenario experiment bottom DIN: control run (black line) and non-sewage (red line) at select MB stations in 2013.

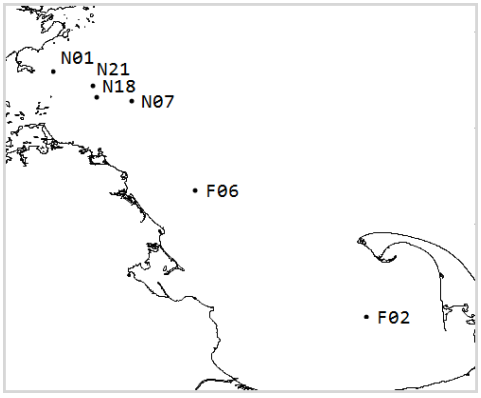

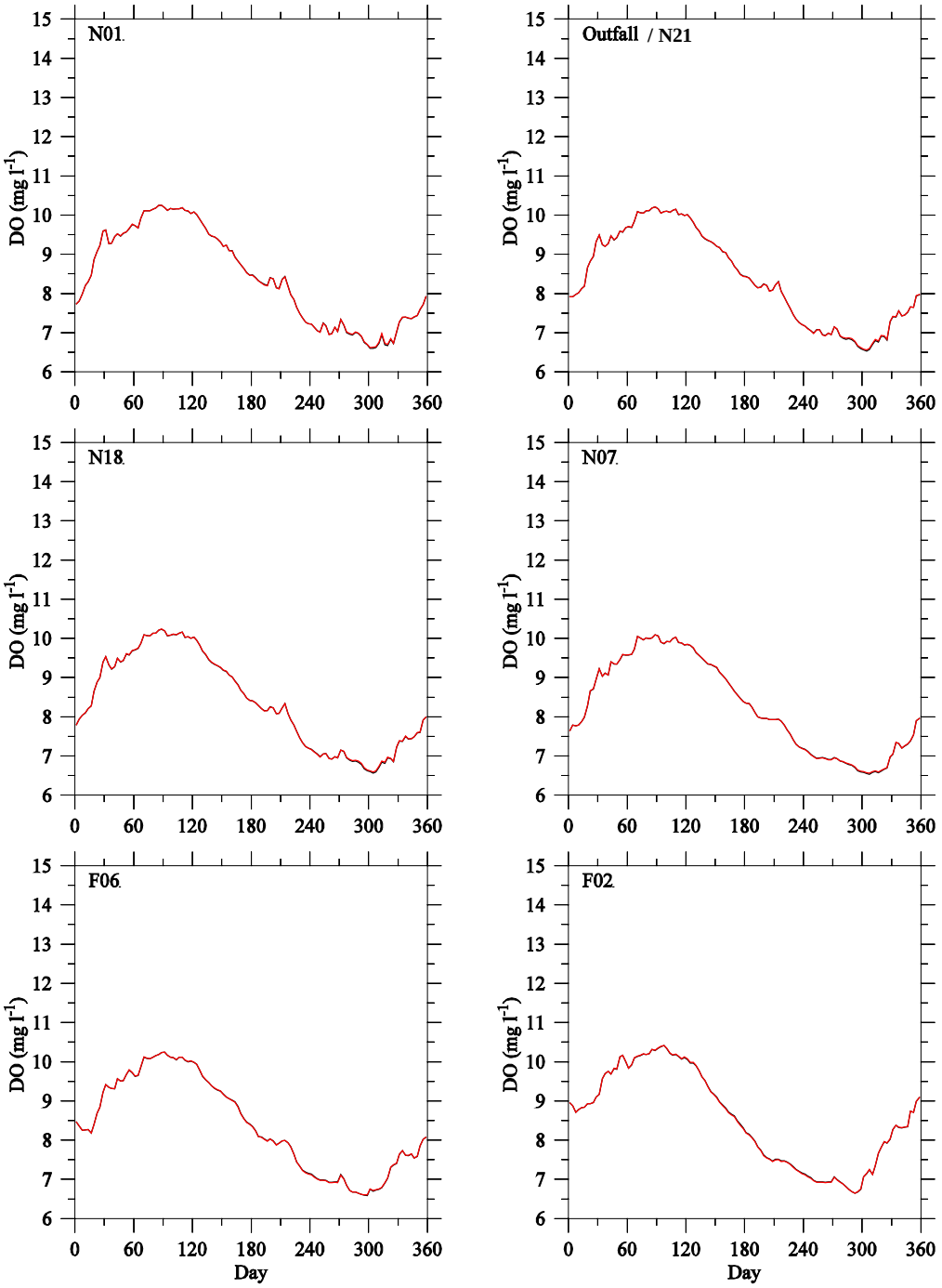

Figure 4.4 Scenario experiment bottom DO (mg L^{-1}): control run (black line) and non-sewage (red line) at select MB stations in 2013.

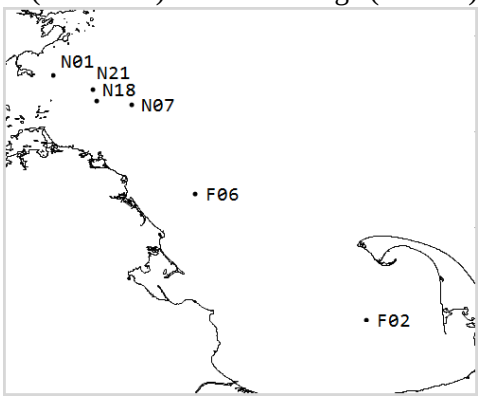

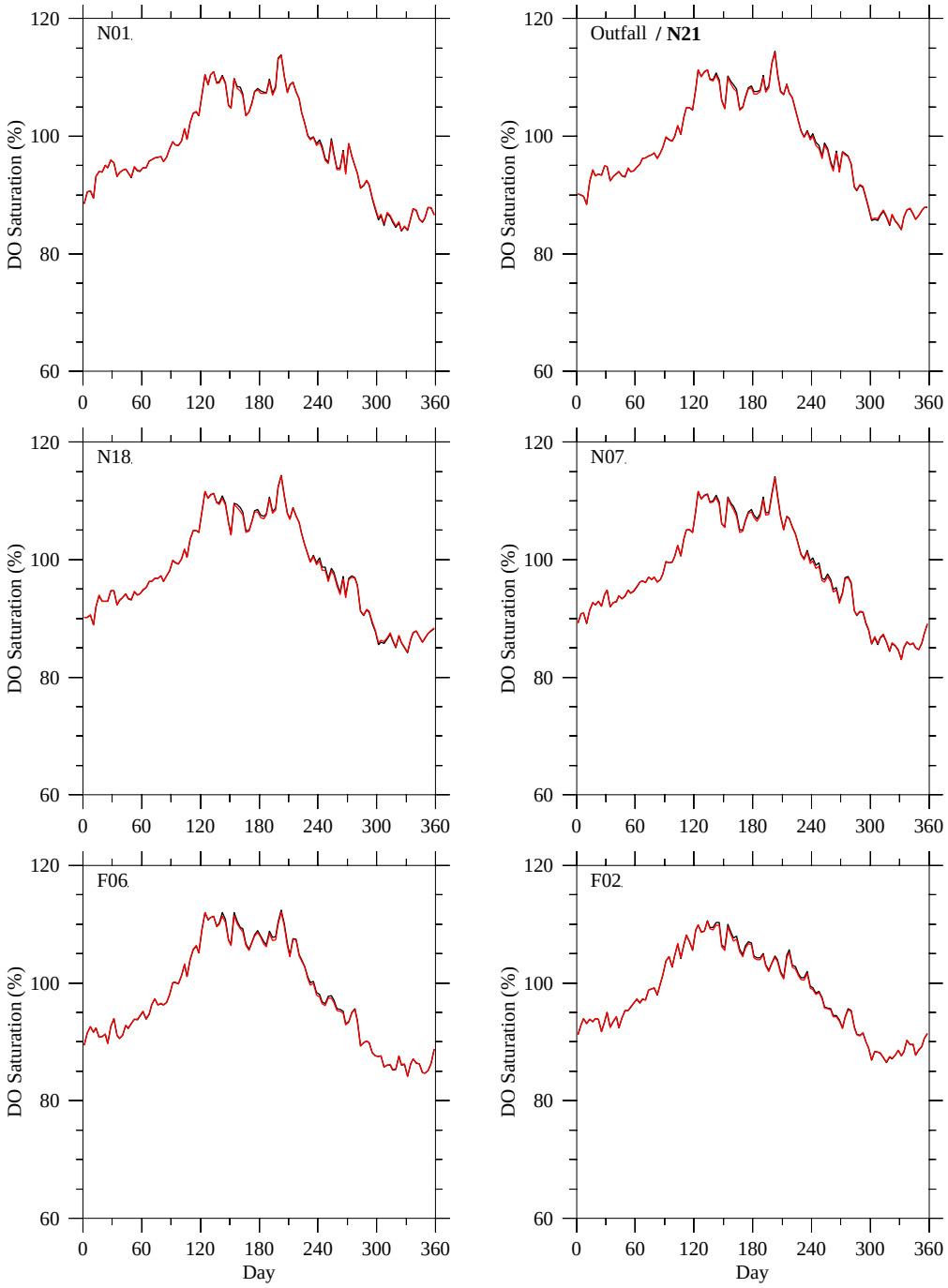

Figure 4.5 Scenario experiment surface DO saturation (%): control run (black line) and non-sewage (red line) at select MB stations in 2013.

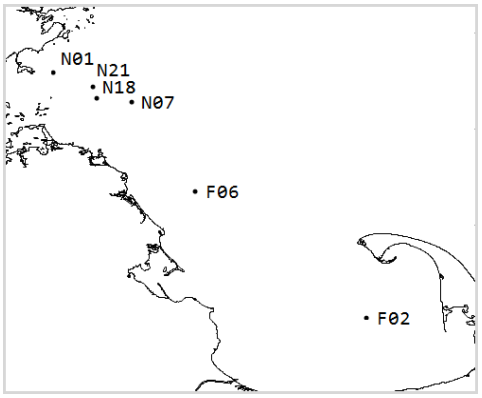

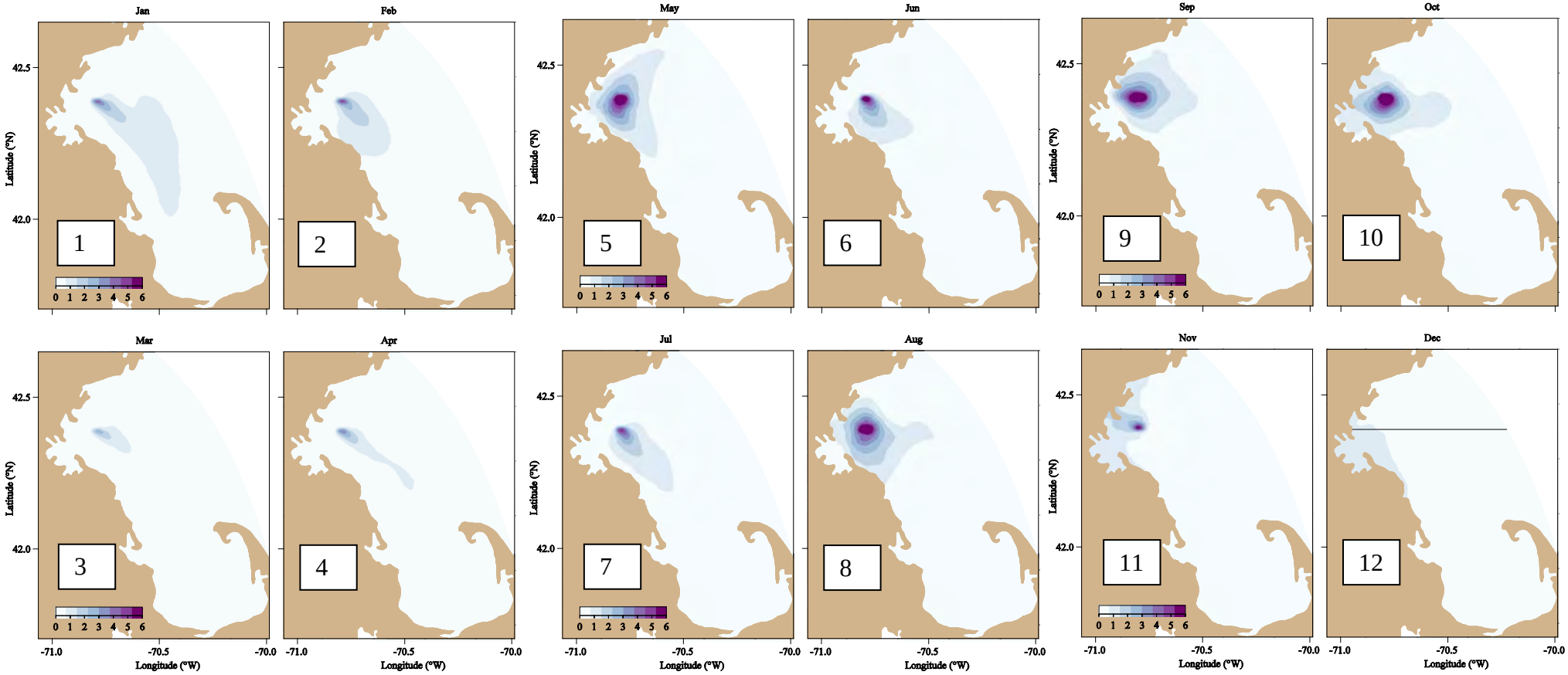

Figure 4.6 Differences in bottom NH_4^+ (μM) between control and non-sewage experiments at end of each month, 2013.

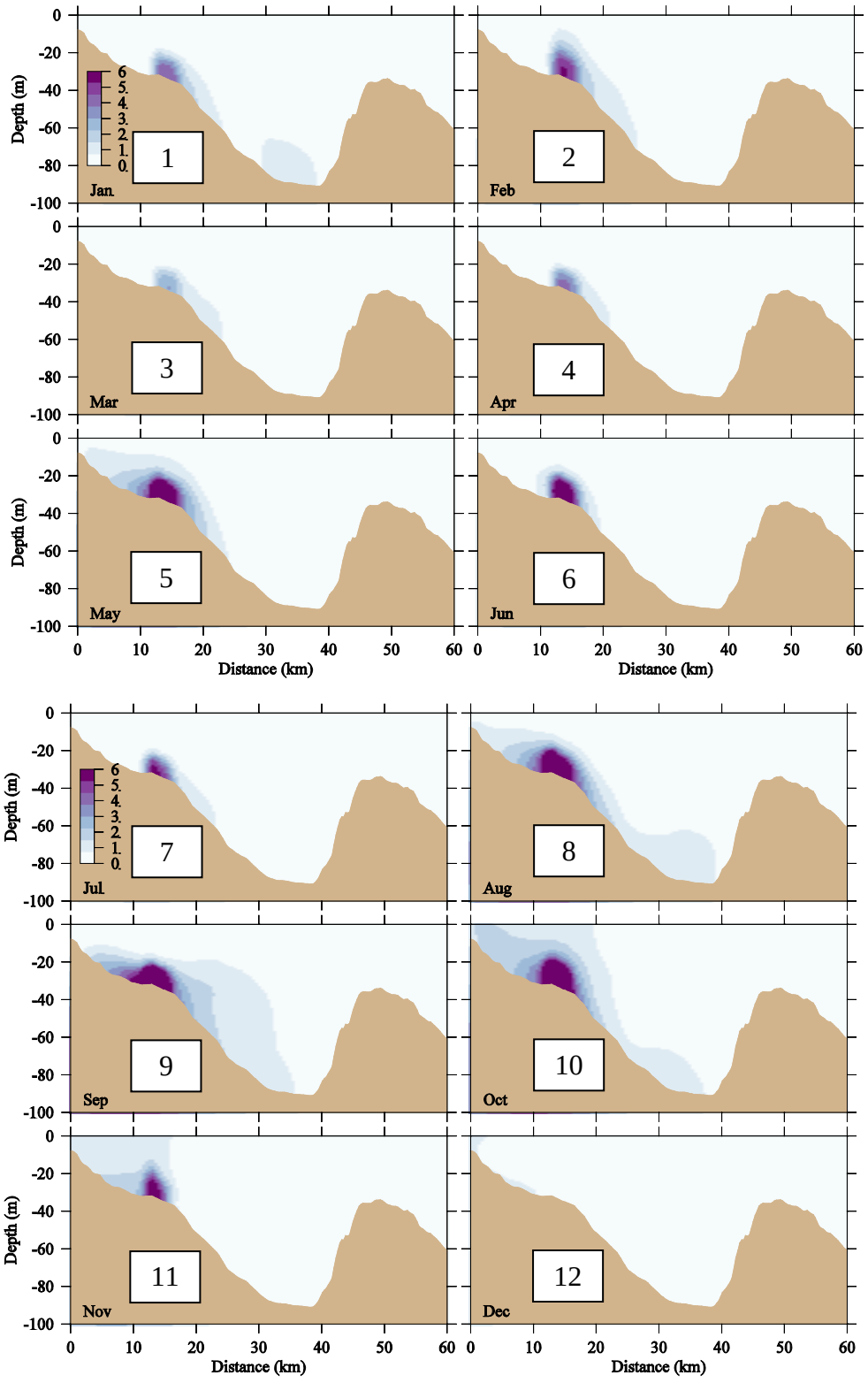

Figure 4.7 Differences in NH_4^+ concentration (μM) between control and non-sewage experiments on west-east transect across MWRA outfall at end of each month, 2013.

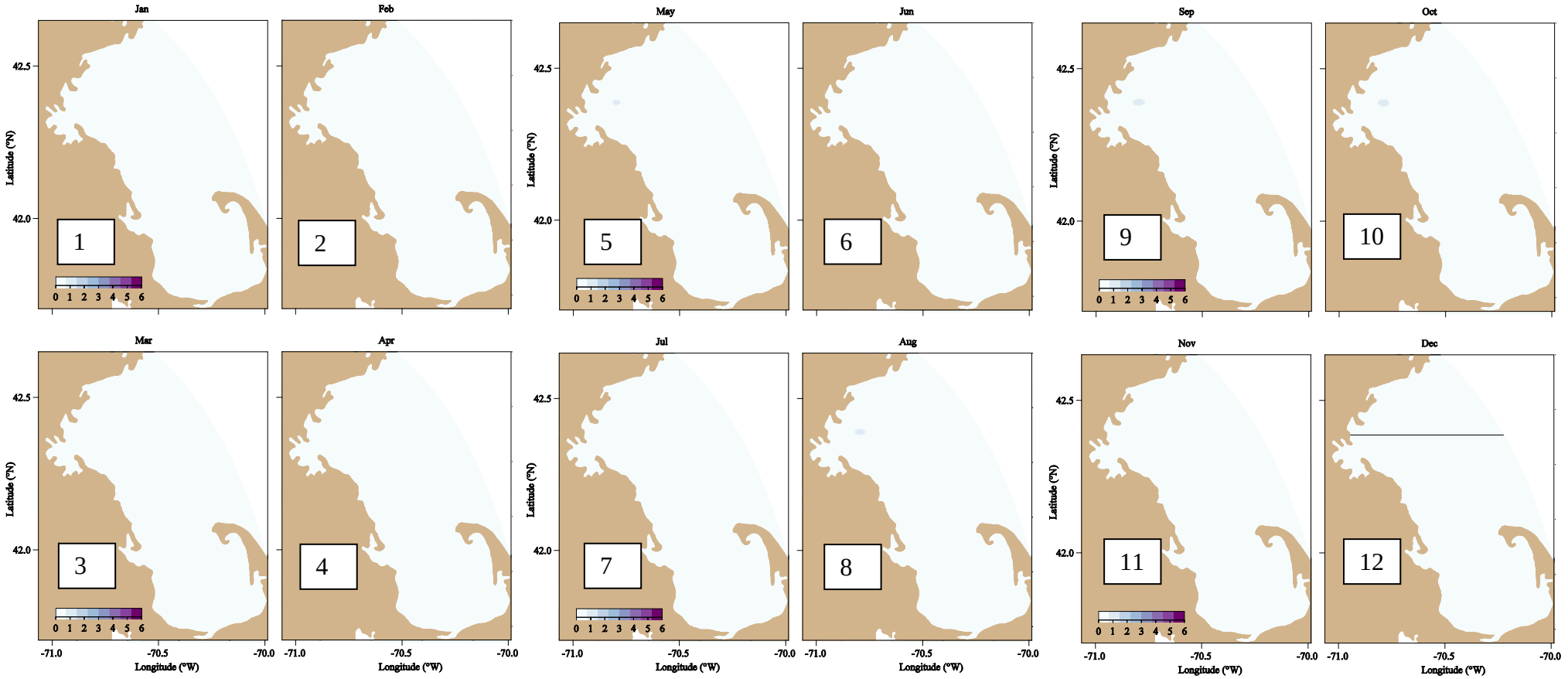

Figure 4.8 Differences in bottom NH_4^+ (μM) between run with nutrient load of 1.1X relative to the control, and the control, at end of each month in 2013.

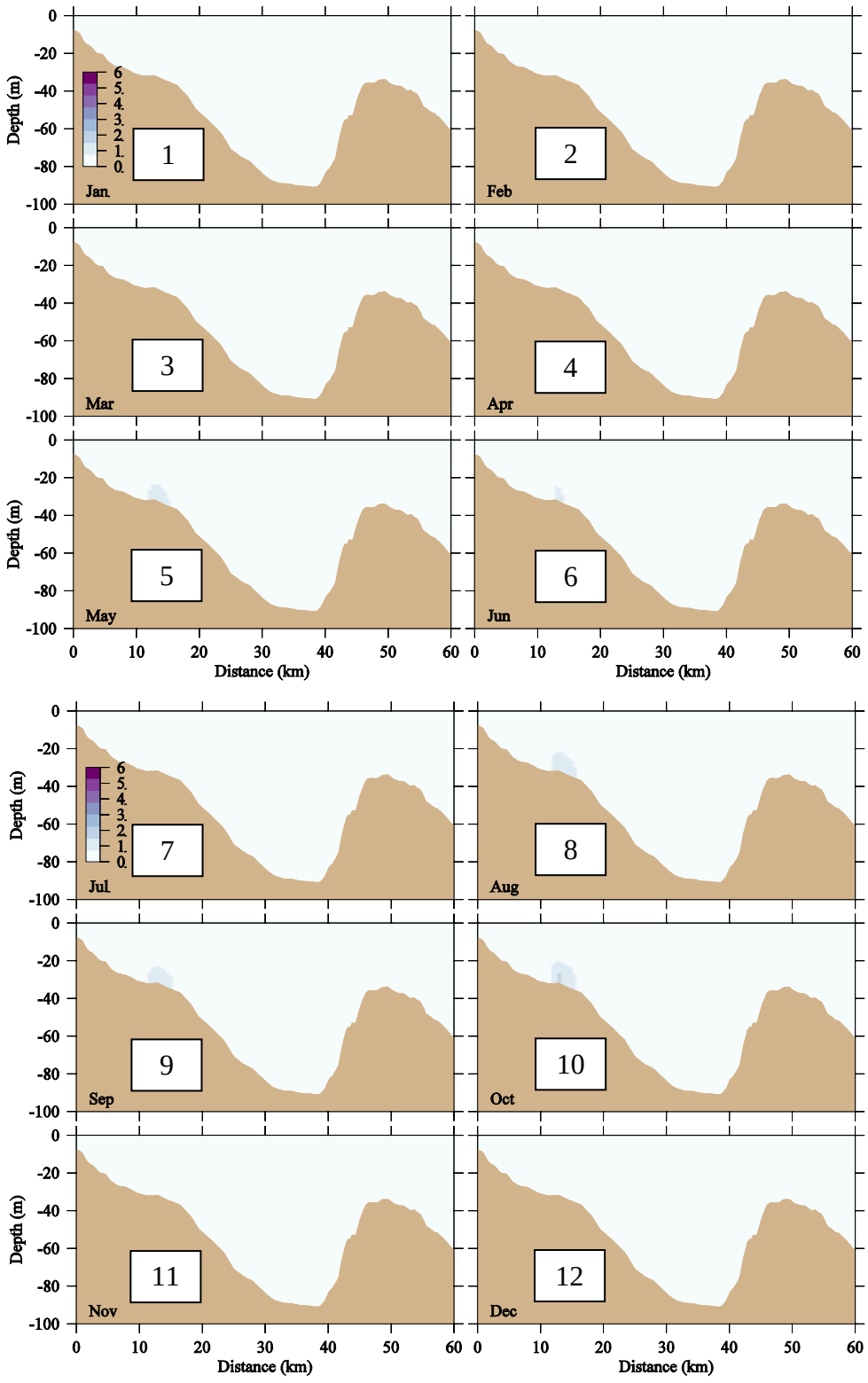

Figure 4.9 Differences in NH_4^+ (μM) between run with nutrient load of 1.1X relative to the control, and the control, on west-east transect across MWRA outfall at end of each month in 2013.

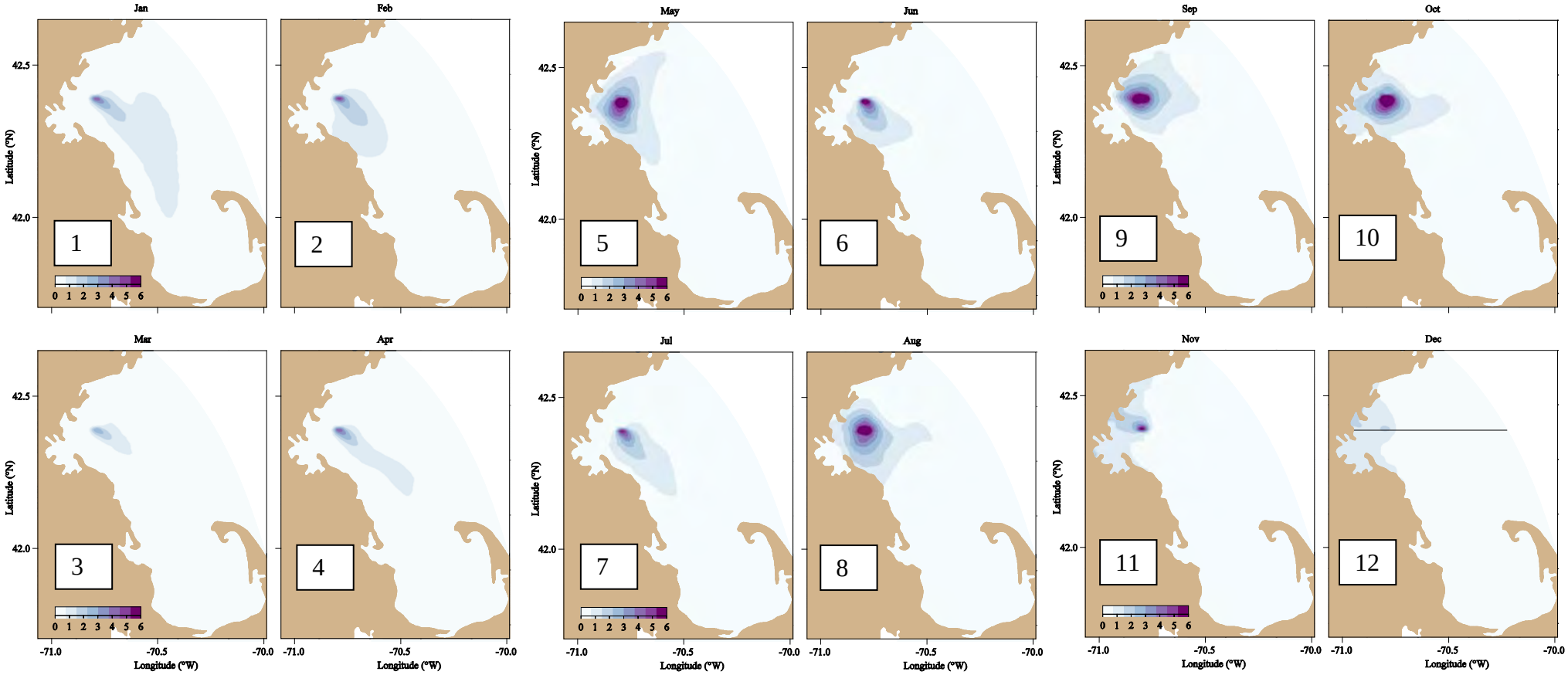

Figure 4.10 Differences in bottom NH_4^+ (μM) between run with nutrient load of 2X relative to the control, and the control, at end of each month in 2013.

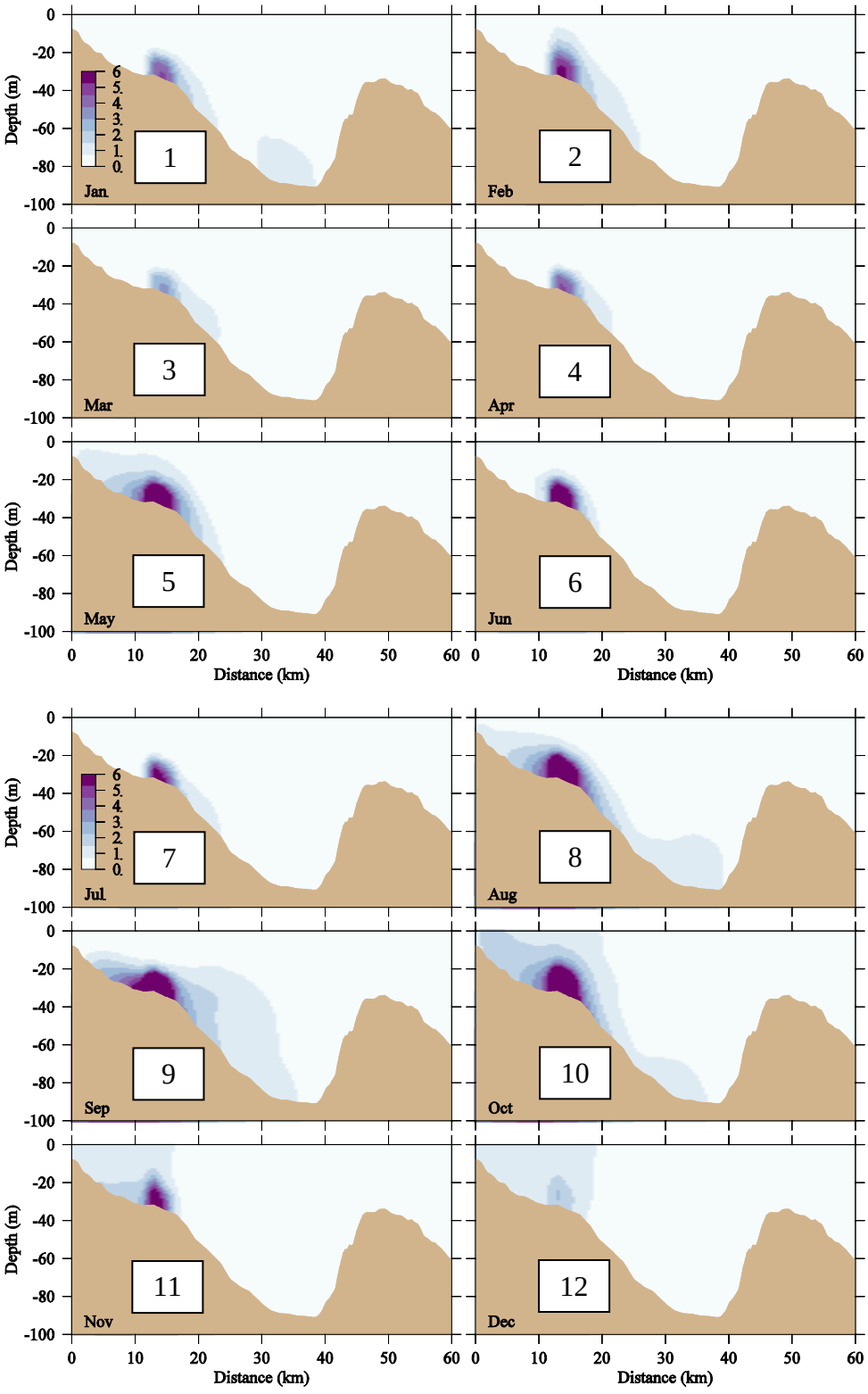

Figure 4.11 Differences in NH_4^+ (μM) between run with nutrient load of 2X relative to the control, and the control, on west-east transect across MWRA outfall at end of each month in 2013.

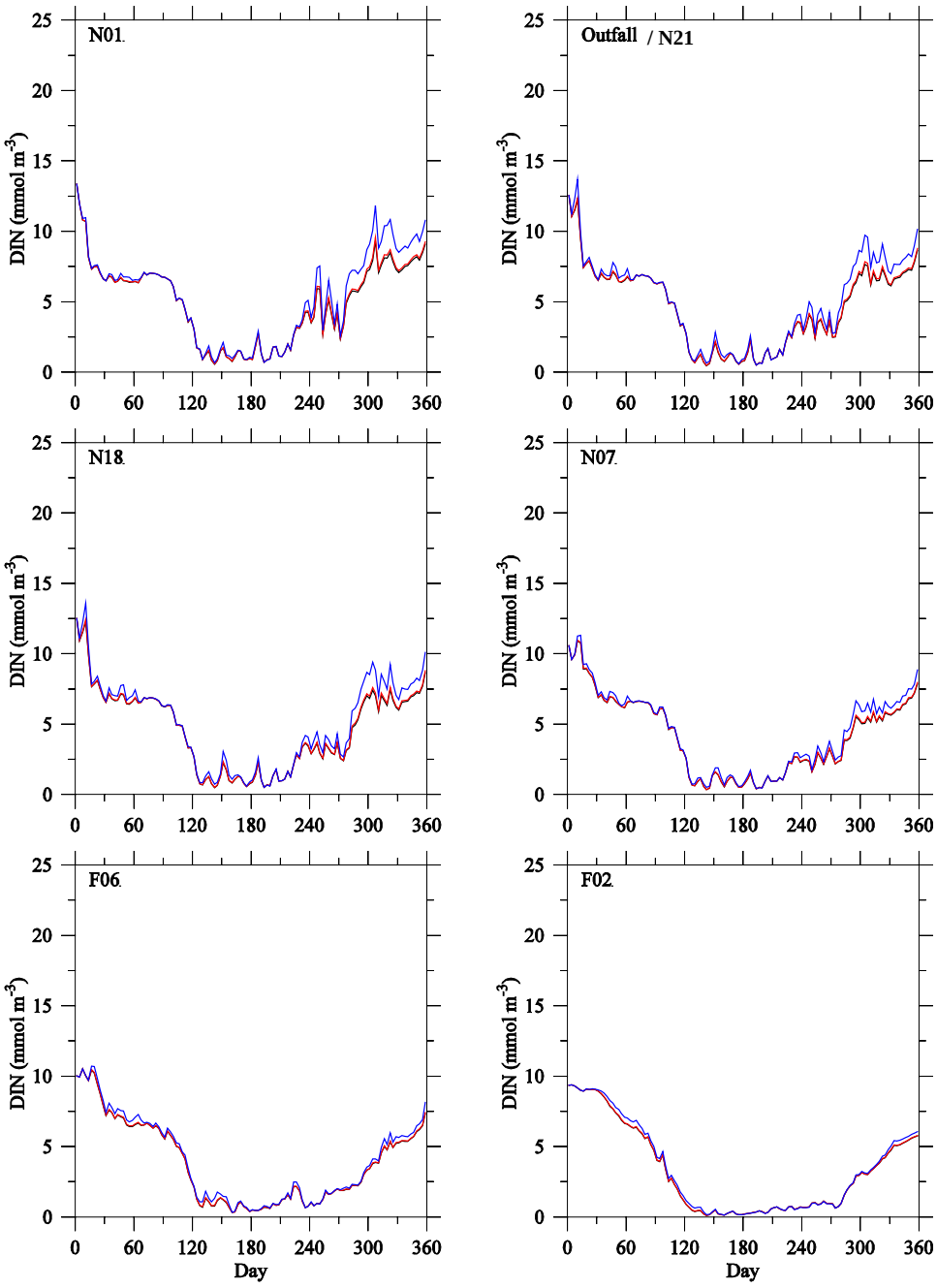

Figure 4.12 Surface DIN concentrations in runs with nutrient load of 1X (black), 1.1X (red), and 2X (blue) relative to the control, at select MB stations in 2013.

Where the three traces overlie each other, only the blue appears; where red and black overlie each other but differ from blue, only the red appears.

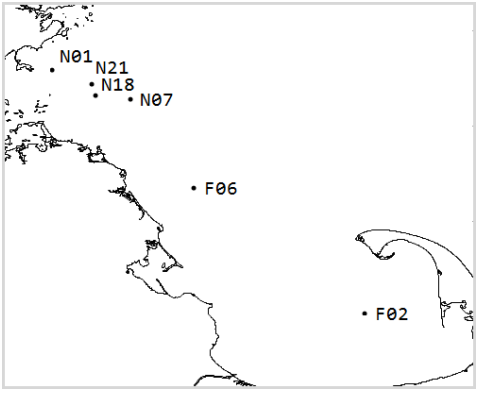

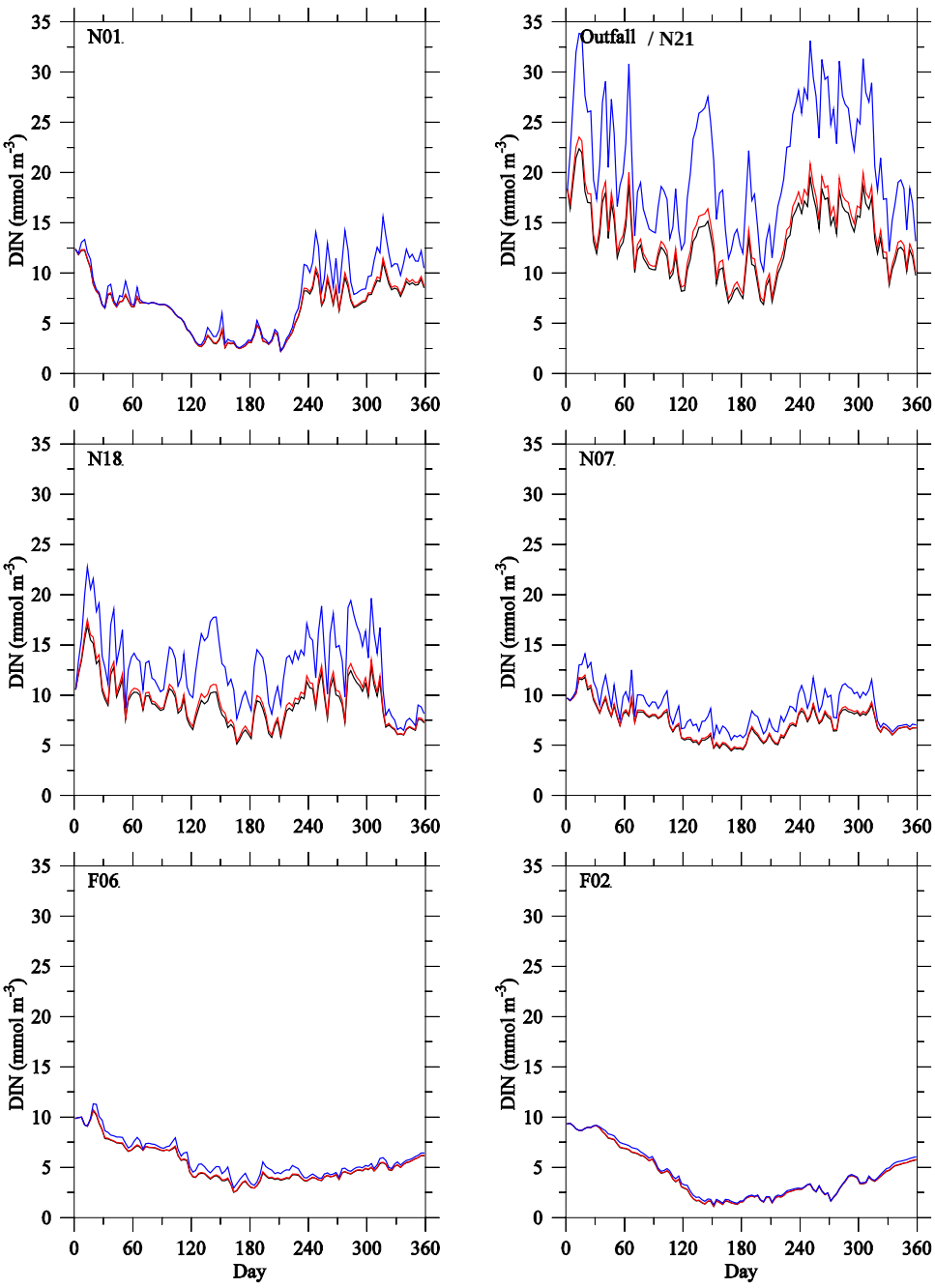

Figure 4.13 Bottom DIN concentrations in runs with nutrient load of 1X (black), 1.1X (red), and 2X (blue) relative to the control, at select MB stations in 2013, shown as in Figure 4.12.

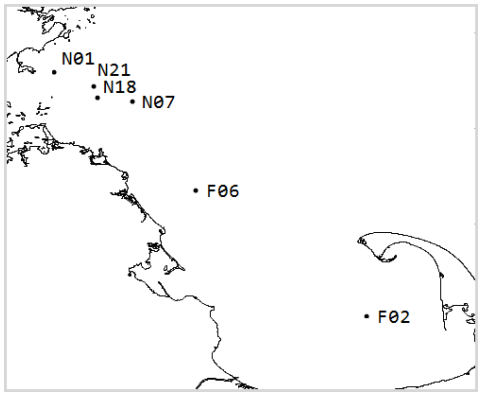

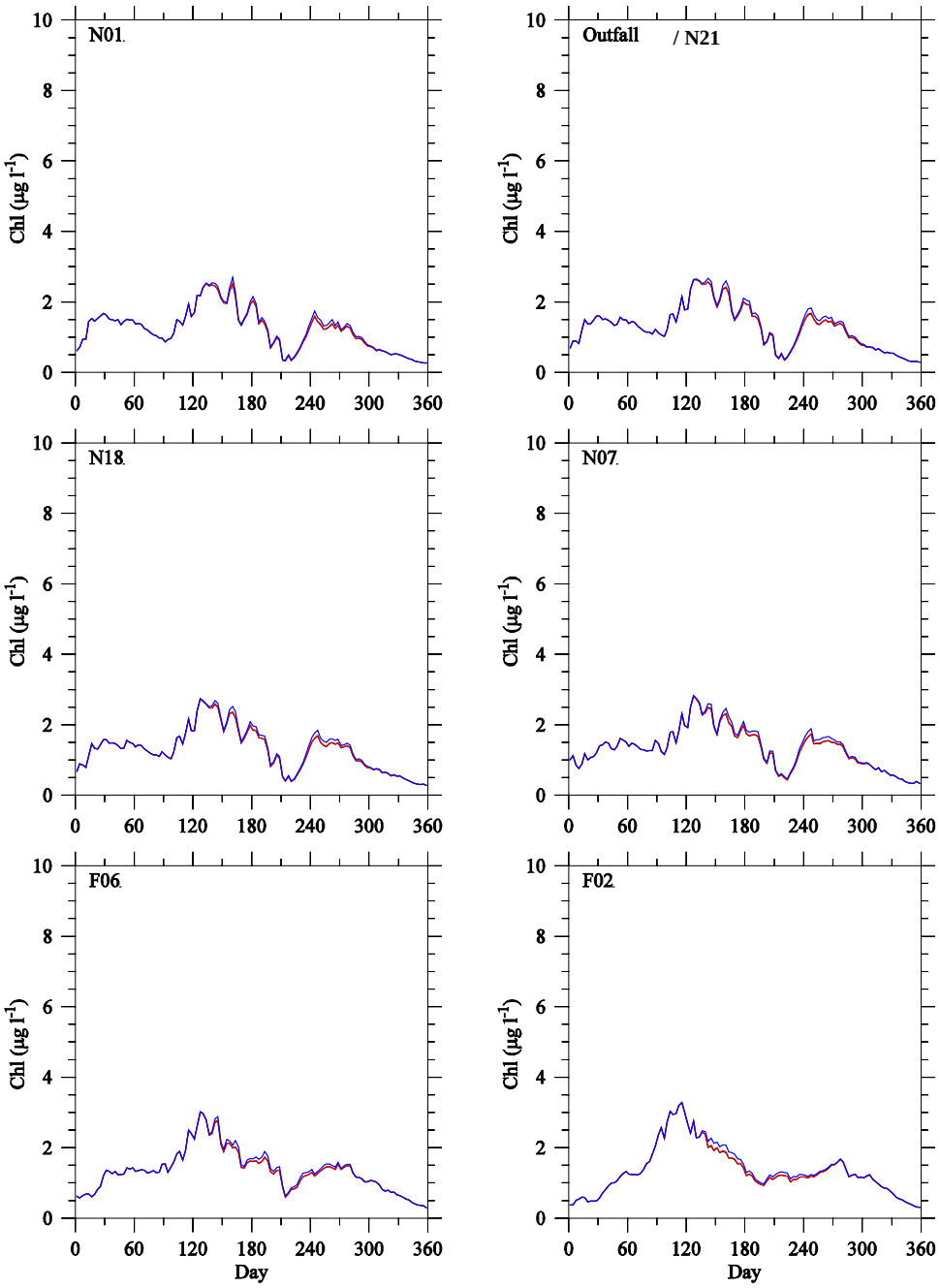

Figure 4.14 Surface chlorophyll concentrations in runs with nutrient load of 1X (black), 1.1X (red), and 2X (blue) relative to the control, at select MB stations in 2013, shown as in Figure 4.12.

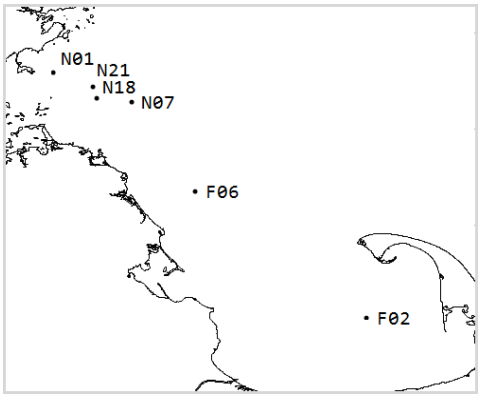

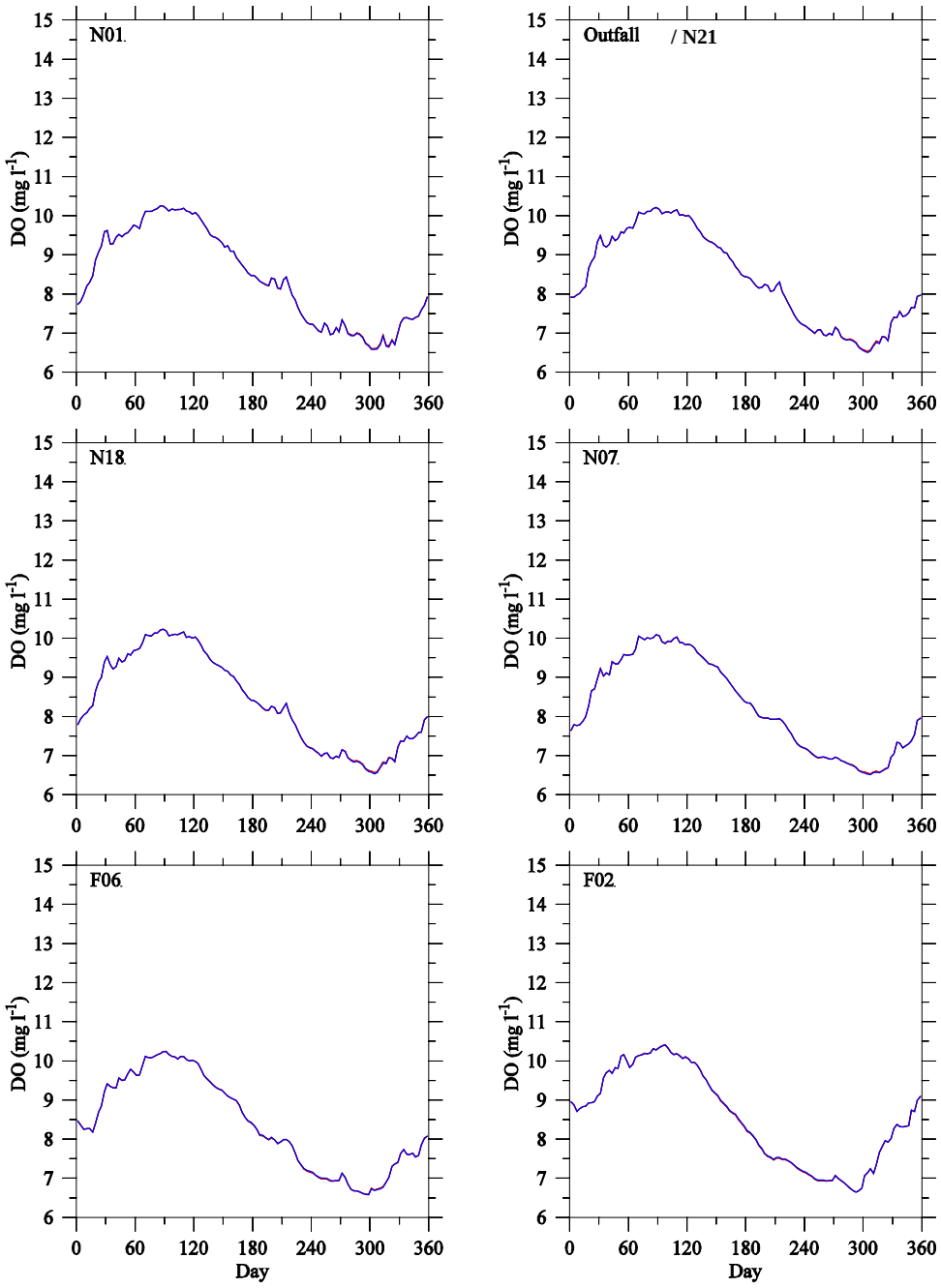

Figure 4.15 Bottom DO (mg L^{-1}) concentrations in runs with nutrient load of 1X (black), 1.1X (red), and 2X (blue) relative to the control, at select MB stations in 2013, shown as in Figure 4.12.

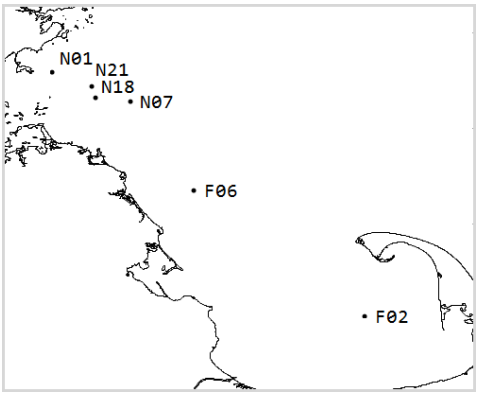

Massachusetts Water Resources Authority
Charlestown Navy Yard
100 First Avenue
Boston, MA 02129
(617) 242-6000
www.mwra.com